

Università degli Studi di Padova
Facoltà di Ingegneria
Corso di Laurea in Ingegneria dei Materiali

Dipartimento di Ingegneria Industriale – DII
Dipartimento di Tecnica e Gestione dei Sistemi Industriali – DTG

**Effect of cryolite content on the chemical and physical
properties of a NaCl-KCl salt flux for aluminium scrap
refining**

**Effetto della quantità di criolite sulle proprietà fisiche e chimiche di un sale di
flussaggio a base di NaCl-KCl per la raffinazione dei rottami di alluminio**

Relatore: Ch.mo Prof. Giulio Timelli

Co-relatrice: Prof.ssa Gabriella Tranell

Laureanda: Veronica Milani

Matricola: 1241696

Ringraziamenti

Vorrei esprimere i miei più sentiti ringraziamenti al Prof. Giulio Timelli per la passione trasmessami per il mondo della metallurgia, nonché per avermi seguito e permesso con inesauribile pazienza di condurre questo lavoro di tesi.

Un sincero ringraziamento anche alla Prof.ssa Gabriella Tranell ed alla Dott.ssa Alicia Vallejo-Olivares, che mi hanno supportato nello svolgimento di una parte sperimentale del progetto presso l'NTNU, in Norvegia.

La mia più umile e sincera riconoscenza va a Sergio, per l'amore più puro ed incondizionato che mai avrei pensato di avere il privilegio di incontrare. Grazie per l'assiduità e la spontaneità con cui mi supporti e sopporti ogni giorno.

Anna, Eleonora, Maddalena, ed Aurora, un grazie speciale va a voi, che siete una presenza costante, incoraggiante ed imprescindibile, senza la quale non sarei in grado di immaginare il mio cammino in questa vita.

Un doveroso ringraziamento agli zii Manu e Luca ed ai nonni, che conoscono ogni sfaccettatura del mio (non sempre facile) carattere, e, nonostante ciò, mi supportano e amano senza riserve. Nonna, zia, grazie per essere da sempre il mio spirito guida ed il mio più prezioso esempio a cui aspiro con enorme ammirazione.

Infine, ma non per ultimi, ringrazio in modo particolare Carlo, mamma e papà. Temo che un centinaio di pagine non siano abbastanza per dedicarvi i miei riconoscimenti. Nelle peggiori avversità come nei momenti più felici siete sempre il mio primo pensiero. Vi devo tutto.

Abstract

Salt fluxes with fluoride additions are necessary for the recycling process of contaminated and oxidised aluminium scrap. Cryolite is a particularly effective fluoride in increasing the secondary metal recovery. This thesis work investigates the effect of various cryolite additions in the range 2-15 wt.%, on the melting behavior, viscosity, and chemical properties of a 95%-5% wt. NaCl-KCl salt flux mixture. A thermodynamic software was used to perform a preliminary investigation of the salt mixtures. The melting properties of the samples were evaluated by means of differential scanning calorimetry (DSC). Viscosity measurements of the molten salts were carried out by means of a rotational rheometer. The Al_2O_3 dissolution ability of the salt was evaluated as the weight loss of alumina spheres in the molten salt. Finally, the dissolution time of the salt mixtures in water, which is relevant for the recovery of salt cakes, was assessed. The DSC results showed a decrease in the salt melting point for an increasing cryolite content, in disagreement with the thermodynamical calculations. A maximum value of viscosity was found at 5 wt.% cryolite. Higher cryolite contents in the salt led to higher rates of alumina dissolution and to an increase in the time needed for the dissolution of salt in water.

Sommario Esteso

La rapida intensificazione dei fenomeni legati al surriscaldamento globale, le cui evidenti conseguenze divengono sempre più gravi, richiede misure tempestive da parte dei governi, delle industrie e dei singoli cittadini per contrastare il cambiamento climatico. L'inarrestabile aumento delle attività umane quali la crescita industriale, la deforestazione, l'utilizzo di energia da fonti non rinnovabili, ed i sistemi di trasporto, hanno portato all'immensa crescita delle emissioni dei gas serra, le quali

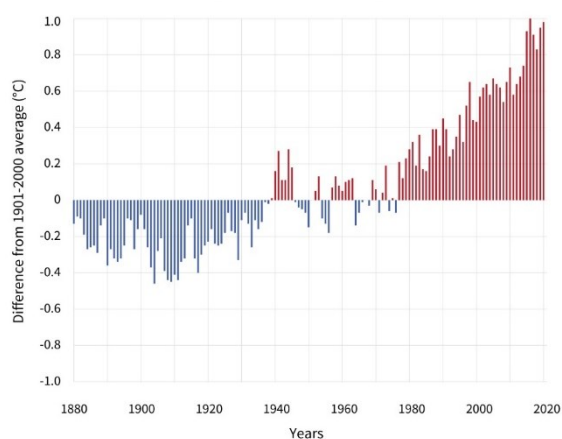


Figura 1 – Temperatura media della superficie terrestre dal 1880 al 2020 [1].

contribuiscono all'innalzamento della temperatura media globale. La superficie terrestre continua a scaldarsi irrefrenabilmente: l'incremento stimato della temperatura media globale è di 1.19 °C rispetto all'era preindustriale (1880-1900) [1], come mostrato in

Figura 1. La principale causa del surriscaldamento globale è attribuibile alle emissioni dei gas serra, i quali permangono nell'atmosfera accumulando calore ed aumentandone la temperatura. Il 76.2 % delle emissioni totali è legato all'utilizzo dell'energia per diversi impieghi, tra cui la produzione di energia elettrica, il riscaldamento, i trasporti, l'edilizia. Seguono come principali responsabili di emissioni di gas serra l'agricoltura ed i processi industriali [2]. Le conseguenze del surriscaldamento globale sono notevoli, e stanno avendo ripercussioni sempre più evidenti: da ondate di calore anomale ed intensificazioni di precipitazioni in alcune aree allo scioglimento dei ghiacci ed all'innalzarsi del livello del mare in altre zone. Incendi, siccità, diffusione di epidemie, distruzione di ecosistemi: sono solo alcuni degli effetti legati al cambiamento climatico [3].

Allo scopo di soddisfare i bisogni della popolazione attuale senza compromettere il futuro delle prossime generazioni, sono essenziali misure immediate per contrastare il surriscaldamento globale. Tra le numerose soluzioni vi sono il passaggio da combustibili fossili a fonti rinnovabili per la produzione di energia, il recupero e la protezione di foreste ed oceani, e l'implementazione di economie

circolari. Quest'ultima prevede la riduzione dei consumi di beni ed energia, il riutilizzo dei prodotti, ed il riciclo.

Nel contesto di un'economia circolare, l'ottima riciclabilità dell'alluminio nonché le sue eccellenti proprietà specifiche conferiscono al metallo un ruolo cruciale nel contrastare il surriscaldamento globale. Il 75% di tutto l'alluminio prodotto nel corso della storia è infatti ancora in uso oggi, grazie alla possibilità di fondere e riciclare i rottami d'alluminio con minime perdite di metallo [4]. Inoltre, con una densità di 2700 kg/m^3 , pari ad un terzo di quella dell'acciaio, l'alluminio presenta eccellenti proprietà specifiche. Questo lo rende un materiale competitivo per alleggerire strutture e sistemi di trasporto: ad esempio, veicoli più leggeri consentono di ridurre il consumo di carburante, nonché le emissioni di CO_2 . Altre caratteristiche che rendono questo metallo competitivo per svariate applicazioni sono l'ottima resistenza alla corrosione, l'eccellente formabilità, la buona conducibilità elettrica e termica, nonché la sua versatilità grazie alla possibilità di alligazione per diversificarne le proprietà chimiche, meccaniche e termiche.

Nonostante i diversi vantaggi risultanti dal suo impiego, il principale inconveniente dell'utilizzo dell'alluminio è la grande quantità di energia richiesta per la sua produzione primaria, ovvero la produzione del metallo a partire dai minerali di bauxite. Il processo di produzione primaria si articola in due fasi: la prima, conosciuta come Processo Bayer, prevede la conversione dei minerali di bauxite in allumina, Al_2O_3 . La bauxite viene lavata, frantumata e filtrata. Ai minerali viene poi aggiunta una soluzione di soda caustica per produrre un liquame che dissolva i composti contenenti alluminio. Successivamente, tutti gli ossidi insolubili vengono separati per sedimentazione, mentre la sospensione rimanente viene filtrata per intrappolare le impurità rimanenti. A seguire, in serbatoi appositi, alla sospensione vengono aggiunti dei cristalli di allumina idrata per promuovere la nucleazione e precipitazione del triidrossido di allumina cristallino, che viene poi filtrato, concentrato e calcinato per ottenere l'allumina [5]. Il Processo Bayer è seguito dal Processo Hall-Heroult, il quale consiste nella dissoluzione elettrolitica dell'allumina in un bagno di criolite a $960 \text{ }^\circ\text{C}$, che costituisce l'elettrolita, per produrre alluminio puro. L'ossigeno viene raccolto agli anodi di grafite, mentre l'alluminio puro si separa dal bagno elettrolitico per gravità al fondo della cella, dove viene raccolto [6].

I processi legati alla produzione dell'alluminio contribuiscono per il 3% alle emissioni totali di gas serra [4]. Nel 2019, l'energia richiesta per la produzione di una

tonnellata di alluminio fu di 14 000 KWh [7]. Oltre ai requisiti energetici ed alle emissioni legate al processo di produzione di alluminio, di notevole interesse ambientale sono anche i prodotti di scarto del processo, ovvero i fanghi rossi, di difficile smaltimento.

Il processo di riciclo dell'alluminio gioca un ruolo cruciale nella sostenibilità in quanto permette di ridurre i requisiti energetici e le emissioni di circa il 95% rispetto al processo di produzione primaria [8], come illustrato in *Figura 2*.

Il processo secondario della produzione di alluminio consente inoltre di ridurre i prodotti di scarto: la produzione di una tonnellata di alluminio primaria genera 3700

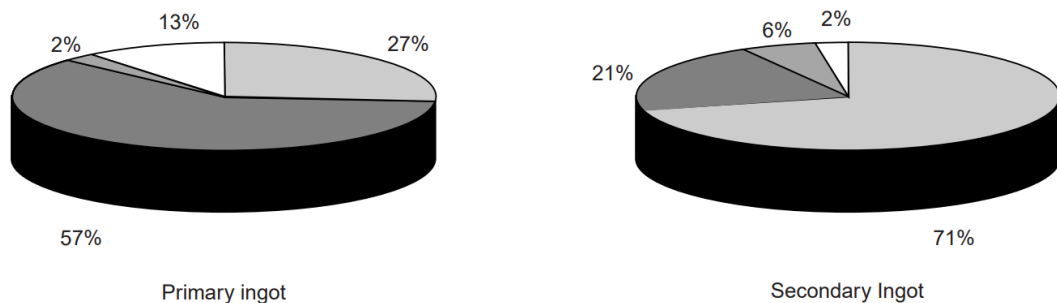


Figura 2 – Requisiti energetici per la produzione di un lingotto da produzione primaria e da produzione secondaria [8].

kg di scarto, mentre una tonnellata di alluminio da riciclo genera 400 kg di scarto per tonnellata di alluminio prodotto [9].

Il processo di riciclo dell'alluminio inizia con la raccolta del rottame, che viene classificato in base alla provenienza: nel caso in cui esso provenga da scarti di produzione industriale, e sia quindi generalmente caratterizzato da composizione nota e privo di impurità, il rottame è classificato come “*new scrap*”. D'altra parte, se il rottame proviene da scarti post-consumo, come ad esempio imballaggi, lattine, e parti di veicoli, esso è classificato come “*old scrap*” [10].

Dopo la raccolta del rottame, esso viene sottoposto a comminazione per conferire le dimensioni adeguate agli step successivi [11]. La comminazione è seguita dallo smistamento del rottame, allo scopo di eliminare contaminanti e materiali estranei come plastica, gomma, vetro ed altri metalli. Diverse tecnologie sono disponibili per lo smistamento del rottame: i classificatori ad aria, i separatori magnetici, le correnti parassite, la separazione per densità e la selezione a mano sono tecniche consolidate per lo smistamento. Negli ultimi anni, lo sviluppo di tecniche ottiche quali la spettroscopia e la fluorescenza a raggi x hanno permesso di dividere anche le leghe di alluminio in base ai principali elementi in lega [11]. Lo smistamento

è seguito dal *de-coating*, volto ad eliminare vernici, carta, ed altri contaminanti dalla superficie del rottame. Questa fase comporta l'utilizzo di processi termici o chimici per l'eliminazione dei contaminanti.

La fase di preparazione del rottame è seguita dalla fusione; sono diverse le tipologie di forni per la fusione del rottame, in base ad una moltitudine di parametri: tra essi la capacità, il costo dell'energia, la contaminazione del rottame e la sua dimensione, e la composizione chimica. I forni più comuni sono quelli a riverbero e quelli rotativi. Quest'ultimi sono più utilizzati dalle raffinerie, in quanto sono adatti a fondere rottame contaminato e con elevata area superficiale. I forni rotativi inoltre presentano efficienze energetiche più elevate [11], consentendo di abbattere le emissioni ed il consumo di combustibile. Questo tipo di forno è particolarmente adeguato alla raffinazione dell'alluminio, ovvero per il processo volto ad eliminare impurezze e contaminazioni dal metallo fuso e, eventualmente, ad aggiungere elementi

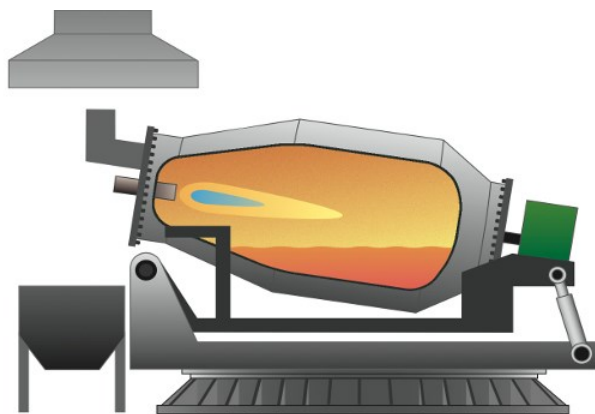


Figura 3 – Rappresentazione schematica di un forno rotativo.

alliganti. I forni rotativi consistono in un cilindro di acciaio rivestito di materiale refrattario, il quale ruota attorno al proprio asse centrale. Un bruciatore è posto ad un'estremità del cilindro e la fiamma è diretta verso le pareti refrattarie per

scaldarle. Questo consente di scaldare la carica di rottame sia per conduzione che per radiazione attraverso i refrattari. I forni rotativi sono dotati di un sistema di smaltimento dei gas di scarico. Una raffigurazione schematica di un forno rotativo è rappresentata in *Figura 3*.

I forni rotativi per la raffinazione dell'alluminio richiedono spesso l'aggiunta di composti chimici, nello specifico sali di flussaggio, che creano uno strato di scoria sulla superficie del bagno di metallo. Essi svolgono tre funzioni principali: proteggono il metallo fuso dall'ossidazione, assorbono impurezze e ossidi dal bagno, e promuovono la coalescenza delle gocce di metallo [12], che altrimenti rimarrebbero intrappolate nella scoria compromettendo la resa del processo di riciclo. I sali di flussaggio consistono tipicamente in miscele di cloruro di sodio (NaCl) e cloruro di

potassio (KCl); una miscela equimolare di essi consente di ottenere il punto di fusione più basso all'eutettico di 657 °C [12]. Dal punto di vista industriale, l'interesse principale è quello di massimizzare la resa di metallo del processo di riciclo mantenendo bassi i costi dell'energia per la fusione del metallo e dei sali.

Poiché le perdite di metallo sono principalmente dovute all'ossidazione ed all'intrappolamento del metallo nella scoria, la coalescenza delle gocce di alluminio gioca un ruolo essenziale nell'aumentare la resa del metallo. Affinchè vi sia coalescenza, le gocce di metallo devono liberarsi dello strato di ossido che le circonda. Diversi studi in letteratura mostrano che i fluoruri, solitamente CaF_2 o Na_3AlF_6 , hanno un impatto notevolmente positivo sulla coalescenza: infatti, nel caso in cui non vengano aggiunti ai sali di flussaggio, la coalescenza è assente o molto scarsa [12-15]. Il meccanismo con cui i fluoruri promuovono la coalescenza non è chiaro in letteratura. Secondo Peterson [12], la rottura dello strato di ossido è correlabile alla capacità dei fluoruri di dissolvere l'ossido di alluminio, mentre secondo Tenorio ed Espinosa [16] i fluoruri accelerano l'eliminazione dell'ossido con un meccanismo simile alla corrosione a caldo. Anche le tensioni interfacciali tra sale e ossido giocano un ruolo essenziale nel promuovere la coalescenza delle gocce di metallo, come suggerito da Roy e Sahai [17].

Anche la viscosità dei sali di flussaggio e della scoria impattano sul grado di coalescenza: infatti, se la viscosità è troppo elevata, ostacola il movimento delle gocce di metallo nella scoria, diminuendo quindi il grado di coalescenza ed il recupero di metallo del processo [14]. L'effetto dei fluoruri sulla viscosità cinematica di una miscela equimolare di NaCl – KCl è stato studiato da Roy, Ye e Sahai [18], i cui risultati sperimentali mostrano un andamento dapprima crescente, poi decrescente all'aumentare della concentrazione dei fluoruri. D'altra parte, i risultati sperimentali di Tenorio et al. [19], mostrano una diminuzione lineare della viscosità all'aumentare della concentrazione di fluoruri.

Il trattamento e lo smaltimento dei prodotti di scarto del processo di riciclo dell'alluminio sono causa di preoccupazione ambientale. Gli scarti, conosciuti anche come "*massi salini*", vanno trattati con estrema cautela vista la loro elevata reattività chimica e la possibilità di generare composti chimici tossici ed inquinanti. Poiché lo smaltimento in discarica dei massi salini in Europa è proibito, solitamente vengono processate per recuperarne i componenti, che solitamente sono sali, parti non metalliche, e alluminio. Spesso, i metodi di trattamento dei massi salini prevedono la

loro dissoluzione in acqua per separare la frazione salina da quella non-metallica e dall'alluminio.

In questo lavoro di tesi, sono state investigate le proprietà chimica e fisiche di un sale di flussaggio a base di 95% NaCl – 5% KCl con aggiunte di criolite tra 0 e 15 % in peso. Sono stati considerati il comportamento a fusione e la viscosità dei sali, nonché la loro abilità di dissolvere l'ossido di alluminio e la loro dissoluzione in acqua al variare della concentrazione di criolite.

È stata eseguita un'analisi termodinamica preliminare tramite il software FactSage, seguita da una Calorimetria Differenziale a Scansione (DSC). Successivamente, la viscosità dei campioni è stata analizzata mediante un reometro rotazionale. La dissoluzione dell'ossido di alluminio è stata valutata in base alla perdita di peso di sfere di alluminio dopo immersione a diversi tempi nei sali fusi. Infine, la dissoluzione del sale in acqua è stata studiata come la perdita in peso dei sali dopo immersione in acqua a diversi tempi di mantenimento.

L'analisi termodinamica preliminare ha rivelato una costanza nella temperatura di solidus per concentrazioni di criolite tra il 2 ed il 15%, mentre la temperatura di liquidus aumenta da 757 a 775 °C all'aumentare della percentuale di criolite, come evidenziato in *Figura 4*.

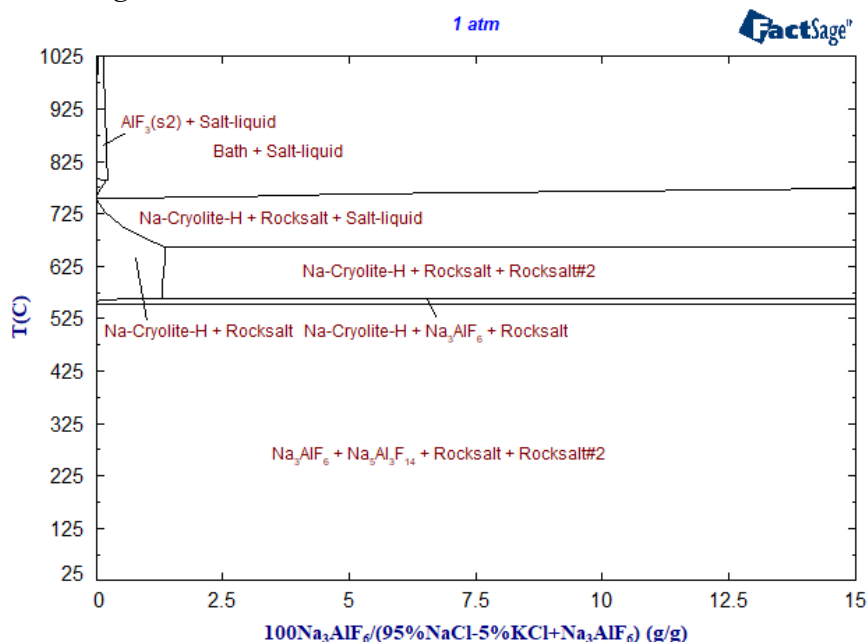


Figura 4 – Diagramma di fase per il sale di flussaggio 95% NaCl – 5% KCl al variare del contenuto di criolite.

I risultati sperimentali dalla DSC rivelano, d'altro canto, una diminuzione sia della temperatura di solidus che della temperatura di liquidus all'aumentare della concentrazione di criolite nel sale, come mostrato in *Figura 5*.

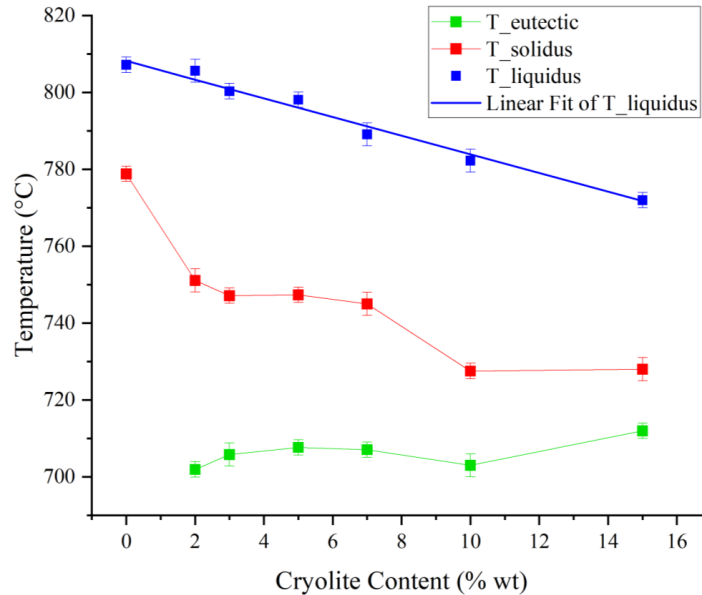


Figura 5 – Andamento delle temperature di solidus, liquidus, e dell'eutettico del sale di flussaggio 95% NaCl – 5% KCl all'aumentare del contenuto di criolite.

Dal punto di vista industriale, la temperatura di liquidus è la più rilevante: essa, infatti, impatta sui requisiti energetici per la fusione del sale, influenzando quindi i costi del processo di riciclo. Una diminuzione della temperatura di liquidus è quindi vantaggiosa in termini di risparmi economici e di riduzione delle emissioni.

I risultati della reologia mostrano un picco di viscosità per la concentrazione di criolite al 5%. In generale, la viscosità dei sali contenenti criolite è sempre più elevata del sale senza aggiunte di criolite, come mostrato in *Figura 6*.

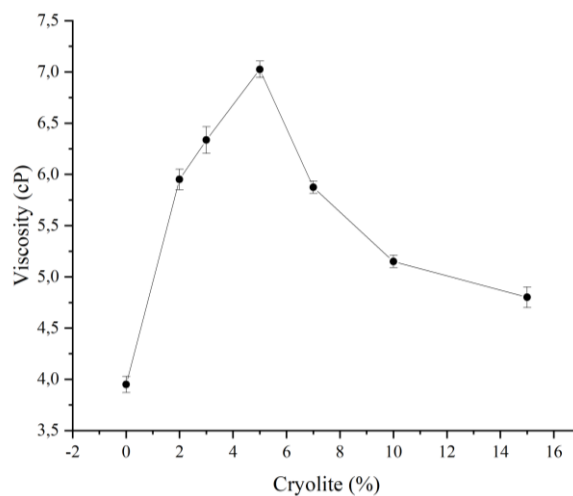


Figura 6 – Andamento della viscosità del sale di flussaggio con 95% NaCl – 5% KCl all'aumentare del contenuto di criolite.

L'aumento di viscosità del sale è un effetto indesiderato dovuto al contenuto di criolite; la viscosità della scoria, infatti, ostacola il movimento delle gocce di metallo e riduce il grado di coalescenza, impattando negativamente quindi sul recupero di metallo del processo.

I risultati degli esperimenti sulla dissoluzione dell'ossido nel sale fuso mostrano un aumento della perdita in peso delle sferette di allumina all'aumentare della concentrazione di criolite nel sale. Tale effetto è più marcato quando il contenuto di criolite nel sale è pari o maggiore a 7% in peso, come si può notare in *Figura 7*.

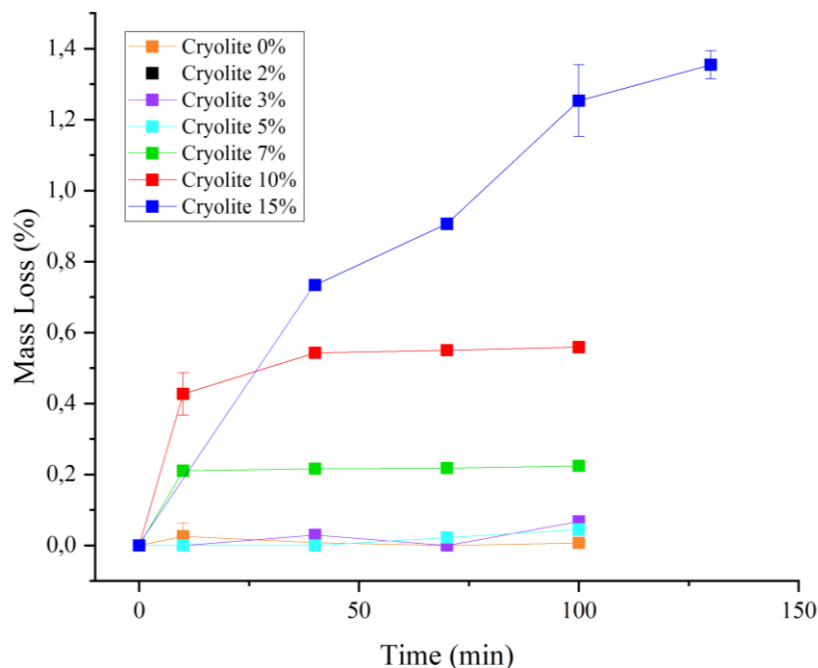


Figura 7 – Dissoluzione delle sferette di allumina nel sale fuso a diversi tempi di permanenza ed al variare del contenuto di criolite nel sale.

L'effetto del contenuto di criolite sulla dissoluzione dell'allumina è correlabile alla capacità del sale nel dissolvere l'ossido, e quindi di rilasciare le gocce di metallo dallo strato di ossido che le circonda. Questo è rilevante dal punto industriale poiché un aumento della coalescenza implica un aumento del recupero di metallo del processo di riciclo.

I risultati sperimentali della dissoluzione del sale in acqua mostrano che, all'aumentare del contenuto di criolite, la dissoluzione è rallentata, specialmente per percentuali di criolite sopra al 10%. La dissoluzione del sale in acqua è rilevante dal punto di vista industriale, nello specifico nel trattamento dei prodotti di scarto, poiché impatta sui tempi di ciclo.

Per concludere, dai risultati sperimentali, contenuti elevati di criolite nel sale analizzato hanno un effetto positivo sulle temperature di liquidus e solidus, nonché sulla dissoluzione dell'ossido. Tuttavia, la presenza di criolite aumenta la viscosità del sale, ostacolando la coalescenza delle gocce di metallo, nonché rallenta il processo di dissoluzione del sale in acqua, il quale è rilevante per il recupero dei massi salini.

Table of contents

Introduction.....	9
1 Aluminum’s role in sustainable development	14
1.1 Global warming and its causes	14
1.2 Consequences of global warming.....	16
1.3 The need for sustainable development	18
1.4 The role of Aluminum in circularity and sustainability	20
1.4.1 Primary Aluminum Production.....	23
1.4.2 Secondary Aluminum Production.....	26
2 Aluminum recycling and refining by means of salt fluxes.....	29
2.1 The recycling stages	29
2.1.1 Preparing the scrap charge.....	29
2.1.2 Melting technologies.....	33
2.1.3 Melt refining	34
2.1.4 Casting	36
2.2 The use of salt fluxes in rotary furnaces for Al refining	36
2.2.1 Rotary Furnaces	37
2.2.2 Salt fluxes.....	38
2.3 Parameters of salt fluxes affecting metal recovery, energy requirements and costs	40
2.3.1 Salt Factor	40
2.3.2 Effect of increased NaCl:KCl ratio.....	41
2.3.3 Coalescence of metal droplets.....	42
2.3.4 Melting Point	49
2.3.5 Impurities removal	49
2.4 The role of cryolite additions in salt fluxes.....	50
2.4.1 Effect of cryolite on salt fluxes’ density and viscosity	51
2.4.2 Effect of cryolite concentration on coalescence.....	51
2.5 Treatment and disposal of salt cakes	54

2.5.1	Traditional salt cake treatment method	55
2.5.2	In-house treatment of salt cake	57
2.5.3	Alternative salt cake treatment processes	57
3	Material and Methods	60
3.1	Raw materials	60
3.1.1	Sample preparation	61
3.2	Thermodynamics	61
3.3	Physical Characterization	62
3.3.1	Thermal Analysis	62
3.3.2	Viscosity Measurements	66
3.4	Chemical Characterization	68
3.4.1	Alumina Dissolution	68
3.4.2	Salt dissolution in water	69
4	Results and Discussion	71
4.1	Thermodynamic calculations	71
4.2	Thermal Analysis	74
4.2.1	Wetting Furnace	74
4.2.2	DSC Analysis	77
4.3	Viscosity Measurements	83
4.4	Alumina Dissolution in the molten salt mixtures	85
4.5	Salt dissolution in water	86
5	Conclusions and future perspectives	89
6	References	92
	Appendix A	100
	Appendix B	102

List of Figures

Figure 1.1 Global average surface temperature from 1880 to 2020. [1].....	14
Figure 1.2 World Greenhouse Gases Emissions, 2018 [2]	15
Figure 1.3 Predicted impact and risks of global warming up to 2°C, according to IPCC [3]	17
Figure 1.4 – Weight saving in car components when substituting other competing materials with aluminum [31].	21
Figure 1.5 – Schematic representation of the alumina production from bauxite ores in the Bayer Process, adapted from [5].	24
Figure 1.6. Greenhouse gas emissions from aluminum production [6]	25
Figure 1.7. Energy consumption for (a) primary and (b) secondary ingots production [8]	27
Figure 2.1 – Schematic representation of (a) drum and (b) overhead-belt devices for magnetic separation of aluminum scrap [10].	31
Figure 2.2 – Conveyor-type eddy current separator for aluminum scrap [10]......	31
Figure 2.3 – Schematic representation of a rotary degasser for molten aluminum. Adapted from [36].	35
Figure 2.4 – Schematic flow chart of the common steps involved in the aluminum recycling process.	36
Figure 2.5 – Schematic representation of a tilting rotary furnace [39].	38
Figure 2.6 – NaCl – KCl binary phase diagram [41].	39
Figure 2.7 – Characteristic materials used for salt fluxes [20]......	40
Figure 2.8 - Schematic representation of the stripping of the oxide layer. (a): contact of oxide layer and molten salt; (b) and (c): openings develop in the oxide layer and the salt penetrates between the oxide layer and the metal. (d): the oxide layer is stripped away [4].	42
Figure 2.9 – Effect of fluoride concentration and temperature on metal recovery [47].	44
Figure 2.10 – Coalescence rate at 830°C [49]......	45
Figure 2.11 Variation of kinematic viscosity of equimolar NaCl-KCl with mole % additives [18]......	47
Figure 2.12 – Densities of molten NaCl – KCl with fluorides additions [18].	47

Figure 2.13 – Equilibrium constant for the impurities removal reactions [20].....	49
Figure 2.14 - Schematic representation of the parameters affecting the efficiency of salt fluxes in the recycling process.....	50
Figure 2.15 – Recovered metal from UBC [12].....	52
Figure 2.16 – Coalesced metal droplets at different cryolite concentrations [60].	52
Figure 2.17 – Influence of the presence of cryolite and of oxide content in the slag on the coalescence efficiency at a duration of 7 minutes for the melting of the aluminum chips [55].....	53
Figure 2.18 – Magnesium content in coagulated metal droplets and coalescence efficiency in salt slags with varying cryolite content [61].	54
Figure 2.19 – Schematic representation of the traditional process to treat salt cakes [21].	56
Figure 3.1 – Schematic representation of the wetting furnace [65].	63
Figure 3.2 – Determination of the characteristic temperatures from the DSC analysis. T_i : initial peak temperature; T_e : extrapolated onset temperature; T_p : peak maximum temperature; T_o : peak offset temperature; T_f : final peak temperature [67].....	65
Figure 3.3 – Theta Industries Rheotronic Rotating Viscometer used for the viscosity measurements.	66
Figure 3.4 – Graphite spindle used for the viscosity measurements.....	67
Figure 4.1 – Phase diagram of 95 % wt NaCl – 5 % wt KCl with cryolite additions up to 15% wt.	71
Figure 4.2 – Phase diagram of 70% wt NaCl – 30% wt KCl with cryolite additions up to 15%.	72
Figure 4.3 – Phase diagram of 50% wt NaCl – 50% wt KCl with cryolite additions up to 15% wt.	73
Figure 4.4 – Experimental melting sequence of a 95% wt NaCl – 5% wt KCl with 15 % wt cryolite addition (a) 640 °C; (b) 710 °C; (c) 731 °C; (d) 760 °C.	75
Figure 4.5 – Wetting furnace - Softening temperature of the salt mixtures as the cryolite content increases.	76
Figure 4.6 – DSC curves of the 95% wt. NaCl – 5% wt. KCl with (a) 0% cryolite; (b) 2% cryolite; (c) 3% cryolite;(d) 5% cryolite; (e) 7% c10ryolite; (f) 10% cryolite; (g) 15% cryolite.	78
Figure 4.7 – Eutectic, solidus and liquidus temperatures of the 95% wt NaCl – 5% wt KCl salt mixtures as the cryolite content increases from 0 to 15% wt.	80

Figure 4.8 – Comparison between the solidus temperature obtained from the DSC analysis and the softening temperature obtained from the wetting furnace experiments.	81
Figure 4.9 - DSC curves of the (a) 70% wt. NaCl – 30% wt. KCl and (b) 50% wt. NaCl – 50% wt. KCl, both with 2% cryolite additions.	82
Figure 4.10 – Viscosity of the 95% NaCl - 5% KCl at 820°C and 170 RPM at different cryolite content.	83
Figure 4.11 – Al ₂ O ₃ dissolution in the molten 95%NaCl-5%KCl salt mixtures at varying cryolite concentrations.	85
Figure 4.12 – Salt dissolution in water as a function of time for different cryolite contents.....	86

List of Tables

Table 3-1 – Chemical composition of the salt mixtures.	60
Table 4-1- Solidus temperature of the salt mixtures with cryolite additions according to the phase diagrams obtained with FactSage.	73
Table 4-2 – Softening point of the salt mixtures obtained by melting the samples in the wetting furnace.....	75
Table 4-3 – Characteristic temperatures obtained from the DSC curves of the 95% wt. NaCl – 5% wt. KCl with different cryolite contents.....	79
Table 4-4 – Eutectic, solidus, and liquidus temperature obtained from the analysis of the extrapolated temperatures from the DSC curves for the 95% wt. NaCl – 5% wt. KCl with increasing cryolite content.....	79
Table 4-5 - Characteristic temperatures obtained from the DSC curves of the 70% wt NaCl – 30% wt KCl and the 50% wt NaCl – 50% wt KCl with 2 % cryolite additions.	82
Table 4-6 – Eutectic, solidus and liquidus temperatures obtained from the analysis of the characteristic temperatures of DSC curves for the salt mixtures.	82

Introduction

Aluminum is the second most used metal in the world. Its low specific weight, good corrosion resistance, high electrical and thermal conductivity, and the versatility of its manufacturing processes have made aluminum a competitive material for several applications: these include packaging, building and construction, the automotive field as well as aerospace applications.

Despite the benefits arising from aluminum applications, the metal requires a substantial amount of energy for its primary production, that is, the production of aluminum from bauxite ores [8]. Primary aluminum originates from the Bayer process, which involves the processing of bauxite ores to obtain alumina, Al_2O_3 . The Bayer process is followed by the Hall-Heroult process, which consists of the electrolytic conversion of alumina into pure aluminum metal. Due to its strong affinity with oxygen, a great amount of energy is required to produce metallic aluminum: the primary production process is one of the most energy-intensive industrial processes and it accounts for approximately 3% of all greenhouse gases emissions [4]. Other environmental concerns of the primary production of aluminum are the production of air pollutants and the solid waste arising from the process, also known as red mud.

The environmental issues arising from aluminum production must be thoroughly addressed in view of global warming. The world's population is witnessing the consequences of the extreme rise in the global average surface temperature, which has increased by 1.19 °C from the pre-industrial period [1] and continues to rise. The increment in the global average surface temperature is mainly due to the emission of greenhouse gases, which absorb heat in the atmosphere and cause rises in its temperature. The consequences of global warming are innumerable: from extreme heat waves and intensifying heavy rainfall to the melting of glaciers and rising sea levels; from wildfires and the reduction of snow cover and sea ice to the destruction of ecosystems and the loss of biodiversity [3].

Due to the urgent need to tackle climate change, aluminum plays a crucial role in the context of circularity and sustainability. Not only does it allow to produce light-weight transport, which implies reduced fuel consumption and emissions, but its recycling process leads to a reduction of greenhouse gases emissions and energy consumption by up to 95% [8]. Aluminum demand continues to increase: the demand

for aluminum products is predicted to increase by 81 % by 2050 [7]. In view of meeting the increasing demand as well as reducing the greenhouse gases emissions to tackle climate change, the aluminum sector will need considerable efforts in improving its technologies and processes.

The secondary production of aluminum, that is, the recycling process of aluminum, starts with the collection of scrap. The scrap is generally classified according to the origin: *new scrap* originates from the industrial waste of metal-processing industries and usually is characterized by low impurities content and known composition. *Old scrap* arises from post-consumer utilization and often contains a higher amount of impurities and its composition is usually unknown. The collection of the scrap is followed by its comminution and sorting to confer the scrap charge its proper size and eliminate contaminants and other materials such as plastic, rubber, glass, and other metals. Some routes of scrap preparation also involve thermal or chemical processes to de-coat the scrap with the aim to eliminate paints, paper, humidity, and other contaminants from the scrap surface. The de-coating process may be followed by an agglomeration phase in the case of aluminum pieces of very small size, which oxidate more easily [10].

The scrap preparation phase is followed by the melting process. Different furnaces are available to melt the scrap according to several parameters such as capacity, production volume, energy requirements and cost, scrap type, origin, and contamination, and final product chemical composition. Rotary furnaces are a suitable choice for processing heavily oxidized and contaminated scrap with unknown composition. Compared to other furnaces used for re-melting aluminum scrap such as reverberatory furnaces, rotary furnaces allow the reduction of emissions and fuel consumption as well as higher melting efficiencies [11].

Rotary furnaces consist of a rotating refractory-lined steel cylinder with a flame burner to melt the aluminum scrap. Melting contaminated scrap in rotary furnaces usually requires the addition of salt fluxes to refine the molten metal. Although the term fluxing stands for all additions of chemical compounds in the treatment of molten aluminum, solid fluxes are the most utilized for this purpose. Salt fluxes, which generally consist of a NaCl-KCl mixture with fluorides additions, perform three main functions: they cover the molten metal to prevent its oxidation, they collect impurities and oxides from the metal bath, and they promote the metal droplets' coalescence by freeing them from the surrounding oxide layer [12]. Different percentages of NaCl and

KCl can be used as a salt flux; however, an equimolar mixture of NaCl-KCl allows to obtain the lower melting point at approximately 665 °C, as they form an eutectic point.

The salt flux, by collecting oxides and impurities from the molten scrap, forms a slag layer on top of the molten metal bath which entraps droplets of molten metal. A salt flux containing only chlorides is not sufficient to promote the metal droplets' coalescence, therefore fluorides are also added, as they allow to increase the metal yield of the re-melting process. The fluorides, which often consist of CaF₂ or Na₂AlF₆, strip the oxide layer surrounding the molten metal droplet, which is then free to coagulate with other droplets and coalesce [20]. The mechanism by which fluorides act is not completely understood in the literature. According to Peterson, the rupture of the oxide layer is related to the fluoride's ability in dissolving aluminum oxide [12]. Tenorio and Espinosa suggested that the rupture of the oxide layer is enhanced by fluoride additions according to a mechanism similar to the hot corrosion process, which helps release the molten metal from the surrounding oxide layer [16]. Interfacial tensions between the salt and the metal also play a crucial role, as suggested by Roy and Sahai [17], in enhancing the coalescence and the coagulation of metal droplets.

The slag's viscosity also affects the metal recovery: if the viscosity increases, it hinders the movements of the metal droplets and therefore leads to a reduction of the metal yield. The slag's viscosity is affected mainly by the presence of oxides and non-metallic particles, which already at a content of 10% can drastically increase the viscosity [15]. The fluoride's effect on viscosity has also been investigated in literature: according to Roy, Ye, and Sahai, the kinematic viscosity of an equimolar NaCl-KCl salt flux increases before decreasing again by the addition of fluorides [18]. On the other hand, the findings of Tenorio et al. [19] show a linear decrease of the viscosity as the fluoride content increases.

The treatment and disposal of the waste product from the secondary aluminum production, also known as *salt cake*, must be addressed properly for its significant environmental concern. Usually, salt cakes are either treated for recovery of their components or stored in controlled landfills. As landfilling is forbidden in Europe due to the high reactivity of salt cakes to form pollutants and toxic compounds, its treatment for recovery is the most ecological choice. Some routes of salt cake treatment involve its dissolution in water to separate the salt fraction from the non-metallic components [21].

In this thesis work, a 95% wt NaCl – 5% wt KCl salt flux with cryolite (Na_3AlF_6) additions has been investigated from a physical and a chemical point of view, as a function of the cryolite content. The melting behavior, the viscosity, the ability of dissolving alumina, and the salt dissolution in water have been studied.

1 Aluminum's role in sustainable development

Sustainable development and the implementation of a green economy are critical factors in mitigating climate change. In this context, the role of aluminum production and recycling will be discussed.

1.1 Global warming and its causes

As a consequence of the rapid growth of the global population, energy demands, products fabrication, deforestation, and utilization of transport have enormously increased. All these factors related to human activities have led to an increment in greenhouse gases emissions, which contribute to global warming and climate change. Earth's surface continues to increasingly warm, the years 2016 and 2020 being the hottest years on record since record-keeping began in 1880 [22]. The global average surface temperature was 0.98 °C warmer than the twentieth-century average and 1.19 °C warmer than the pre-industrial period (1880-1900) [1], as can be seen in *Figure 1.1*.

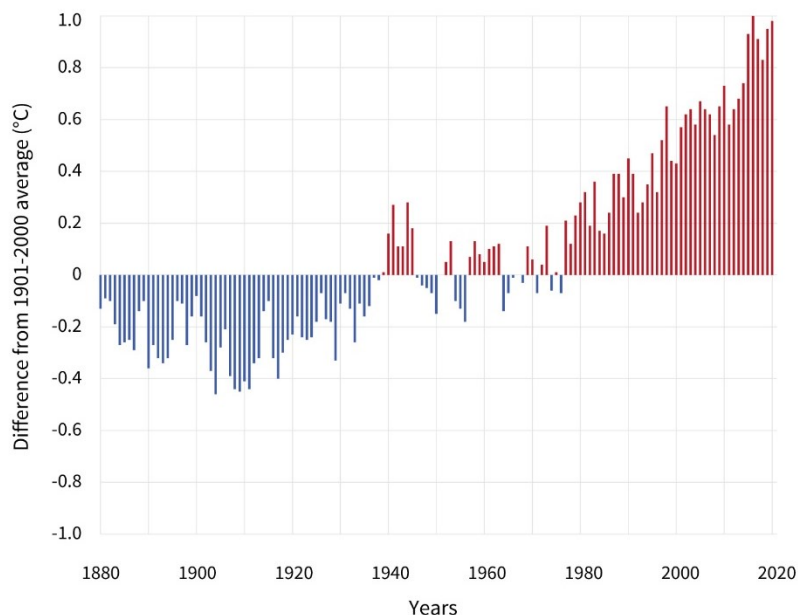
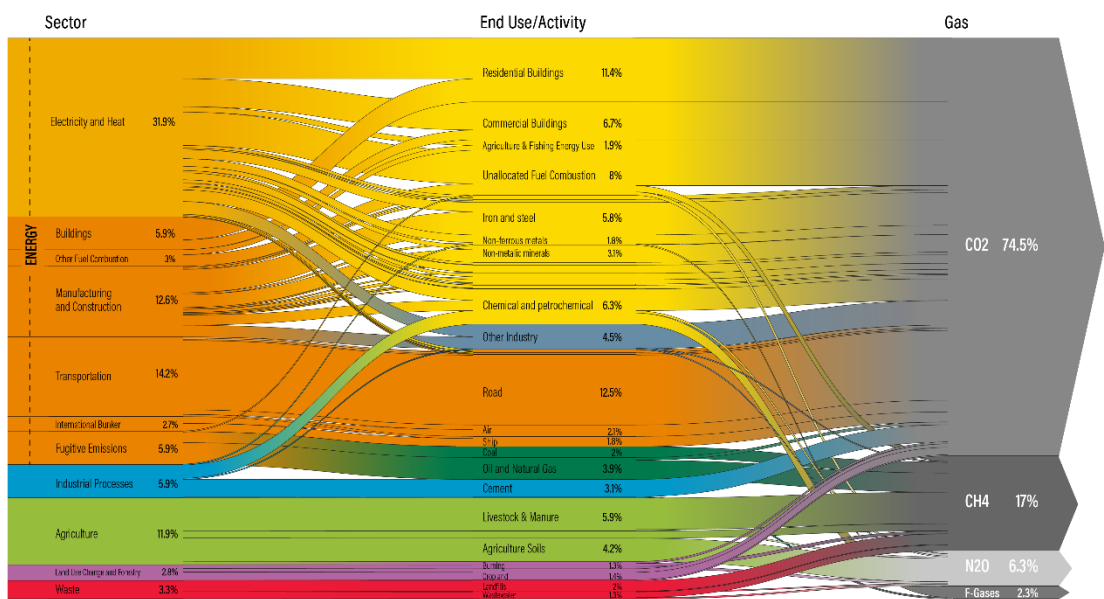


Figure 1.1 Global average surface temperature from 1880 to 2020. [1]

The main cause responsible for this increment in global average surface temperature is the emission of greenhouse gases (GHGs), which absorb heat in the atmosphere and cause rises in its temperature. Carbon dioxide (CO₂) is mainly produced by burning fossil fuels and by industrial processes such as iron and cement production. CO₂ is the main greenhouse gas emitted through human activities, accounting for 79% of all greenhouse gases emissions in the U.S. in 2020 [23]. Other greenhouse gases are methane (CH₄), nitrous oxide (N₂O), and fluorinated gases such as perfluorocarbons and hydrofluorocarbons. Methane is emitted when producing fossil fuels such as coal, natural gas, and oil, but it is also a result of agricultural practices and livestock. Nitrous oxide is also a result of industrial and agricultural practices.

Figure 1.2 displays on the left the sources, divided by sector, of the world's greenhouse gases emissions in 2018. The energy sector, represented in orange colors, is the largest



Source: Greenhouse gas emissions on Climate Watch. Available at: <https://www.climatewatchdata.org>

WORLD RESOURCES INSTITUTE

Figure 1.2 World Greenhouse Gases Emissions, 2018 [2]

emitting sector, accounting for 76.2% of total emissions, followed by agriculture and industrial processes. It is interesting to note how much transportation, electricity, and heat affect the amount of emissions just in the energy sector. Another point worth mentioning is that cement production process accounts for 3.1% of total greenhouse gases emitted in 2018. On the right side of the graph, the percentages of the greenhouse gases are shown, carbon dioxide being by far the most prominent at 74.5%, followed by methane at 17% and nitrous oxide at 6.3% [2].

Although CH₄, N₂O and fluorocarbon gases constitute a smaller percentage of the total greenhouse gases emissions, some gases are more effective than others at increasing the average global temperature. To understand the impact of each greenhouse gas on the atmosphere and compare the GHGs, a Global Warming Potential (GWP) was developed. It is a measure of how much energy the emissions of 1 ton of a gas will absorb over a given period, relative to the emissions of 1 ton of carbon dioxide (CO₂). The larger the GWP, the more a given gas warms the Earth compared to CO₂ over that time period, which is usually 100 years. As an example, the estimated GWP for methane is 28-36, whereas that of nitrous oxide is approximately 256-298 [24].

1.2 Consequences of global warming

Although a roughly 1 °C increase in global average temperature may seem small, Earth's soil and oceans' tremendous size and heat capacity must be considered. This significant increment in accumulated heat is not only causing extreme seasonal temperature rises all over the world, but it is also leading to the reduction of snow cover and sea ice, melting of glaciers, intensifying heavy rainfall in some zones and drought in others, as well as reducing habitats for plants and animals and expanding them for others. These events affect all regions in the world: from wildfires in Australia to extreme heat in European cities, from rising sea levels caused by ice melting to floods in India, Nepal, Bangladesh, and Myanmar. Other regions, such as Southern Africa and Central and Southern America, suffer from a severe lack of water [25]. The phenomena arising from global warming affect both animals and humans. The destruction of ecosystems leads to a severe loss of biodiversity as well as it forces animals to abandon their habitat, increasing the possibility of zoonoses by altering host-pathogen interactions [26]. Higher temperatures are also making it easier for mosquitos to spread diseases, such as dengue fever. Climate change is also having drastic consequences on hunger: after years of decline, hunger in the world is rising again due to droughts and floods which drastically affect crops [25]. Global attention is also growing on the issue of migration due to weather-related disasters: According to the Internal Displacement Monitoring Center (IDMC), in some areas of the world such as the Americas, Europe, and Central and Southern Asia, climate disasters caused

more internal displacement than war in 2021 [27]. The world is already witnessing and suffering from the repercussions of the changing weather patterns; however, the consequences could be even more disastrous if the global warming issue is not addressed properly. With the Paris Agreement in 2015, nearly all countries in the world have endorsed in tackling climate change by limiting global warming well below 2 °C, preferably below 1.5 °C. If action is not taken, the outcome will adversely affect every ecosystem. Future scenarios which are likely to occur are depicted in the Intergovernmental Panel on Climate Change (IPCC) Special Report “*Global Warming of 1.5 °C*” [3], based on the available literature. According to the report, climate models project substantial differences in average temperature, hot extremes, heavy precipitations, and drought between present-day and global warming of 1.5°C, and between 1.5°C and 2°C.

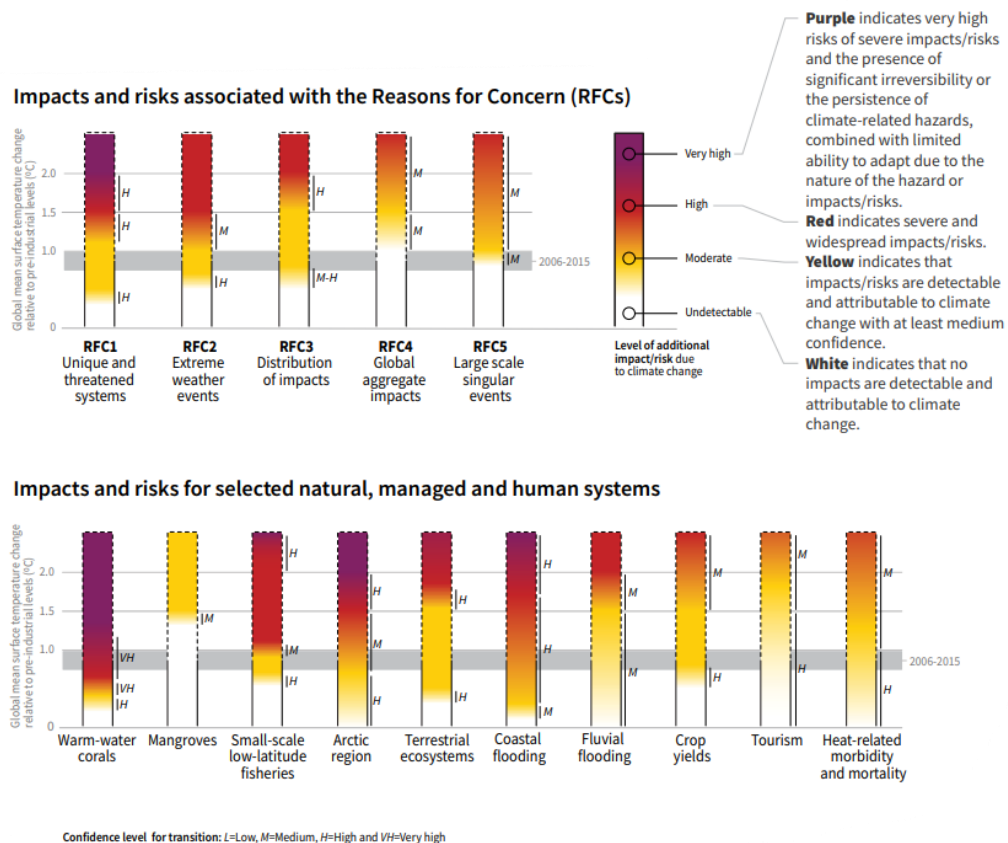


Figure 1.3 Predicted impact and risks of global warming up to 2°C, according to IPCC [3]

Figure 1.3 shows the impacts and risks of global warming up to 2 °C associated with the Reasons for Concern, RFCs, above, and for some natural, managed, and human systems, below. Reasons for Concern summarize key implications of global warming for people, economies, and ecosystems. Unique and threatened systems (RFC1) refers to ecological and human systems that have restricted geographic ranges

constrained by climate-related conditions and they include coral reefs, the Arctic and its indigenous people, glaciers, and biodiversity hotspots. Extreme weather events (RFC2) concern risks and impacts to humans and ecosystems from extreme weather events such as heatwaves, heavy rain, drought and associated wildfires, and coastal flooding. The distribution of impacts (RFC3) indicates consequences that affect particular groups due to the uneven distribution of climate change threats. Global aggregate impacts (RFC4) include global monetary damage, global-scale degradation, and loss of ecosystems and biodiversity, whereas large-scale singular events (RFC5) are large and often irreversible changes in systems such as the disintegration of the Greenland and Antarctic ice sheets. The graphs in *Figure 1.3* clearly display how, already at 1°C temperature increase, represented by the gray line, some risks and impacts are already having severe consequences, in some cases even irreversible. It is also evident that predictions for temperature increases of 1.5 °C and 2 °C would imply even more catastrophic effects.

1.3 The need for sustainable development

To meet the needs of today's population without compromising the future of the next generations, the United Nations as well as other international organizations and governments have embraced the concept of sustainable development. Their challenge is to promote well-being worldwide by addressing hunger and poverty as well as protecting ecosystems and reducing the impact of climate change. To avoid the predictions for a temperature increase of 2 °C or above from occurring, ambitious and vital actions must be taken. It is essential that governments and organizations not only participate in tackling global warming, but they should also inform citizens about the importance of their role on an individual level. According to the Emissions Gap Report 2021 by UN Environment Programme [28], to achieve the Paris Agreement goal of keeping global warming below 1.5 °C, the world should halve the greenhouse gases emission in the next eight years. However, many national plans delay climate action until 2030.

Considering the future scenarios caused by climate change stated in Paragraph 1.2, it is clear that actions must be taken promptly to hinder global warming. Reducing greenhouse gases emissions plays the most crucial role in tackling climate

change. As follows are presented some of the key measures for governments and international organizations to achieve decarbonization, that is, moving away from systems that cause carbon dioxide emissions:

- Economies need to shift from fossil fuels to renewable and low-carbon energy sources. Energy consumption, as already seen in *Figure 1.2*, accounts for the largest part of GHGs emissions. Hence, the necessity for a shift toward greener economies, based on existing technologies such as wind, solar, wave, tidal, and geothermal power.
- Restore and protect forests and oceans, since they contribute in absorbing large amounts of carbon dioxide from the atmosphere.
- Transportation methods should also shift towards sustainability. Solutions include improving and adopting greener and smarter public transport and incentives for electric vehicles.
- Carbon Capture and Storage (CCS). This technology allows to capture carbon dioxide from the atmosphere, transport it and store it safely underground. Carbon Capture and Storage technology has proved to be efficient in the decarbonization of the electricity system as well as in that of the steel and cement industries, which give a conspicuous contribution to greenhouse gases emissions. Despite CCS's technical maturity, it has yet to be applied on a large enough scale to meet the ambitions to mitigate climate change, the main challenge being constituted by its costs [29].
- Energy efficiency of private and public buildings should be improved to decrease power consumption. Buildings' energy efficiency enhancement solutions include improving thermal insulation as well as installing solar panels.
- Supporting and investing in businesses that use and promote sustainable practices. For governments, as an example, this could imply incentives for businesses that make green and sustainable development choices.
- Circularity should be the foundation for countries' economies. By transforming the way we produce and use products, the main benefit of a circular economy is the CO₂ emissions reduction; however, it could also lead to innovation, implementation of new jobs, more durable products as well as raw materials

conservation. The basic assumptions for circularity are reducing consumption of goods and energy, reusing sources and products, remanufacturing, and recycling. If the aim to reach net-zero emissions seems like an ambitious challenge, a study has shown that by implementing a circular economy in the production of four key materials (cement, plastic, steel, and aluminum), it would be possible to achieve the net-zero emissions goal by 2050 [30]. As a matter of fact, the study claims that, by replacing fossil-fuels-derived energy with renewable and greener energy, the total emissions would be reduced by 55%. The remaining 45% of total emissions arise from products manufacturing, that is, land management, buildings construction, vehicles, food and clothes, and other daily-use goods. To reduce such emissions, it is necessary to re-think the way products are made: possible solutions include substituting materials with ones that are more durable and/or recyclable, designing for circularity, improving waste management, or, if feasible, eliminating waste.

Given the strong necessity to shift to a green and circular economy based on sustainable development to mitigate climate change, the next section will focus on the role of aluminum manufacturing and utilization in this context.

1.4 The role of Aluminum in circularity and sustainability

Aluminum is the second-most used metal in our economy, mainly for transportation, packaging, and buildings. As sustainability should become customers and industries' top priority, aluminum constitutes a reasonable choice in tackling climate change for the following reasons:

- Recyclability: nowadays, 75% of the aluminum ever produced in history is still in use, thanks to the possibility of remelting and recycling aluminum scrap infinitely with minimal metal losses [4]. This represents an advantage with respect to other materials such as plastics since their recyclability is limited due to the breaking of the structure of the polymeric chains.

- Low specific weight: aluminum has a density of 2700 kg/m^3 , approximately one-third compared to that of steel [31]. This means it is possible to obtain lighter structures with high specific strength both in building constructions and in the automotive sector, as well as in the construction of aircrafts. Since the weight of vehicles directly impacts the fuel consumption, manufacturing light-weight cars is necessary to reduce emissions as well as to increase the vehicles’

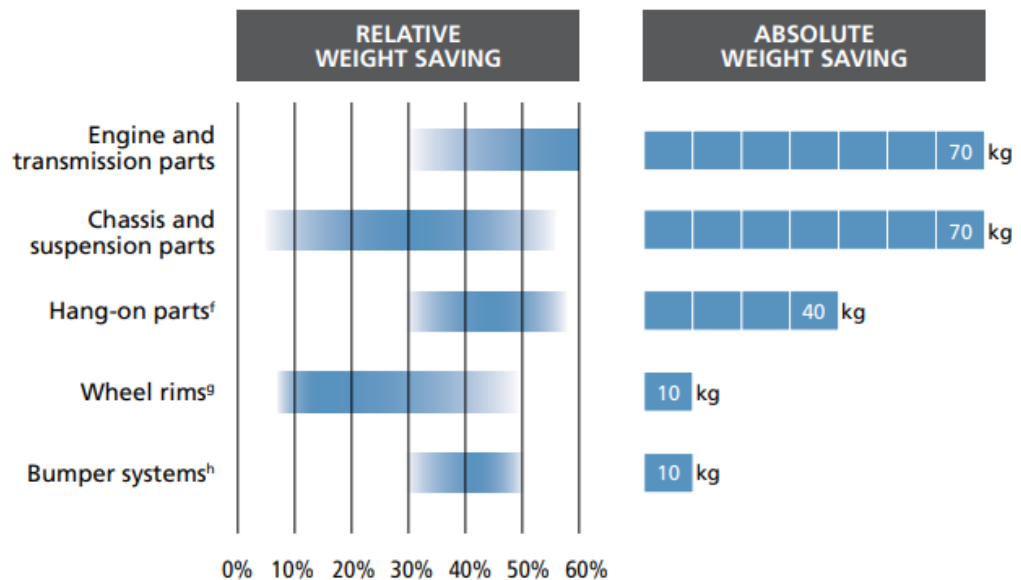


Figure 1.4 – Weight saving in car components when substituting other competing materials with aluminum [31].

fuel efficiency. According to a report from the European Aluminum Association [31], substituting other competing materials with aluminum in car components such as bumpers, wheel rims, engine and transmission parts allows a weight saving of up to 50 %, as can be seen in *Figure 1.4*.

The report also states that the manufacturing of an aluminum-intensive vehicle could lead to the reduction of its total weight by one-third compared to an average car. Furthermore, for an average-sized car traveling 15000 km per year and containing 140 kg of aluminum, the average fuel saving would be of 65 liters per year.

- Corrosion resistance: in the pH range of 4.5-8.5, a protective oxide layer forms on the surface of aluminum, protecting it from corrosion. Passivation confers good corrosion resistance and durability to aluminum when used in a suitable environment. These properties are exploited, for example, in structural components in buildings and vehicles, as well as solar panels and wind

turbines, making them lighter and more durable compared to other materials [32].

- Good formability: the high ductility and relatively low melting point of aluminum can be translated into a variety of manufacturing technologies [32], including extrusion and casting. This could also allow choosing the most sustainable process to obtain the same component.
- Good conductivity: aluminum exhibits good electrical and heat conductivity, making it suitable for energy-efficient systems for heat transfer and electrical transmission [32].
- Possibility of alloying: aluminum alloys can be tailored according to the type of application and the necessities of its utilization by adding alloying elements which will influence the alloy's properties such as strength, stiffness, temperature resistance, and bendability [32].
- Impermeability: aluminum is also employed in packaging for food, beverages, and pharmaceutical products since it is chemically inert and acts as a barrier from contamination [32].
- Abundancy: aluminum is one of the most abundant metals in the earth's crust [5].

Despite these advantages arising from the use of aluminum, its main drawback is the substantial amount of energy required to carry out the primary production (that is, the process to obtain aluminum from mineral ores) of the metal. In the next section, the process to obtain primary aluminum is described, to give an insight into the energy expenses it requires as well as to allow a comparison with the recycling process.

1.4.1 Primary Aluminum Production

Primary aluminum originates from two processes: the Bayer process through which alumina is obtained from bauxite ores, followed by the Hall-Heroult process in which alumina is converted into pure aluminum metal. The first step of the Bayer Process involves the washing, crushing, and screening of the bauxite ores. The ores are then mixed in a caustic soda (NaOH) solution to produce a *slurry* of sodium aluminate ($\text{Al}(\text{OH})_4\text{Na}$). The following step, also known as digestion, involves the solubilization of the slurry with a solution of sodium hydroxide at 110-270 °C under pressure. Digestion allows to ensure that all aluminum-containing compounds are dissolved in a sodium aluminate solution. In the following step, also known as clarification, the insoluble oxides are separated from the sodium aluminate solution by settling at the bottom of the vessel. While the aluminum-containing compounds remain dissolved in the caustic soda, the settled residue (also known as “red mud”) is removed from the solution. The remaining liquid is pumped through a series of filters to trap particles of impurities. The following step involves the precipitation of alumina hydrate in precipitation tanks, where solid seed crystals of alumina hydrate are added to promote the nucleation and precipitation of crystalline aluminum trihydroxide ($\text{Al}_2\text{O}_3 \cdot 3\text{H}_2\text{O}$). The solid precipitate of aluminum trihydroxide is then filtered and concentrated by evaporation and, in the last step of the Bayer process, calcinated at 950-1000 °C to remove the water content and obtain alumina [5]. A schematic representation of the Bayer Process, adapted from [5], is reported in *Figure 1.5*.

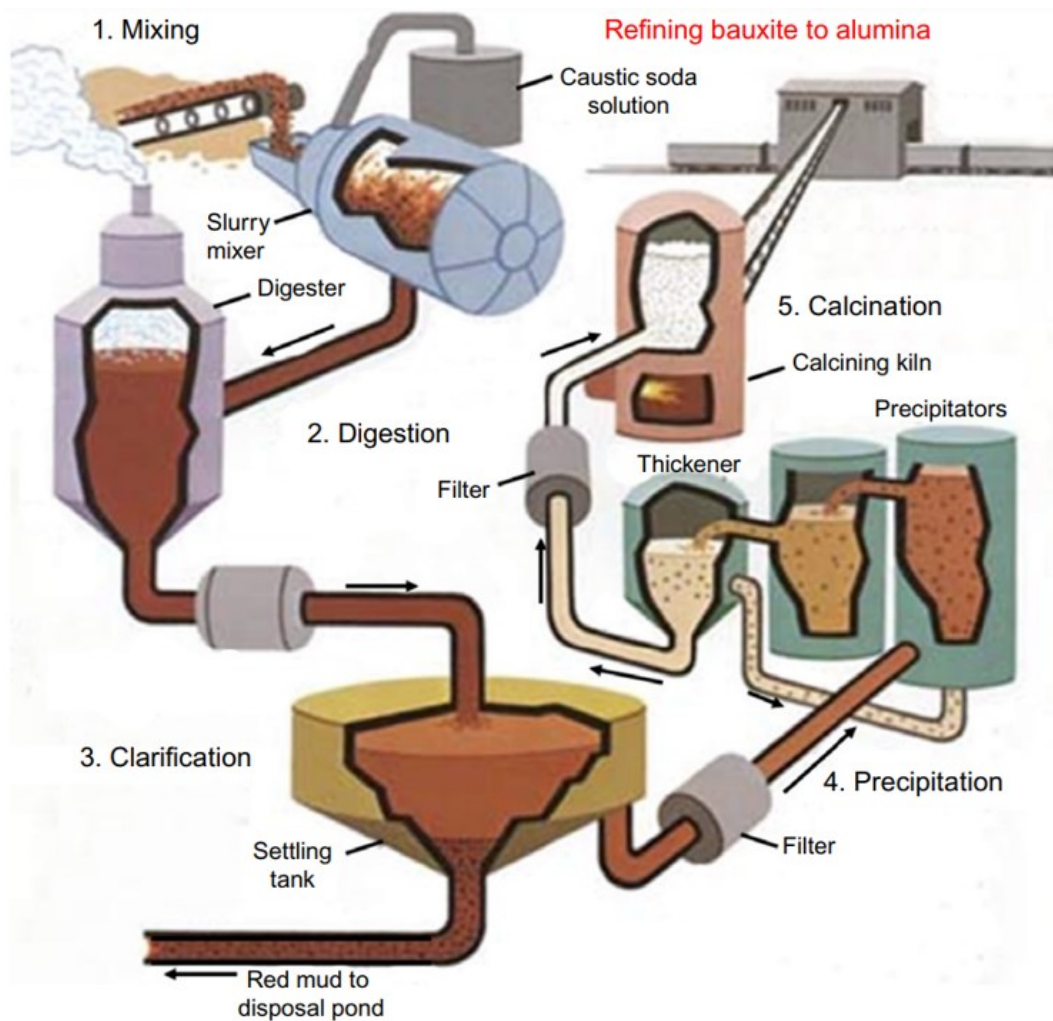
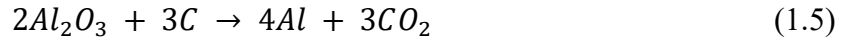
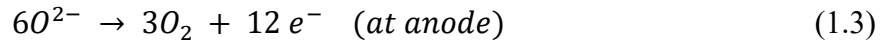


Figure 1.5 – Schematic representation of the alumina production from bauxite ores in the Bayer Process, adapted from [5].

The Bayer process is followed by the Hall-Heroult electrolytic process, through which alumina is smelted by electrolytic dissolution in a cryolite bath to produce pure aluminum metal. The process involves the dissolution of Al_2O_3 in an electrolytic cell in which the graphite cell lining constitutes the cathode, whereas graphite anodes are suspended on the molten bath. The molten bath is composed of cryolite (Na_3AlF_6) at a temperature of approximately 960°C and when the current passes in the cell, alumina is reduced. The oxygen is collected at the carbon anode, where a reaction takes place to form carbon dioxide. The pure aluminum metal separates from the electrolyte by gravity and settles at the bottom of the cell, where it is collected. The net electrolytic reduction reactions involved in the process are [6]:



Due to its strong tendency to recombine with oxygen, a great amount of energy is required to produce metallic aluminum. The Hall-Heroult process is followed by a refining process of the aluminum, which removes impurities such as sodium, calcium oxide, and hydrogen. The processes to obtain primary aluminum constitute the negative side of the utilization of the metal: aluminum is an effective choice in terms of sustainability and circularity due to the reasons stated before, for example lightweight transports and recyclability. On the other hand, aluminum production is also one of the most energy-intensive industrial processes and it accounts for approximately 3% of all GHGs emissions [4]. In 2019, the power consumption to produce one ton of aluminum was more than 14000 kWh [33]. To have a more comprehensive overview of aluminum production's carbon footprint, however, more factors that contribute to it must be considered: as an output of the process there are also air pollutants (particulate matter, sulfur dioxide, nitrogen oxide, carbon monoxide, fluorides, etc. [6]) as well as solid waste, also known as *red mud*. All these factors, including energy consumption, contribute to greenhouse gas emissions and are

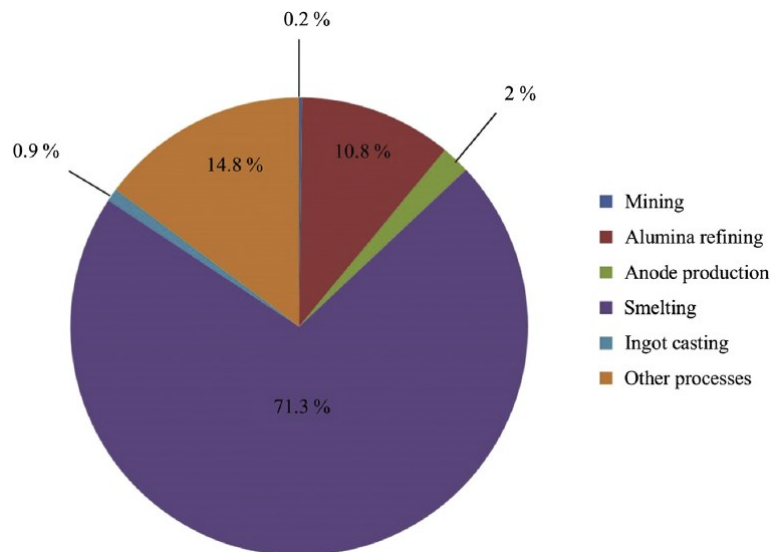


Figure 1.6. Greenhouse gas emissions from aluminum production [6]

represented in *Figure 1.6*. Other processes include ingot casting, transport of materials, semi fabrication, and recycling processes.

Aluminum demand continues to increase: the International Aluminium Institute predicts demand for aluminum products will increase by 81 % by 2050 [7]. If the aim is to meet the increasing demand as well as to reduce the greenhouse gases emissions from its production, the aluminum sector will need huge efforts in improving its technologies and processes.

1.4.2 Secondary Aluminum Production

The term *secondary* indicates aluminum produced by recycling aluminum scrap from industrial waste and discarded consumer items, which is remelted in furnaces, cast, and subsequently manufactured in aluminum fabricating facilities. The process starts with the collection of scrap, which includes *new scrap*, originating from metal-processing industries, and *old scrap*, i.e. post-consumer scrap. The scrap is then transported to the recycling plant, sorted, and cleaned to prepare it for remelting. The preparation includes sorting through a magnet to ensure the absence of steel as well as de-coating by hot air blowing. The next step involves melting at approximately 700 °C of the scrap in furnaces [9]. The molten bath is often covered by chemical compounds also known as salt fluxes, which form a protective layer on top of the liquid metal to prevent it from oxidating. The salt fluxes also function as refining agents, by removing impurities from the molten bath. The last step involves casting the molten metal in ingots, which are then transported to industries for manufacturing. Secondary aluminum production will be discussed more in detail in Chapter 2; in this section the focus is on the comparison with primary aluminum production in terms of emissions and energy requirements: the recycling process can reduce GHGs emissions and energy consumption by up to 95 % [6].

The pie charts in *Figure 1.7* show the energy requirements to produce a mass of one ton of primary and secondary aluminum ingot. Secondary aluminum only requires approximately 6% of the energy consumed by primary aluminum production [8]. Not only this allows to reduce the costs of the metal, but also the focus on recycling on aluminum is essential to reduce greenhouse gases emissions with the goal to mitigate global warming, especially if aluminum demand is expected to keep rising in the next decades. Another benefit of secondary aluminum compared to primary aluminum is the reduction of waste: in primary production, one ton of aluminum generates 3700 kilograms of waste, mainly *red mud*. Recycling of aluminum, on the contrary, produces 400 kilograms of waste per ton of aluminum produced [9].

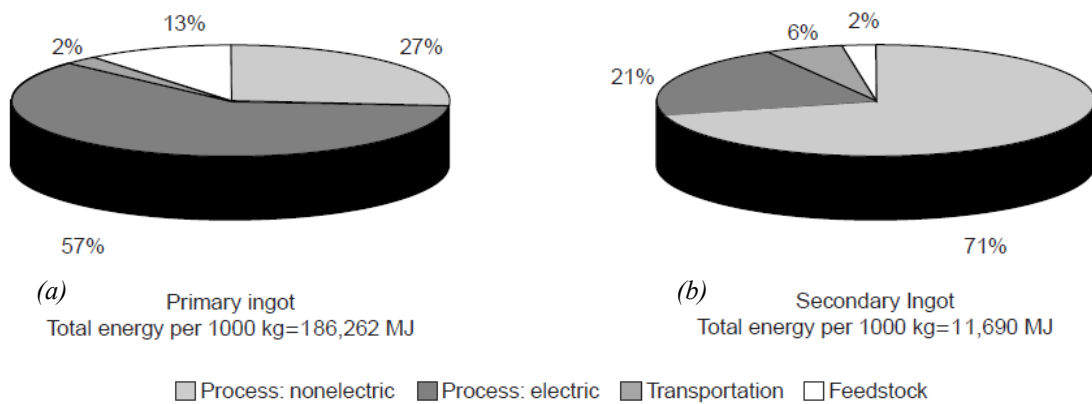


Figure 1.7. Energy consumption for (a) primary and (b) secondary ingots production [8]

Despite the advantages recycling generates, the process is not without challenges. One of them involves control of impurities and the quality of secondary alloys: especially in old scrap, alloys compositions and the presence of impurities can vary to a great extent. Improvements in sorting the scrap, controlling the impurities, and refining secondary alloys are important requirements to obtain high-quality secondary aluminum products. Another challenge in recycling of aluminum is the treatment and disposal of solid residues arising from the process: these are known as *salt cakes* and are mainly composed of salt mixtures and aluminum compounds. The next chapter will focus on the state of the art in the recycling of aluminum by salt flux utilization and common industrial practices.

2 Aluminum recycling and refining by means of salt fluxes

This chapter intends to provide the reader with a detailed description of the technologies and equipment used in the secondary aluminum production process, as well as to present an overview of the current state of the art regarding the use of salt fluxes for aluminum recycling.

2.1 The recycling stages

In this section the steps involved in aluminum recycling will be discussed, starting from the preparation of the scrap, which is the raw material of the aluminum recycling process. The most common industrial melting technologies will be presented, as well as the casting of secondary aluminum products.

2.1.1 Preparing the scrap charge

The final quality and chemical composition of secondary alloys depend on the origin of the scrap as well as on the preliminary treatment of the scrap charge prior to its melting. These treatments are carried out in order to increase the bulk density of the scrap, to eliminate non-aluminum elements, as well as to reduce the amount of impurities [11].

As follows, the steps involved in preparing the aluminum charge prior to melting the scrap are presented.

2.1.1.1 Scrap Collection

The first step of the recycling process usually involves the collection of scrap. Scrap can be divided into two types, according to its origin. If the scrap derives from manufacturing processes' discards, such as trimming, turnings, croppings, it is usually referred to as "*new scrap*". Examples include gates and risers from casting operations. New scrap usually consists of alloys with known composition, free from coatings and

dirt. On the other hand, if the scrap originates from post-consumer discards, it is usually referred to as “*old scrap*” [10]. Old scrap can be categorized into the main sectors of aluminum utilization: transportation, packaging, building, wire and cable, and other [10]. This kind of scrap is often characterized by the presence of impurities, coatings, and a wide range of usually unknown alloy compositions [8].

2.1.1.2 Scrap Pre-melting Treatments

This phase of the recycling process is crucial when aiming to eliminate or reduce contaminants from the charge as well as to ensure the scrap has the correct size for the melting phase. The scrap treatments prior to the melting phase are described as follows:

1. Comminution: scrap with excessive dimensions is often cut into smaller pieces or shredded during the phase also known as *comminution* [10]. According to Capuzzi and Timelli [11], comminution aims to confer a proper size distribution to the scrap, as well as to increase its bulk density and eliminate parts which may form assemblies to prepare the scrap for further processing. Typical devices utilized for comminution are shears, shredders, and crushers, according to the origin and the size of the scrap [10].
2. Sorting: this phase allows eliminating any contaminants or other materials such as plastic, other metals, rubber, or glass, which are inevitably present in the scrap charge. Air classifiers, magnetic separators, Eddy currents, separation by density and hand screening are often used as consolidated methods for the purpose of sorting [11]. Air classifiers are useful to separate scrap from lighter fractions such as plastics and paper by means of an upwards air flow which lifts the light materials away from the metal fraction. Magnetic separation is employed to capture and collect iron or Nickel-based alloys by means of a magnetic device, while the non-magnetic fraction of the scrap will stay on a separate conveyor. A schematic representation of common methods for magnetic separation, drum and overhead-belt separators, is shown in *Figure 2.1* [10].

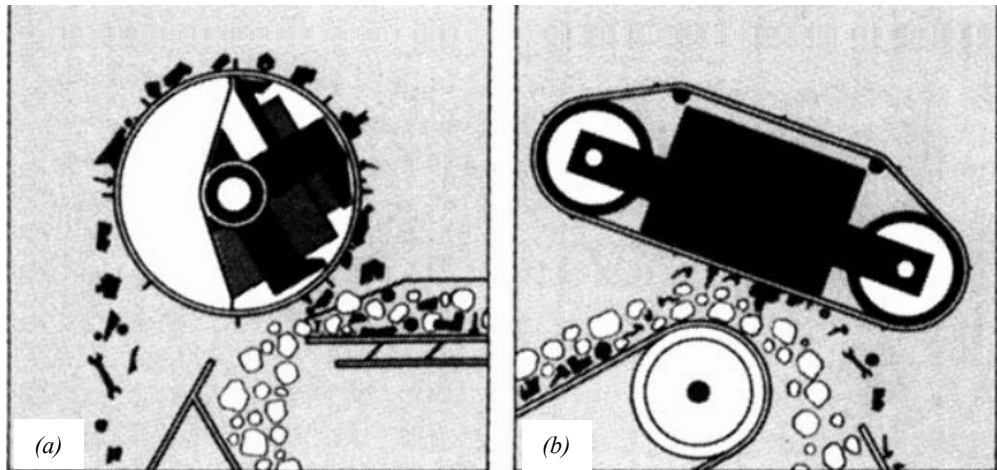


Figure 2.1 – Schematic representation of (a) drum and (b) overhead-belt devices for magnetic separation of aluminum scrap [10].

The eddy current separation method exploits a time-variable magnetic field to generate electromotive forces perpendicular to the magnetic field itself, according to Faraday’s law. If the magnetic field encounters a conductive object of a certain material, the induced electromotive forces generate a magnetic field in the object itself, depending on the material’s conductivity.

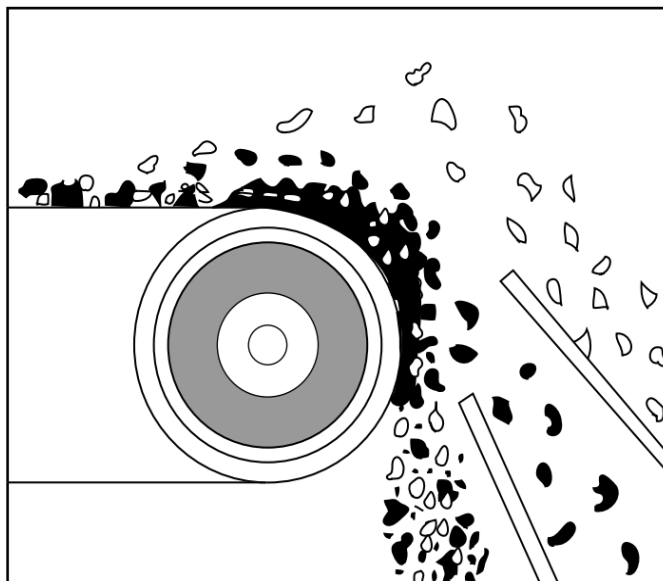


Figure 2.2 – Conveyor-type eddy current separator for aluminum scrap [10].

The eddy current phenomenon is exploited in aluminum scrap sorting with different technologies; one of the main applications is the conveyor-type eddy current separator shown in Figure 2.2.

Separation by density methods exploit media (which can be wet, such as slurries, or dry, such as sand with air flowing to control its density) with

When the material encounters a magnetic field with reversed polarity, a repulsive Lorentz Force deflects the object from its path. The extent of the deflection of the object from its path mainly depends on the material’s conductivity and density [10]. The

known density to separate aluminum scrap from contaminants [11]. The main concept of this application is that materials with a higher density compared to that of aluminum will sink, whereas the lighter materials will float, allowing the collection of aluminum scrap. Separation by color allows separating coated from bare scrap, while spectroscopy and sensors technologies such as x-ray fluorescence (XRF) and laser-induced breakdown spectroscopy have also become widely used in the recent years as they are capable to separate alloys according to the major alloying elements [11, 34]. The separation of aluminum scrap based on the alloy composition is of great concern especially for wrought alloys, as they have low tolerances for the presence of impurities such as iron, copper, zinc, and silicon [10]. Since casting alloys generally contain greater amounts of alloying elements compared to wrought alloys, a technique has been developed to separate the two types of alloys: due to the presence of alloying elements, casting alloys have a lower melting point than wrought alloys. By means of the *hot-crushing* technique, the mixed alloys are crushed at temperatures close to the solidus temperature. This will lead to the partial melting and deformation of the casting alloy pieces, whereas the wrought alloy fragments will remain undeformed. The mixed alloys are then separated by screening [11]. The techniques described above all aim to tackle the problem of the presence of impurities in secondary alloys at the solid state by sorting and separating aluminum scrap; impurities removal from the secondary aluminum at the molten state will be described in detail in Section 2.3.5.

3. De-coating: The sorting procedure is usually followed by the de-coating of the scrap, which aims to eliminate paints, paper, and other contaminants from the surface of the scrap as well as to minimize the oxidation of the scrap surface [10]. De-coating often involves thermal or chemical processes to eliminate organic and inorganic compounds. Chemical processes are usually more complex compared to thermal processes; however, the thermal method is not able to eliminate inorganic compounds such as TiO_2 , which is often present as coating and inevitably will be present in the secondary product as an impurity [11]. Two main techniques have been developed to thermally de-coat the aluminum scrap: the first one involves exposure of the scrap for long times at temperatures in the range of 480-520 °C. In this way, metal oxidation is

minimized; however, the main drawback is that the lower temperatures may result in incomplete de-coating. The second technique involves a short exposure of the scrap at higher temperatures, typically in the range of 590-620 °C. The risk of this method is the high oxidation rates of the scrap if the exposure at the high temperature prolonged [10].

4. Agglomeration: Some routes of scrap preparation also involve agglomeration of aluminum pieces of very small size into bales or briquettes. This allows to ease the handling and transportation of the scrap as well as it reduces its possibility of absorbing moisture [10]. Furthermore, very small pieces such as turnings have a large surface area/volume ratio, which leads to higher oxidation rates during melting [8, 9]. This topic will be discussed in more detail in *Section 2.3.3* in terms of the metal yield in the recycling process.

2.1.1.3 Pre-heating and Charging

Pre-heating the charge is often a desirable option to limit the amount of humidity and organic compounds, which can cause safety concerns such as explosions. Moreover, preheating the charge also allows to mitigate heat losses in the melting furnace as well as it allows to reduce the time required for the melting process. The efficiency of the melting process may be further increased by pre-heating the charge with the exhaust gases coming from the melting process itself [35]. After preheating, the scrap is charged into the furnace. The scrap should be charged in the furnace as quickly as possible to avoid oxidation, which leads to metal losses and consequently to a lower metal yield of the recycling process [11].

2.1.2 Melting technologies

After charging, the scrap is melted in a *melting furnace*. The molten aluminum is then transferred to a *holding furnace* for metal treatment: here, the alloy will be adjusted to the final composition by eliminating the impurities and adding pure alloying elements such as Silicon, Copper, and Manganese. Different furnaces are available to melt the scrap, according to several parameters: these include capacity,

energy cost, scrap contamination and size, and final product chemical composition. The most common furnaces are reverberatory furnaces and their derivations, which are used by remelters, and rotary furnaces, which are generally used by refiners and when the scrap has a large surface area and is heavily contaminated [9]. Reverberatory and rotary furnaces are both fired with fossil-fuels, commonly natural gas, as opposed to electric furnaces, where no gases are fired [11]. When selecting a furnace for melting aluminum scrap, two main parameters must be considered: the metal yield of the process and the production volume. Rotary and reverberatory furnaces are characterized by a higher production volume compared to electric and crucible furnaces; on the other hand, the highest metal yield can be obtained by reverberatory and electric furnaces. Electric furnaces are of common use in facilities for melting internally produced scrap and where the production volume is low. On the other hand, reverberatory furnaces allow to treat greater amounts of scrap, however they are characterized by low energy efficiency and a high metal oxidation rate. Rotary furnaces are more energy-efficient than reverberatory furnaces and are used for the treatment of highly contaminated scrap as well as dross from primary and secondary aluminum production [10,11]. Rotary furnaces usually require the addition of chemical compounds, specifically salt fluxes. Rotary furnaces and salt fluxes will be discussed in detail in *Section 2.2* and *2.3*, as the utilization of salt fluxes is the focus of this study.

2.1.3 Melt refining

Refining of the molten metal is carried out to achieve a satisfactory metal quality of the secondary product by removing or limiting the quantity of impurities. The impurities of greatest concern commonly consist of hydrogen, reactive metals (mainly sodium, calcium, and magnesium), and inclusions [10].

The presence of hydrogen in the molten metal usually arises from humidity (typically originated from a wet scrap charge), from turbulence in the melt, and from the combustion products from the firing of fossil-fuels containing H₂. Since hydrogen is insoluble in aluminum at the solid state, its presence will generate porosities in the cast product. For hydrogen to abandon the molten metal, its partial pressure must be reduced: a well-established method to achieve this is degassing. Typically, argon or

nitrogen gas bubbles are injected in the melt by an impeller. The process decreases the partial pressure of hydrogen in the bubbles, enhancing the absorption and diffusion of H_2 into the bubbles which then rise to leave the melt [10, 36], as can be seen in *Figure 2.3*.

Recent technologies have combined the degassing method with the addition of salt fluxes in a technique also known as “gas fluxing” [37]. Calcium, sodium, and magnesium can be removed by means of chlorine gas injection in the melt,

which reacts with these impurities to form compounds which will go into the slag. However, the utilization of chlorine gas leads to the formation of compounds of environmental concern. For this reason, solid salt fluxes are the most common technology for impurities removal from the molten metal and will be furtherly discussed in Section 2.3.5.

To remove some metals that have not been removed by physical separation of the scrap, selective melting, or “*sweating*”, can be performed: it consists of the exposure of the scrap charge at certain temperature intervals below the melting point of aluminum. This leads to the melting of the metals with melting points lower than that of aluminum, such as tin, lead, and zinc. These can be easily removed before melting the aluminum scrap [37].

Inclusions are solid particles present in the molten aluminum and mostly consist of oxides. They can cause defects in the solidified metal and constitute points of weakness of the cast products. Inclusions may be removed from the melt by sedimentation, depending on the particles size and density; however, a more efficient way for inclusions removal is through flotation: the inclusions are captured by gas bubbles, such as those injected for degassing, and are transported to the slag. The most efficient way for inclusions removal is filtration, where typically ceramic foam filters are used to capture the inclusions and prevent them from re-entering the molten metal [10, 37].

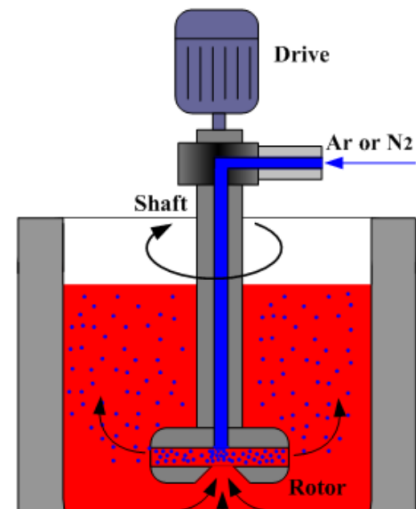


Figure 2.3 – Schematic representation of a rotary degasser for molten aluminum. Adapted from [36].

2.1.4 Casting

The last phase of the recycling process involves casting, when the alloy temperature and composition requirements are met. Cleaner scrap is usually remelted for continuous casting to produce wrought alloys, whereas contaminated scrap is cast into ingots by refiners [4].

An illustrative flow chart of the common steps involved in a typical route of aluminum recycling and refining is shown in *Figure 2.4*.

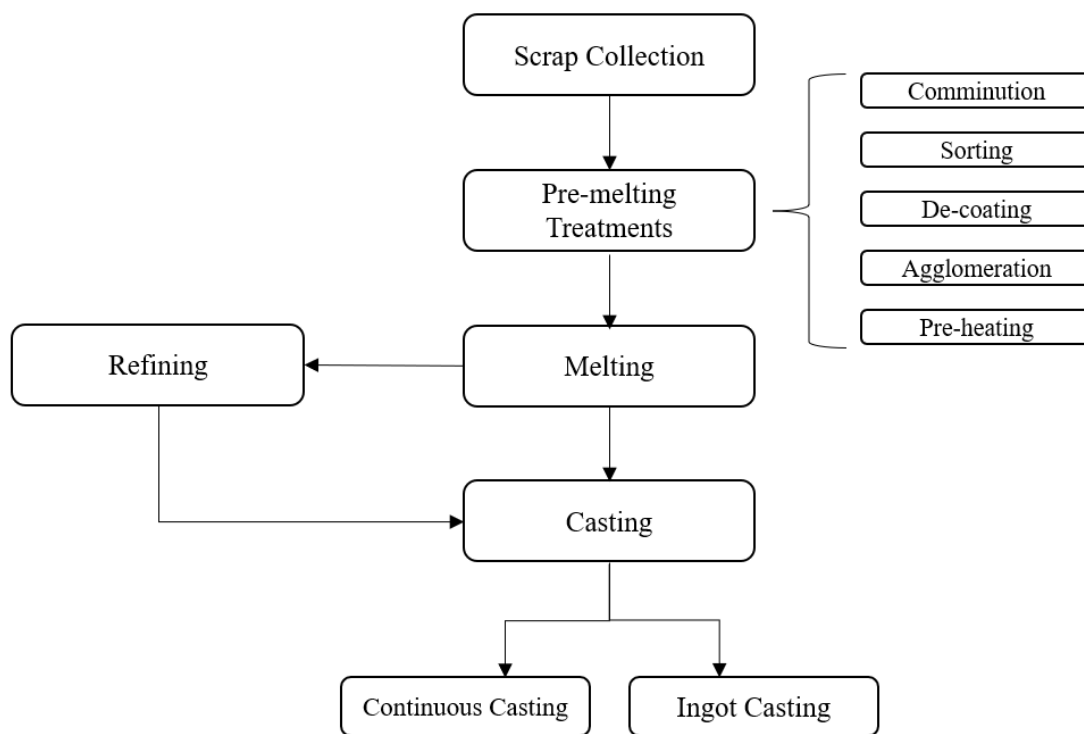


Figure 2.4 – Schematic flow chart of the common steps involved in the aluminum recycling process.

2.2 The use of salt fluxes in rotary furnaces for Al refining

While pre-melting treatments of the aluminum scrap such as sorting and de-coating contribute to decrease the amount of impurities of the charge at the solid state, aluminum refining is carried out to remove dissolved impurities present in the metal at the molten state. The most used method for refining the molten metal is fluxing, which consists of the addition of chemical compounds or gases to the molten metal

[34]. Solid inorganic salts, also known as salt fluxes, are frequently used. They usually perform three main functions: they protect the molten bath from oxidation, collect impurities from the metal, and promote metal droplets coalescence [12]. The next sections will provide a detailed insight both on rotary furnaces and on salt fluxes.

2.2.1 Rotary Furnaces

While in America and in the rest of the world reverberatory furnaces are more common, in Europe most of secondary aluminum is produced in rotary furnaces [38]. Although reverberatory furnaces are less expensive and need less maintenance, rotary furnaces are the preferred kind of melting furnaces by refiners as they are faster, more efficient, and suitable for processing contaminated mixed scrap or scrap with a large surface area. As a matter of fact, rotary furnaces allow to reduce emissions and fuel consumption, and improve melting rates as the rotary movement improves heat transfer to the charge. For this reason, they are preferred by refiners in Europe, where the energy costs are high [11].

Rotary furnaces consist of a refractory-lined steel cylinder rotating around its central axis. Their holding capacity usually ranges from 10-60 tons [4], however larger furnaces can reach up to 100 tons of capacity. An oil or gas burner is placed on the door at one end of the cylinder and its flame is directed to the refractory walls to heat them. The melt is therefore heated indirectly through conduction and radiation by the refractories. Fixed-axis rotary furnaces have been the common technology for decades, however the use tilting rotary furnaces has increased, as they allow to obtain higher energy efficiency, lower operating costs, and improved metal recovery [5]. Furthermore, the use of tilting rotary furnaces reduces the flux consumption compared to the fixed-axis rotary furnace [5]. Tilting rotary furnaces, as suggested by the name, can be tilted to facilitate the operations of scrap charging and molten metal and slag discharging [10]. Rotary furnaces are equipped with a system for off-gas collection. A schematic representation [39] of a rotary furnace is shown in *Figure 2.5*.

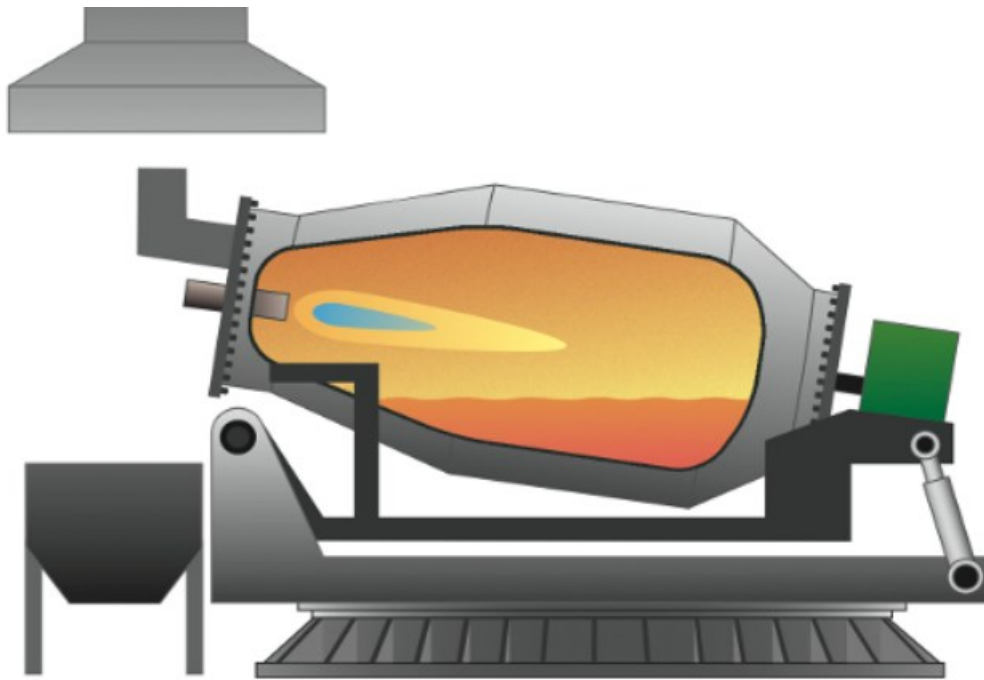


Figure 2.5 – Schematic representation of a tilting rotary furnace [39].

2.2.2 Salt fluxes

The furnace design itself is not sufficient for the refining of scrap, therefore fluxing is carried out. The term fluxing represents all additions of chemical compounds during the metal treatment process to perform several functions. Utigard et al. [20] proposed to subdivide the functions of salt fluxes into five categories: cover, cleaning, drossing, refining and wall-cleaning. These fluxes are employed coordinately in the molten bath to meet the requirements of the secondary aluminum product. Peterson [12] proposed three primary requirements of fluxes for aluminum melting: a flux should cover the metal to protect it from oxidation, it should dissolve and collect impurities and oxides, and it should strip away the oxide layer on the metal surface to promote metal droplets coalescence. Salt fluxes are able to remove dissolved impurities in the molten metal such as Ca, Sr, Na, Mg, and Li by serving as catalysts for their equilibrium oxidation reactions: these impurities, by oxidating, will leave the molten metal by either settling at the bottom of the furnace or by floating to the slag layer on top of the melt [34].

It is also necessary that the salt does not contaminate or react with the metal, and only those chloride salts more stable than aluminum chloride can be used as flux components. This allows to only select those salts composed of alkali and alkaline earth elements [5]. When also considering the costs for the inorganic salts, even fewer options are left. Salt fluxes are usually blends of chlorides, typically sodium chloride (NaCl) and potassium chloride (KCl) with additions of fluorides. Mixtures of $MgCl_2$ -KCl are also used. However, since $MgCl_2$ is expensive and hygroscopic, they are only used when treating alloys with very limited contents of sodium and calcium and when the magnesium content is above 2% [40]. The use of NaCl-KCl mixtures is common since they allow to lower the melting temperature of the flux: they form an eutectic point at 657 °C, as shown in the NaCl - KCl phase diagram in *Figure 2.6* from Beheshti [41].

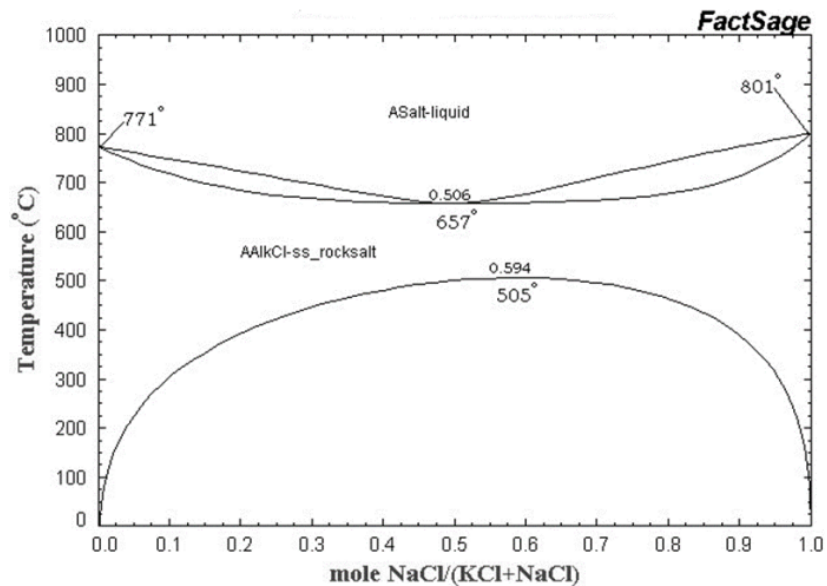


Figure 2.6 – NaCl – KCl binary phase diagram [41].

50% *wt.* NaCl – 50% *wt.* KCl mixtures are common in the United States and Asia, whereas 70% *wt.* NaCl – 30% *wt.* KCl blends are used more frequently in Europe [4]. Some of the most used materials for salt fluxes are displayed in *Figure 2.7*.

Chemical	Molecular Mass (g/mol)	Solid Density (g/cm ³)	Melting Point (°C)	Boiling Point (°C)
LiCl	43.39	2.068	605	1,325
NaCl	58.44	2.165	801	1,413
KCl	74.56	1.984	770	1,500
CaCl ₂	110.99	2.15	782	1,600
MgCl ₂	95.22	2.32	714	1,412
AlCl ₃	133.34	2.44	190	177.8
BaCl ₂	208.25	3.92	963	1,560
LiF	25.94	2.635	845	1,676
NaF	41.99	2.558	993	1,695
KF	58.1	2.48	858	1,505
CaF ₂	78.08	3.18	1,423	2,500
MgF ₂	62.31	3.18	1,261	2,239
AlF ₃	83.98	2.882	—	1,291*
Na ₃ AlF ₆	209.94	2.9	1,010	—
LiNO ₃	68.94	2.38	264	600 [†]
NaNO ₃	84.99	2.261	307	380 [†]
KNO ₃	101.11	2.109	339	400 [†]
Li ₂ SO ₄	109.94	2.221	859	high
Na ₂ SO ₄	142.04	—	897	—
K ₂ SO ₄	174.27	2.66	1,069	1,689
CaSO ₄	136.14	2.61	1,450	high
MgSO ₄	120.37	2.66	—	1,124 [†]
Li ₂ CO ₃	73.89	2.11	723	1,310
Na ₂ CO ₃	105.99	2.532	851	high
K ₂ CO ₃	138.21	2.42	894	high
MgCO ₃	84.32	2.96	—	350 [†]
CaCO ₃	100.09	2.71	1339	850

* Sublimes
† Decomposes

Figure 2.7 – Characteristic materials used for salt fluxes [20].

2.3 Parameters of salt fluxes affecting metal recovery, energy requirements and costs

Nowadays, solid salt fluxing is the most used technology for impurities removal from molten aluminum. There are several parameters influencing the metal yield, that is, the amount of metal produced compared to the mass of scrap. The chemical composition of the secondary aluminum and the metal yield are controlled not only at the solid state by scrap selection, as mentioned before, but also at the molten state by controlling the process parameters. The next sections aim to provide an insight of the crucial parameters which affect the metal yield, the energy requirements and the costs in the aluminum refining process.

2.3.1 Salt Factor

The quantity of salt plays an important role in the efficiency of the melting process, as it impacts on production, energy, and disposal costs,. The amount of salt

needed in the process is related to the quality of the scrap through the *salt factor* (SF), which describes the proportion between the amount of salt and the non-metallic scrap components of the scrap [4], as shown in (2.1).

$$\text{Salt Factor} = \frac{\text{mass of salt}}{\text{mass of non metallic components}} \quad (2.1)$$

Salt factors ranging from 1.5 to 2 are frequent in the aluminum recycling process in fixed rotary furnaces, whereas in tilting rotary furnaces the salt factor can be lowered to 0.5 [4]. Capuzzi et al. [42] conducted a series of experiments to investigate the effect of salt quantity on the metal recovery by melting several types of scrap under a NaCl-KCl-Na₃AlF₆ salt flux, both in a rotary and in a crucible furnace. The results showed that, by increasing the salt factor from 1.55 to 1.65, it is possible to obtain higher metal recovery. A similar trend was also found by Pirker et al. [43], whose results also show, for the same amount of salt, a decrease of metal yield if the scrap bears a high organic content.

2.3.2 Effect of increased NaCl:KCl ratio

Although decreasing the KCl amount leads to an increment of the melting temperature of the flux, aluminum remelters have a strong motivation in lowering the KCl amount due to its higher costs if compared to NaCl. In literature, there is a limited amount of studies concerning the effect of lowering the amount of KCl in the salt flux. Pirker et al. [43] investigated the effect of decreasing KCl amounts on metal recovery by melting scrap turnings in a rotary drum furnace as well as by melting chips in an electrical resistance furnace. The experiments showed a limited or very little effect on the metal recovery as the amount of KCl decreased.

Bolivar and Friedrich [44] also performed a series of tests to determine the effect of increased NaCl/KCl ratios on the metal recovery. The series of experiments involved the use of two different salt factors of 2 and 1.5, respectively. Although the tests were performed at a small scale, with less than 100 grams of aluminum, the results showed a limited reduction of the metal recovery.

Besides the cost considerations, an additional advantage in lowering the KCl amount is the decrease of the vapor pressure in the slag and thus lower evaporation from the slag [43].

2.3.3 Coalescence of metal droplets

Since metal losses are mainly caused by oxidation and metal entrapment in the slag [45], a crucial role in increasing the metal recovery is played by the metal droplets' coalescence. For coalescence to occur, the oxide layer must be stripped away in order for the metal droplets to coagulate and enter the metal bath through the salt slag. Roy and Sahai [13] suggested that the stripping of the oxide layer occurs in a three-steps process, as also shown in *Figure 2.8*:

1. Openings develop in the oxide layer. The weakening of the oxide is due to the expansion of molten aluminum at high temperatures, which causes thermal stresses to arise in the oxide layer.
2. The salt penetrates between the oxide layer and the metal.
3. The oxide layer is stripped away.

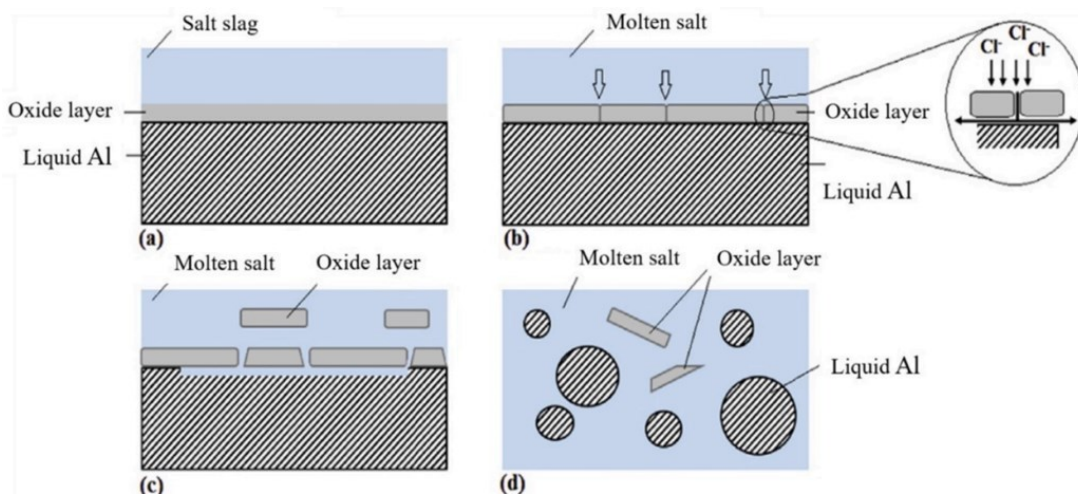


Figure 2.8 - Schematic representation of the stripping of the oxide layer. (a): contact of oxide layer and molten salt; (b) and (c): openings develop in the oxide layer and the salt penetrates between the oxide layer and the metal. (d): the oxide layer is stripped away [4].

The experiments to investigate coalescence involve melting of aluminum scrap under a salt flux in a crucible, where the mixture is then left to solidify. After the salt and the metal have solidified, they are removed from the crucible and the salt is removed by dissolution in water to evaluate the coalescence of the metal. Experiments

are based either on measuring the time needed to reach complete coalescence or on evaluating the coalescence rate after a given time. Nowadays, there is no standard method to evaluate the coalescence efficiency. Other measurements to estimate the coalescence ability of a salt involve the investigation of the wetting ability of a salt on aluminum or alumina, as well as the study of interfacial tensions. However, these methods cannot be considered a direct measurement of coalescence, as stated by Peterson [12].

Presence of fluorides

Several studies [12-14, 20, 46-49] have proved that the additions of fluorides in the NaCl – KCl salt flux leads to a significant increase in coalescence by causing the rupture and stripping of the oxide layer. As a matter of fact, when no fluorides were added to the salt flux, the coalescence of metal droplets was absent or very poor, unless stirring was carried out to break the oxide layer. The mechanism of breaking and stripping of the oxide layer by fluorides is not completely understood. Peterson [12] suggested that a fluoride's ability to destroy the oxide layer is related to its ability to dissolve alumina, Al_2O_3 . Tenorio and Espinosa [16] suggested that the rupture of the oxide layer is enhanced by fluoride additions according to a mechanism similar to the hot corrosion process, which assists the release of the molten metal from the surrounding oxide layer.

These mechanisms related to the alumina dissolution may help to understand the rupturing mechanism of the oxide layer. On the other hand, different authors [13, 46, 47, 50] agree that the stripping of the oxide layer is linked to a decrease of the interfacial tension between the salt and the metal, which enhances the affinity between the salt and the metal and facilitates the stripping of the oxide. At the same time, an increased interfacial tension between oxide and metal facilitates the coagulation of metal droplets and thus the coalescence. Roy and Sahai [17] suggested that the decrease in interfacial tension between salt flux and molten metal is related to the adsorption of surface-active elements at the salt-metal interface. An electrochemical process was suggested by Jordan and Milner [51] and by Storchai and Baranov [52] to explain the stripping of the aluminum oxide layer. According to the authors, the aluminum acts as the anode and the oxide as the cathode, while the salt flux functions as the electrolyte.

Types and concentrations of fluorides and slag temperature

It is widely acknowledged in literature that a pure NaCl – KCl mixture is not sufficient to enhance the coalescence [12, 13, 20, 46], . However, the effect on coalescence of fluoride's type and concentration is not very well understood, as the experimental results and methodologies vary to a great extent in the literature. In terms of effectiveness of the different kinds of fluorides and their concentration in the salt flux, there is no consensus in literature. Utigard et al. [20] investigated the effect on coalescence of 5% additions of fluorides (MgF_2 , CaF_2 , AlF_3 , LiF , Na_3AlF_6 , NaF , KF) on an equimolar NaCl – KCl salt flux. The results showed that the fluorides that allowed to reach an excellent grade of coalescence in a very short time (less than one second) were Na_3AlF_6 , NaF , and KF . These findings are similar to the ones obtained by Roy and Sahai [13], who investigated fluorides' effect on efficiency of coalescence as a function of time. According to the coalescence ability, the fluoride-containing salts were classified into 4 different categories: excellent, good, moderate, or poor. Additions of 5% weight of NaF , KF , LiF , or Na_3AlF_6 to the equimolar NaCl – KCl salt flux were found to have excellent coalescence ability. Peterson [12] also investigated

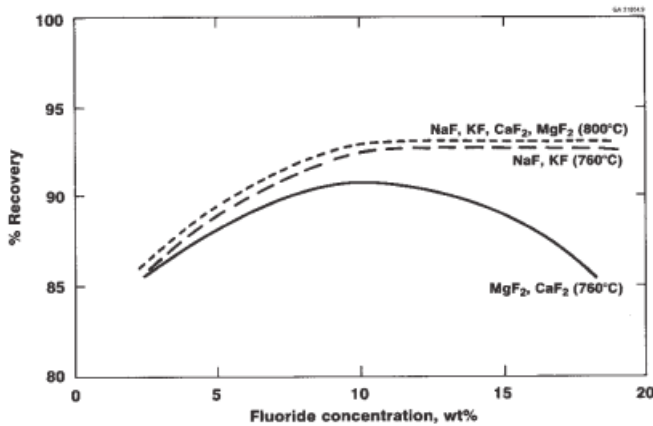


Figure 2.9 – Effect of fluoride concentration and temperature on metal recovery [47].

the coalescence times and efficiency of 5% fluoride (AlF_3 , BaF_2 , KF , LiF , CaF_2 , NaF , MgF_2 , Na_2SiF_6 , $NaAlF_4$, Na_3AlF_6 , $KAlF_4$) additions to an equimolar NaCl – KCl salt flux. The study revealed that the aluminum-fluoride containing salts (AlF_3 , $NaAlF_4$, Na_3AlF_6), except for $KAlF_4$, were the best coalescing agents, given the rapid time and degree of coalescence. Van Linden and Stewart [47] investigated the effect of CaF_2 , NaF , KF and MgF_2 additions to the equimolar NaCl – KCl flux at 760 °C and 800 °C. The percentages of fluorides varied from 3 % to 18 % weight. The results showed different values of metal recovery not only depending on fluoride type and concentration, but also on the temperature. At 800 °C, the behavior of the different fluorides was similar: the metal recovery increased with fluorides additions up to 10% and then stabilized for greater concentrations of additions. At 760

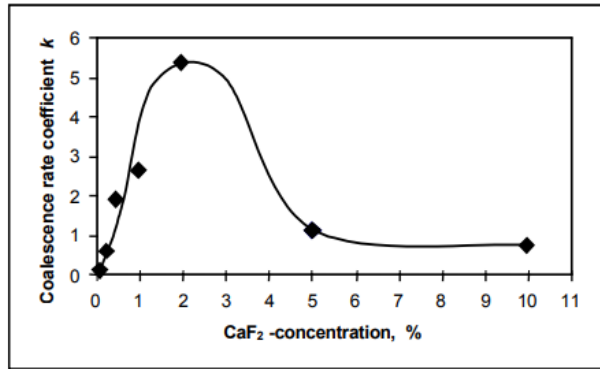


Figure 2.10 – Coalescence rate at 830°C [49].

°C, NaF and KF were found to be more effective in terms of metal recovery than MgF₂ and CaF₂. The results are shown in *Figure 2.9*. Sydykov et al. [49] also found that an increase in temperature of the slag from 750 to 850 °C led to an increased metal yield. They conducted their experiments in a rotary kiln using a 70 % NaCl – 30% KCl salt flux recovered from slag, with fluoride additions. The aim of the study was not only to determine the effect of slag temperature on metal yield, but also to compare the coalescence efficiency of CaF₂ and cryolite. Their results showed that, at 830 °C, a maximum of coalescence rate for a CaF₂ concentration of approximately 2%, as can be seen in *Figure 2.10*. They found that the type of fluoride was not significant on the metal yield. This is in contrast with the findings of Capuzzi et al. [53], who investigated the effect of remelting aluminum scrap under different salt flux systems. The salt to scrap ratio ranged from 0 to 4 and three types of salt were used: an industrial salt and a recycled salt both with CaF₂ additions, and an experimental salt with cryolite additions. They found that complete coalescence was only achieved with the salt containing cryolite. As a matter of fact, additions of CaF₂ from 2 to 6% did not determine a positive effect on the metal coalescence.

Since many of the experiments in literature were conducted at a small scale and with very high salt/scrap ratio, they cannot be considered fully representative of the industrial practice. However, to some extent, they can help understand how to improve the coalescence and the metal recovery in the remelting and refining of aluminum scrap.

Oxide content in slag, slag's viscosity and density

Another consideration worth mentioning is that most of the tests were carried out with high salt/scrap ratio and when the salt flux was free from oxides and impurities, which only corresponds to the beginning of the process in the industry. As the slag collects more contaminants and oxides, its viscosity increases, hindering the

salt/metal separation and consequently the coalescence of metal droplets. This can be further explained by analyzing the settling velocity of a metal droplet in the slag, which can be described as follows, according to Stoke's Law:

$$V = \frac{2r^2(\rho_M - \rho_S)g}{9\eta_S} \quad (2.2)$$

where V is the velocity of the droplet, r its radius, ρ_M the density of the molten metal, g the gravitational acceleration, and ρ_S and η_S the density and viscosity of the slag, respectively. As can be understood from Eq. (2.2), as the viscosity of the slag increases, the velocity of the metal droplet decreases, delaying or stopping the drop from entering the molten metal pool. Strong evidence exists in literature of the deleterious effect of oxides in the slag on the coalescence. Sully et al. [54] studied the effect of oxides on flux viscosity and found that an oxide concentration of just 10% was enough to impede coalescence. This is in accordance with Thoraval and Friedrich's study [55]: the experiments were conducted in a lab-scale tilting rotary furnace (TRF) to investigate the effect of oxide and cryolite content in the slag on the coalescence. The results showed that oxides suppress the positive effects of cryolite additions, thus hindering the coalescence. A similar trend was also found by Sydykov et al. [49]. By analyzing the effect of the presence of Al_2O_3 in the slag, the results showed that the alumina content in the flux increased the metal content in the slag and therefore led to metal losses. Xiao, Reuter and Boin [15] also investigated the effect of non-metallic particles (NMPs) on the slag viscosity. They found that the viscosity increases with the addition of NMPs, and after a critical value of NMPs volume percentage of 10%, the viscosity increased drastically.

The viscosity of the slag is also influenced by the type and concentration of added fluorides. However, in literature there are few studies which investigated this topic, and they are not in accordance. Roy, Ye, and Sahai [18] investigated the effect on kinematic viscosity of KF, LiF, NaF, LiCl, CaF_2 and cryolite to an equimolar NaCl-KCl salt flux at 850 °C by means of a capillary viscometer. In most cases except for KF, the kinematic viscosity decreased before increasing with the additions of fluorides up to 15% weight. The results are reported in *Figure 2.11*.

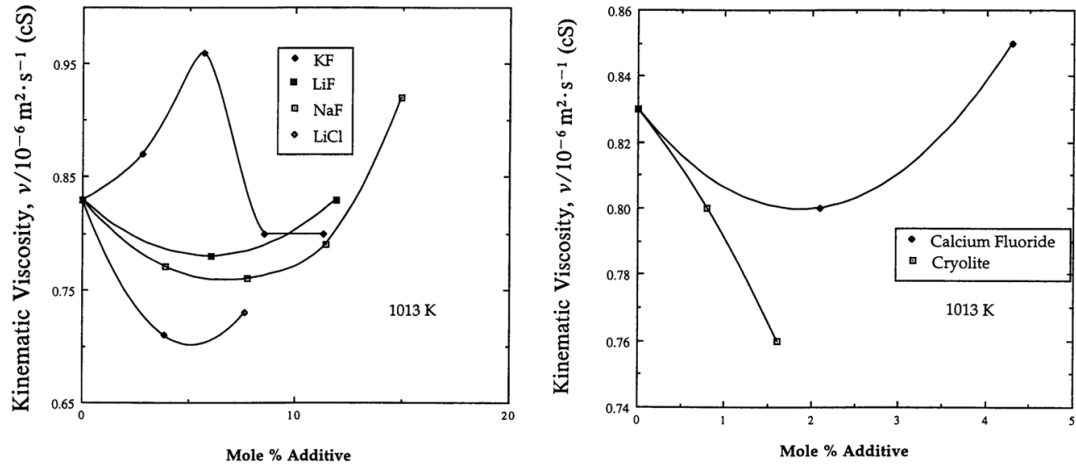


Figure 2.11 Variation of kinematic viscosity of equimolar NaCl-KCl with mole % additives [18].

Tenorio et al. [19] investigated the effect of additions of NaF and KF to an equimolar NaCl – KCl mixture up to 20% weight, by means of the *body falling method* at 760 °C and 810 °C. The experiments showed an approximately linear decrease of the viscosity as the content of fluoride increased. Another parameter to be considered

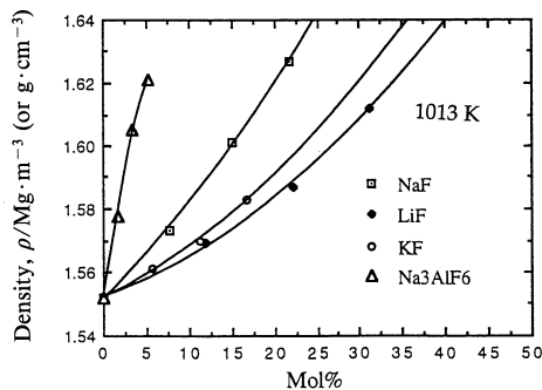


Figure 2.12 – Densities of molten NaCl – KCl with fluorides additions [18].

is the slag density: as the slag collects impurities and oxides, it becomes denser. This could lead to worsening of metal/slag separation, as well as to hindering of coalescence. Roy, Ye and Sahai [18] studied the density of molten NaCl – KCl and of NaCl – KCl with additions of NaF, LiF, KF and cryolite by means of the Archimedean method.

For the NaCl – KCl mixture with no additions, an increase of NaCl from 20 to 80 % mol increased the density approximately from 1.545 g/cm³ to 1.575 g/cm³. Concerning the equimolar NaCl – KCl system with fluoride additions, the results showed an increase of density for all fluorides. The most evident increase in density was found to be caused by cryolite: the increment in density was from 1.55 g/cm³ for 0 % cryolite to 1.62 g/cm³ for just a 5 % cryolite addition, as shown in *Figure 2.12*. The authors also concluded that, because of higher density of the slag, too much fluoride additions can also cause problems in submerging scrap pieces, especially very thin ones such as used beverage containers (UBC).

Presence of coatings and compaction of scrap

As mentioned in Section 2.1.1, scrap pre-treatment is a common industrial practice in the secondary aluminum production, as it allows to obtain higher metal yields. Pre-treatment of scrap includes de-coating and compacting. De-coating is carried out to eliminate the organic content in the scrap, which otherwise leads to a lower amount of metal recovered as well as to a lower quality of recycled aluminum. Compaction of scrap plays a crucial role in reducing its surface area, thus lowering its tendency to oxidation which is a cause for metal losses. This is crucial when treating scrap of small dimensions such as chips, sawings, and turnings, as their surface area to volume ratio is very high.

Vallejo-Olivares et al. [56] studied the effect of compacting aluminum foils into briquettes on metal yield and oxidation. The scrap pieces were melted under a 70 % weight NaCl – 30% weight KCl salt flux with 2% weight addition of CaF₂. The results showed a metal yield above 98 % as well as a lower oxidation rate for the compacted foils. Palimaka [57] investigated the effect of compacting and thermal cleaning of fine aluminum chips (sawings), which are currently not being recycled as scrap by traditional methods using salt flux. The chips were pressed to form compacts and then heated in a furnace under Argon and/or air atmosphere. The compacts were then remelted at 750 °C under an equimolar NaCl – KCl salt flux with cryolite additions. Despite the high salt to scrap ratio of 10, the laboratory results showed a high metal yield (up to 94%) and coalescence (up to 100%) when a two-stage process of thermal cleaning was carried out: the first step involved decomposition of hydrocarbon without oxygen, and it was followed by oxidation at lower temperatures.

Capuzzi et al. [53] studied the coalescence of aluminum alloys according to the presence of coatings and using different salt systems and salt-scrap ratios. Three different subsets of scrap in the form of disks were chosen: clean, coated and thermally decoated at different temperatures. The findings revealed that the presence of coatings can negatively affect the coalescence, which can however be improved by a suitable thermal decoating at 600 °C prior to remelting. Eggen et al. [58] investigated the effect of thermal pre-treatment at different temperatures of household waste, such as cans and foils. The authors found that a higher metal yield was obtained at a temperature of 550 °C compared with 300 °C. Furthermore, they concluded that cans can be recycled

with a modest yield and metal quality, whereas recycling of foils produced a negative yield.

2.3.4 Melting Point

If more energy is required to reach the melting point of the salt flux, the costs of the refining process increase. As mentioned before, to lower the melting point of the salt, blends of NaCl and KCl are used. Majidi et al. [59] investigated the equimolar NaCl – KCl molten flux temperature in the aluminum refining process for the remelting of chips and turnings. The results of the study show that at temperatures below 740 °C refining will not be very effective in terms of oxides and impurities removal, whereas at temperatures above 790 °C hydrogen absorption in molten aluminum is accelerated.

2.3.5 Impurities removal

To maintain the value of the secondary metal, impurities control is one of the key factors in aluminum recycling. The use of fluxing is one of the most common

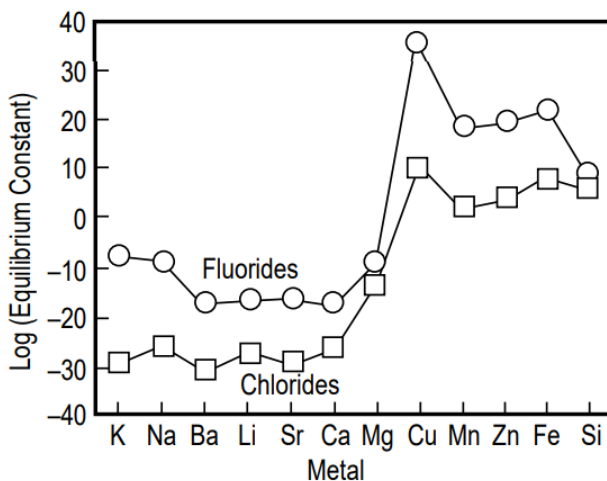
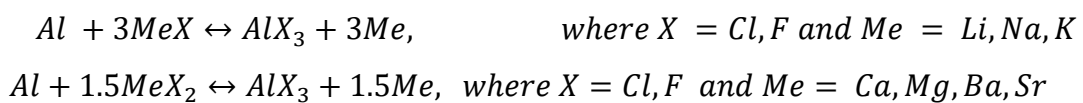


Figure 2.13 – Equilibrium constant for the impurities removal reactions [20].

technologies to remove impurities from the aluminum melt, as they allow to facilitate the removal of Ca, Sr, Na, Mg and Li [20]. The salt fluxes function as catalysts by forming chlorides and fluorides more stable than aluminum. Figure 2.13 shows equilibrium constant based on the following reactions:



When the values of the equilibrium constant are well below one, the reactions are shifted to the left: this implies that aluminum is less reactive than chlorides and fluorides with the metal impurities. This explains the effectiveness of chlorides and fluorides in removing alkali and alkali-earth metal impurities from molten aluminum while maintaining a high metal recovery [20]. The products of the reactions, depending on their density, will separate from the melt either by sedimentation or by floating and migrating to the slag.

The parameters affecting the efficiency of salt fluxes in terms of metal recovery, cost efficiency, and energy requirements discussed in Section 2.3 are summarized in the schematic representation in *Figure 2.14*.

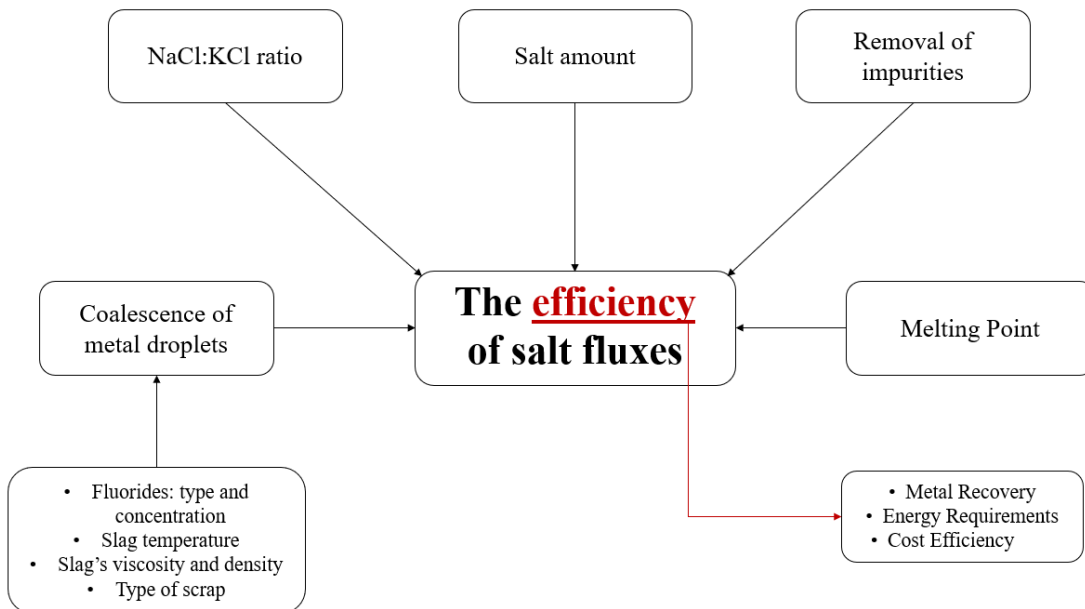


Figure 2.14 - Schematic representation of the parameters affecting the efficiency of salt fluxes in the recycling process.

2.4 The role of cryolite additions in salt fluxes

Several authors agree on cryolite's ability to reach high degrees of coalescence of metal droplets compared to other fluorides [12, 13, 20, 53], as also described in Section 2.3.3. However, some parameters of the recycling process affected by the additions of cryolite are not fully understood. These parameters are discussed in the next sections.

2.4.1 Effect of cryolite on salt fluxes' density and viscosity

As described in Section 2.3.3, Roy, Ye, and Sahai [18] investigated the effect of fluoride additions on molten equimolar NaCl - KCl molten at 740 °C and found that cryolite was the one which had the most sensible impact on density, even for low concentrations (up to 5%). The density increased from 1.55 g/cm³ to 1.62 g/cm³, as shown in *Figure 2.12*.

Roy, Ye, and Sahai also investigated the effect of fluoride additions to the equimolar NaCl – KCl on kinematic viscosity as described in *Section 2.3.3* and shown in *Figure 2.11*. While all fluorides additions up to 20% increased the viscosity except for KF, cryolite decreased the kinematic viscosity of the salt. The variation of kinematic viscosity was, however, only investigated for cryolite additions up to 2%.

2.4.2 Effect of cryolite concentration on coalescence

Several authors have investigated the effect of cryolite concentration on the coalescence of metal droplets and thus on the metal recovery. However, as stated before, the presence of oxides and non-metallic particles (NMPs) in the slag strongly affects its viscosity and hinders the mobility of the metal droplets in the slag. For this reason, it is necessary to distinguish the studies in which the salt flux was free from oxides and NMPs and those in which the slag contained oxides.

Salt fluxes in the absence of oxides and NMPs

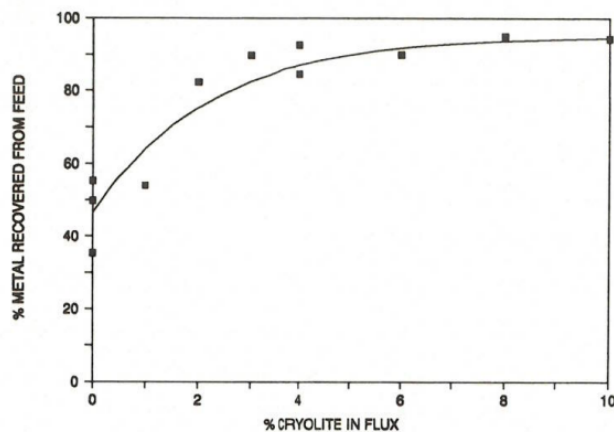


Figure 2.15 – Recovered metal from UBC [12].

consequently 200 grams of UBC were added to the molten flux. The content in the crucible was stirred several times to assist coalescence. The recovery was found to increase significantly with increasing cryolite content in the flux, as can be seen in Figure 2.15. Increasing the content of cryolite in the flux will increase the amount of recovered metal up to a certain limit, then further cryolite additions will not be beneficial.

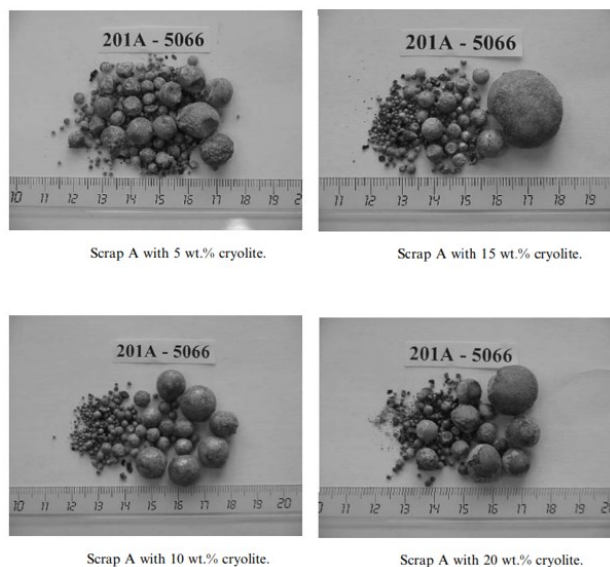


Figure 2.16 – Coalesced metal droplets at different cryolite concentrations [60].

The results showed an increase of the degree of coalescence as the content of cryolite in the flux increased. Figure 2.16 shows the coalesced droplets at the different cryolite percentages in the salt flux.

Peterson [12] investigated the metal recovered from melting decorated UBC (Used Beverage Containers) under a molten equimolar NaCl – KCl salt flux with increasing cryolite concentrations. For the tests, 200 grams of salt flux were molten at 750 °C in a graphite crucible and

A similar trend of increased coalescence with increased cryolite content in the salt flux was found by Xiao and Reuter [60], who investigated the recyclability of different subsets of aluminum turnings under a 70% NaCl – 30 % KCl with cryolite additions up to 20 % weight. The turnings were melted in an alumina crucible at 800 °C with a salt-scrap ratio of 2. The

Presence of oxides and NMPs in the slag

Thoraval and Friedrich [55] studied the effect of different slag compositions on coalescence by means of a lab scale tilting rotary furnace (TRF) to determine the influence of oxides in the slag on metal recovery. The authors melted aluminum chips which were pre-oxidized in order to obtain a thicker oxide layer on the metal. The experiments were conducted at 750 °C using an equimolar NaCl – KCl mixture with additions of non-metallic particles (NMP), both coming from recycled salt slag. The tests were also conducted at different durations to determine the best experimental time for the melting of the chips. The authors found that, by increasing the oxide content in slag, at the same percentage of cryolite addition, the coalescence efficiency decreased significantly, as shown in *Figure 2.17*.

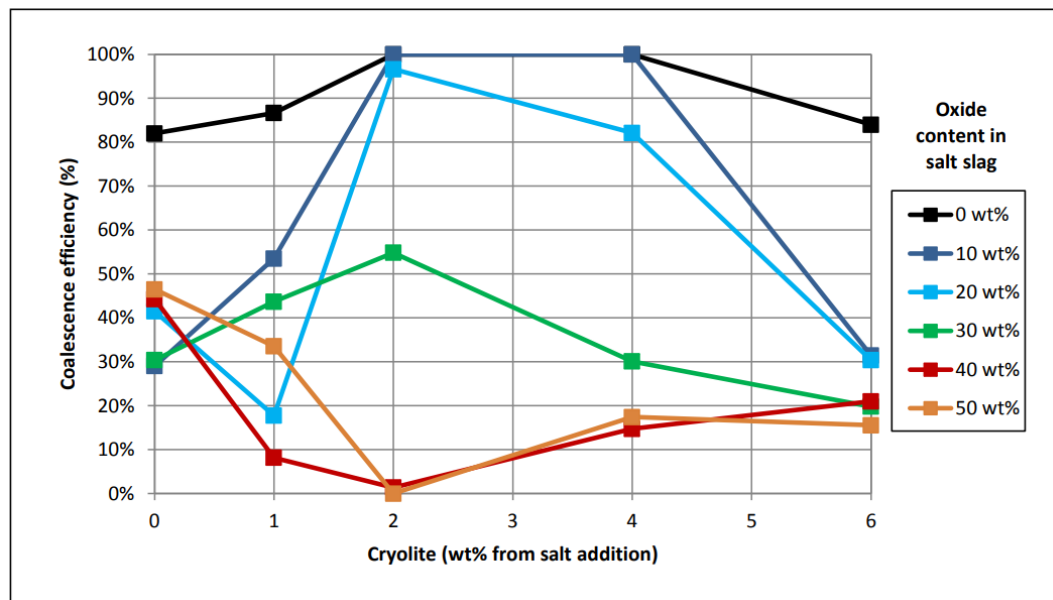


Figure 2.17 – Influence of the presence of cryolite and of oxide content in the slag on the coalescence efficiency at a duration of 7 minutes for the melting of the aluminum chips [55].

Presence of Magnesium in the scrap

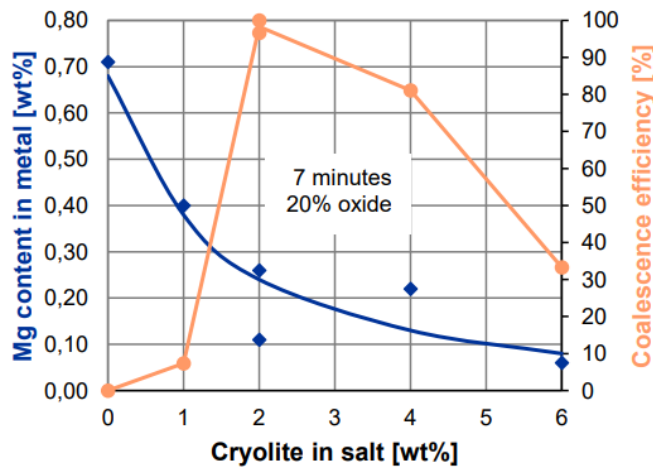


Figure 2.18 – Magnesium content in coagulated metal droplets and coalescence efficiency in salt slags with varying cryolite content [61].

effectiveness of cryolite in the removal of magnesium, they found that a maximum coalescence efficiency was obtained at approximately 2 % cryolite. For higher cryolite concentrations, the coalescence efficiency dropped from above 90 % to 30 %, as can be seen in *Figure 2.18*. By investigating the leaching residues from the remelting by XRD analysis and consequently using the thermodynamic software Factasage, they concluded that cryolite concentrations higher than 2% in the salt flux at temperatures between 700 and 725 °C lead to the formation of perovskite. Perovskite forms a layer around the metal droplets which hinders coalescence.

Besson et al. [14] and Thoraval [61], when investigating the coalescence efficiency of cryolite additions to an equimolar NaCl – KCl salt flux for the remelting of Mg-containing aluminum alloys, found that too much cryolite additions can lead to the formation of unwanted elements. Despite the

2.5 Treatment and disposal of salt cakes

Salt cakes, also known as salt slag or saline slag, are the by-product of aluminum scrap remelting processes where the utilization of salt fluxes is involved. The amount of salt cakes generated during the remelting operations can vary between 30% and 60% of the amount of metal produced, meaning that between 300 and 600 kg of salt slag are produced per ton of recycled aluminum [21]. Their chemical composition can vary to a great extent depending on various factors, such as the type of aluminum scrap being processed, the kind and amount of salt fluxes, and the type of remelting furnace [62].

Generally, salt cakes are a mixture of metal beads, crystallized salt and non-metallic particles and usually contain 5-7% metallic aluminum, 15-30 % aluminum oxide, 30-55% sodium chloride, 15-30% potassium chloride, as well as other compounds such as sulphides, phosphides, carbides, and nitrides [37, 63]. The leachability and high reactivity with humidity and water of salt cakes lead to the formation of toxic compounds, which can harm both living beings and the environment. The high reactivity of salt slags with water can lead to the formation of toxic, poisonous, harmful, and polluting gases and compounds, such as ammonia, methane, hydrogen cyanide, phosphine, and hydrogen sulfide [63]. Salt cakes disposal must be carried out with extremely cautious measures to avoid these compounds polluting air and groundwater, as well as to avoid living beings' exposure to them. Salt slag is classified as toxic and hazardous waste and its treatment, recovery, and disposal is of great environmental and economical concern. Nowadays, landfilling of salt cakes is forbidden in most European countries [62]. The scrap remelters are facing the challenges and environmental and economic issues of treatment and recovery of salt slags processes, which will be described in detail in the next sections.

2.5.1 Traditional salt cake treatment method

The traditional process to treat salt cakes consists, in a first step, the grinding and screening of the solidified salt slag to recover the residues of metallic aluminum. The metal fraction will be separated and sent to remelters for recovery. The remaining mixture of salts, oxides and non-metallic particles is then leached with water in the second step. This phase allows to dissolve the salt in water and to separate it from the oxides by filtration and evaporation of the solution. This step is often carried out at high temperatures and pressure to approach the saturation concentration of the salt in water to minimize the volume of water required for the process [21]. The steam obtained during the evaporation of water can be sent to a cooling tower to reuse the water in the process. To ease the crystallization of the salt after evaporation, crystallites may be added to promote the rapid growth of the crystals. The reaction gases, mainly H_2 , CH_4 , NH_3 and traces of H_2S , HCN , and PH_3 , require careful treatment due to their toxicity and environmental concerns. They are usually subjected to a washing and incineration process or treated by absorption on activated carbon. The residual oxides

slurry from the filtration step is usually subjected to a washing or calcination process to eliminate chlorides to make it suitable to be employed for various uses, some of the most common shown below [37, 63]:

- Construction industry, e.g. filling for cement, pavements, and mortars.
- Chemical industry, e.g. production of aluminum oxides and salts compounds, epoxy resin mortars and inert filling for polymers.
- Metallurgical industry, e.g. synthetic slags for steel refining.
- Agriculture, e.g. artificial soils and fertilizers.
- Mineral wool.

A schematic representation of the traditional treatment process for salt cakes is shown in *Figure 2.19*.

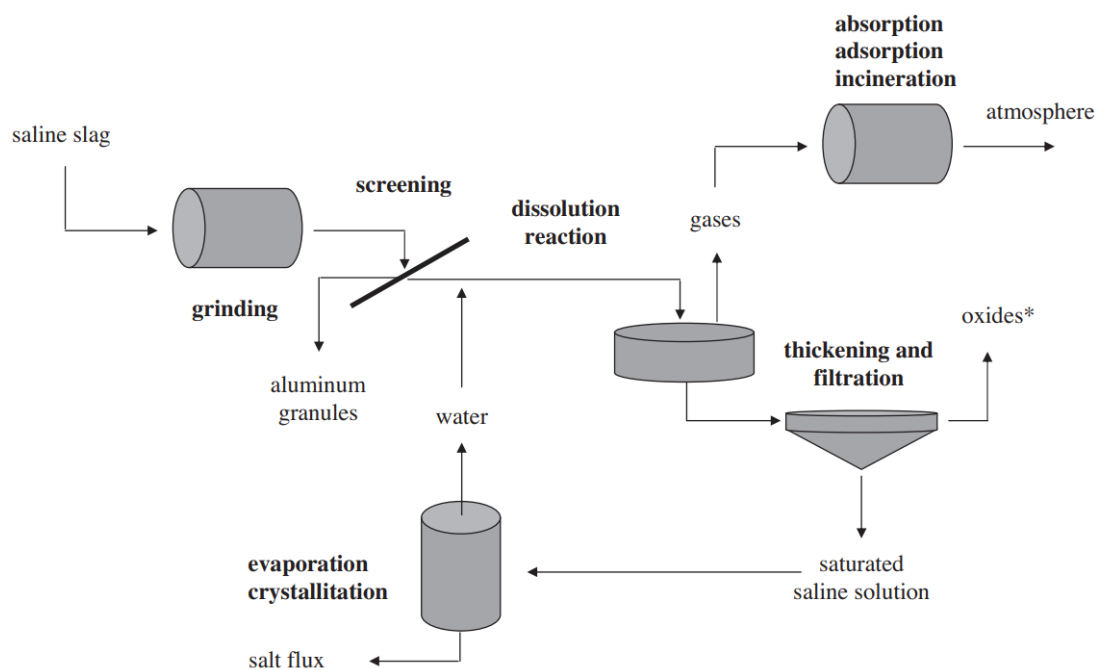


Figure 2.19 – Schematic representation of the traditional process to treat salt cakes [21].

According to Gil and Korili [21], the economic and environmental benefits of the recovery of salt cakes are questionable, when considering the amount of water utilized and the energy costs for the process. According to the authors, if there is no demand nor utilization for the salts and oxides recovered from the process, landfill remains the most convenient option. However, as mentioned before, landfill is prohibited in most European countries due to the hazardous, toxic, poisonous, and

polluting nature of the salt cake. Moreover, according to Tsakiridis [63], landfilling operational costs are very high, and over 80% of the metallic aluminum and essentially all the salts can be recovered, making the process the best option when considering economic and environmental concerns. More solutions are also arising to lower the costs and environmental impact of salt cake treatment, some of which will be discussed as follows.

2.5.2 In-house treatment of salt cake

Due to its high set-up and operational costs, in Europe only nine large-capacity salt slag treatment facilities are present, serving more than 270 aluminum recycling plants. This implies additional costs for the aluminum recycling companies for the storage and transport of the salt slag to the salt cake treatment facilities. A recent project funded by the European Union, *AluSalt* [64], developed full-scale prototype of a small-sized salt slag recycling unit which can be installed at secondary aluminum producing facilities. The adoption of this solution by aluminum remelters not only would imply avoiding the shipment of up to 2 million tons of salt slag across Europe [64], but it would also contribute to reduce aluminum's carbon footprint in the context of a circular and environmentally-friendly economy, as the products of the salt cake recovery can be sold for further utilization.

2.5.3 Alternative salt cake treatment processes

Several studies have shown alternative attempts to innovate the treatment process of salt cakes, with the aim to further enhance the sustainability of the process as well as to reduce the costs related to it. The main alternative salt slag treatment processes were identified by Tsakiridis [63], and are briefly described as follows:

- Freeze crystallization: this process consists of cooling the salt and water solution beyond its saturation point. This will lead the salt to precipitate as crystals, which will then be recovered. From this process it is also possible to recover pure water and magnesium chloride, which would otherwise accumulate as an impurity in the salt flux.

- Solvent/antisolvent process, which can substitute the evaporation step to recover the salts from the salt and water solution. In the process, a concentrated solution containing the salts is fed in an antisolvent reactor with acetone.
- Common ion process, which is based on the addition of compounds containing chloride ions to the saturated salt/water solution to recover the salts after their precipitation and filtration.
- High temperature/high pressure process: this process is based on the idea of increasing the solubility in water of sodium and potassium chloride to reduce the amount of water needed to leach the salts and is carried out at temperatures of 200 °C or 300 °C using pressurized water. As the process is closed, the water is recycled.

Among the promising methods for the reutilization of the solid residue from salt cake is its transformation into zeolite. A recent study by Padilla et al. [62] was conducted with the aim to transform the non-metallic residue of the salt cake into zeolite without the generation of further solid waste from the process. Zeolite consists of crystalline aluminosilicates which show many industrial applications, such as catalysis, removal of metal ions from water, and gas purifications. The methodology followed by the authors in the study consisted in a two-steps procedure: first, the recovery of the salts and the treatment of the reaction gases was carried out. This step allowed to recover approximately 90% of salt as well as 90% of ammonia. The second stage involved the transformation of the residual non-metallic solid into zeolite by a hydrothermal process. The obtained zeolite was characterized and proved to yield suitable features for its employment in the removal of metal ions from water.

3 Material and Methods

This section provides a detailed description of the salt flux characterization and investigation procedure. The first part includes a description of the salts and of the sample preparation. The second part provides an explanation of the methodology to carry out a thermodynamical analysis prior to the experimental part. In the next sections, the characterization techniques and experimental procedures will be illustrated. The methods to carry out thermal analysis, viscosity measurements, as well as to measure the alumina dissolution in the molten salts and the salts dissolution in water will be discussed.

3.1 Raw materials

The salt fluxes studied in this work were composed of sodium chloride, NaCl, (99.5% purity, Fisher Scientific), potassium chloride, KCl, (99.5% purity, Sigma-Aldrich), and cryolite, Na₃AlF₆, (97% purity, Sigma-Aldrich). The salt flux object of this thesis work is a 95 wt.% NaCl – 5 wt.% KCl salt mixture with fluoride additions ranging between 0 wt. % and 15 wt. %. Two other salt flux systems were taken into consideration: a 50% NaCl – 50% KCl and a 70% NaCl – 30% KCl. A 2% weight amount of cryolite was added to both. The chemical composition of the analyzed salts mixtures is summarized in *Table 3-1*:

	Mixture	%wt NaCl	%wt KCl	%wt Na₃AlF₆
1	95-5-0	95	5	0
2	95-5-2	95	5	2
3	95-5-3	95	5	3
4	95-5-5	95	5	5
5	95-5-7	95	5	7
6	95-5-10	95	5	10
7	95-5-10	95	5	15
8	70-30-2	70	30	2
9	50-50-2	50	50	2

Table 3-1 – Chemical composition of the salt mixtures.

3.1.1 Sample preparation

To prepare the samples for further experimental analysis, 300 grams of each mixture composition were prepared. These mixtures were molten in an induction furnace to obtain “*master salts*” to ensure a fixed composition for each mixture. Prior to melting, each powder mixture was weighed according to the composition and mixed to ensure proper homogeneity of the compound. Each powder mixture was then molten at 820 °C in a graphite crucible in the induction furnace under Argon cover to avoid oxidation of the graphite crucible. Before and after each melting, vacuuming by means of a vacuum pump was carried out to ensure the absence of oxygen in the furnace chamber as well as to eliminate any evaporation gases due to the melting. Temperature was recorded by means of an S-type thermocouple during melting. Apertures in the furnace allowed checking if the sample was molten; the molten mixture was then poured in a water-cooled rectangular copper mold by means of a lever connected to the crucible holder. After the sample was solidified and properly cooled, it was collected from the mold.

3.2 Thermodynamics

Prior to performing the characterization of the samples, a thermodynamic analysis by means of a commercial thermodynamic software *Factsage*™ was carried out. The software allows to create phase diagrams by selecting the components of the mixture being investigated. Since the NaCl/KCl ratio in each mixture is constant, it was possible to obtain a binary phase diagram in which the considered variables were the temperature and the amount of cryolite. To set a fixed composition for each NaCl/KCl ratio, three *streams* were created after suited equilibrium calculations. The streams are described as follow:

- Stream 1, i.e. 95% *wt.* NaCl, 5% *wt.* KCl;
- Stream 2, i.e. 70% *wt.* NaCl, 30% *wt.* KCl;
- Stream 3, i.e. 50% *wt.* NaCl, 50% *wt.* KCl;

For each stream, a binary phase diagram was created, by setting as variables the amount of cryolite (Na_3AlF_6) and the temperature.

3.3 Physical Characterization

In the next sections, the methodology to characterize the salt mixtures will be discussed in detail. The experimental procedures to perform the thermal analysis and viscosity measurements will be described, as well as the method to determine the alumina dissolution in the molten salts and the salt dissolution in water.

3.3.1 Thermal Analysis

Thermal analysis of the samples was performed to further understand the melting behavior of the salt mixtures. In particular, the experiments aimed to locate the melting interval as well as to verify the presence of phase transitions and eutectic points of the samples during melting. The melting behavior of salt fluxes is crucial, as the energy required to melt the salts contributes to increase the melting operations costs and the environmental impact. Two sets of experiments were carried out to perform the thermal analysis: a preliminary investigation was conducted by means of a wetting furnace, which was followed by a Differential Scanning Calorimetry (DSC).

3.3.1.1 Wetting Furnace

Wetting furnaces, as suggested by the name, are usually employed to determine the wettability of a material on a substrate material. The contact angle between a molten droplet of sample material and the substrate is measured as an indicator of wettability, using a method also known as the “sessile drop technique” [65]. In this thesis work, however, the wetting furnace was used as a preliminary method to locate the softening interval of the sample prior to the Differential Scanning Calorimetry experiments. The experimental equipment consists of a cylindrical graphite heater placed inside a water-cooled chamber. The graphite heater is surrounded by graphite radiation shields, and inside of it the substrate is placed. Windows on the chamber walls allow digital recording of the sample by means of a camera (Sony XCD – SX910CR, Sony Corporation, Millersville, MD). A pyrometer controls the temperature of the chamber, which can reach up to 2400 °C. A circular graphite substrate with a diameter of 10 mm was used to heat the salt samples. The samples

were obtained by crushing the previously cast and solidified salt mixtures to obtain pieces with a dimension of 2-3 mm and weighing approximately 40 mg. During the experiments, Argon was flushed in the chamber at a rate of 0.1 l/min after vacuuming to remove oxygen from the chamber. A schematical representation of the wetting furnace is presented in *Figure 3.1*.

For the experiments, the temperature was increased up to 600 °C in 3 minutes and then

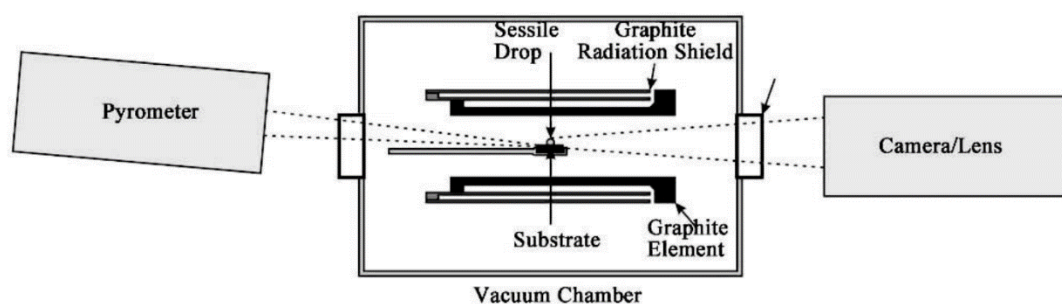


Figure 3.1 – Schematic representation of the wetting furnace [65].

the heating rate was set at 15 °C/min until the sample was observed through the camera to be molten; when the sample was molten the furnace was stopped. Temperature recording was carried out by means of an S-type thermocouple. As the melting interval is approached, the sample assumes the shape of a droplet on the substrate. The temperature at which the sample starts to melt was identified by observing a fixed point of the sample and determining the temperature at which the point started to move.

3.3.1.2 DSC Analysis

Differential Scanning Calorimetry (DSC) is a fundamental tool in thermal analysis, as it allows to detect several transitions such as melting, glass transition, and phase changes of a substance as well as thermal properties such as enthalpy values, specific heat, or latent heat. The heat flow (or power) between a reference material and the sample is recorded upon controlled heating and/or cooling by selecting the desired temperature profile [66]. Only a few milligrams of material are required to run a DSC experiment. The output of a DSC analysis is a graph of the heat flux versus temperature or time, from which it is possible to calculate the specific heat, the enthalpy of fusion and the heat of reaction of the sample if a particular atmosphere is chosen. When a peak appears in a DSC curve, it is associated with thermally activated heat

consumption or production transitions such as melting or crystallization. Other changes in the shape of DSC curves, for example step-like changes, are correlated to other transitions such as glass transitions. In this study, the DSC analysis was not used to investigate the specific heat or the enthalpy of the samples, but to assess the melting temperature of the salt mixtures as the cryolite content increased from 0% to 15% weight. Two main types of Differential Scanning Calorimeters are available [67]:

- Heat-flux DSC: this technology measures the voltage difference between thermocouples connected to the sample and to a reference material. The voltage difference is a measure of the amount of heat required to increase the temperature of the sample and of the reference: when the sample is subject to a transformation such as melting, which is an endothermic phase transition, more heat will have to flow to the sample compared to the reference. Often, the reference consists of an empty pan. In heat-flux DSC, the reference and the sample pans are put on a plate inside the furnace chamber of the apparatus [68].
- Power compensated DSC: this setup allows to quantify the amount of power necessary to keep sample and the reference's temperature at the same value. The sample and the reference are placed in separate chambers. This technology is very sensitive; however, it usually works at lower temperatures compared to heat-flux DSC [68].

For the purpose of this thesis work, a heat-flux DSC apparatus (Linseis STA PT 1600) was utilized in the laboratories of the Norwegian University of Science and Technology (NTNU, Trondheim, Norway). The equipment allows to simultaneously run a DSC analysis as well as a thermogravimetric analysis (TGA) and can work at temperatures up to 1750 °C in controlled atmosphere conditions. The measuring system consists of a plate containing the sample and the reference placed on top of a rod. An S-type thermocouple was used for temperature recording. An empty graphite crucible with a 6.8 mm diameter was used for the zeroline. The *master salts* were crushed to obtain samples weighing approximately 60 mg. The samples were then heated up to 820 °C with a 5 °C/min heating rate; they were left at 820°C for 10 minutes and then cooled to room temperature with a 5 °C/min cooling rate. All experiments were carried out in Argon atmosphere, with a gas flow of 0.2 l/min. The

Linseis STA Evaluation Software present in the PC connected to the equipment allows to control the experimental parameters, the data acquisition as well as the data evaluation.

The curves obtained from the data acquisition software were automatically corrected with the zeroline using the Linseis STA Evaluation Software. By analyzing the reaction peaks of the DSC heating curves, it was possible to obtain the characteristic temperatures of the sample, as also shown in *Figure 3.2* [67]:

- The extrapolated peak onset temperature (T_{onset}) was obtained as the intersection between the descending peak slope, which was obtained as a linearly fitted line, and the baseline. The baseline was obtained as a straight line between the initial (T_i) and final temperature (T_f) of the peak region [67]. The initial and final temperatures of the peak region were identified as deviations from the baseline of the DSC curve. The extrapolated peak onset temperature was determined as the melting point of the sample [67].
- The peak offset temperature (T_{offset}) was obtained as the intersection between the ascending peak slope, which was obtained as a linearly fitted line, and the baseline.
- The peak maximum temperature (T_{peak}) was obtained as the intersection point between the fitted lines of the descending and ascending slopes of the peak. This value can be considered as a good approximation of the liquidus temperature [67].

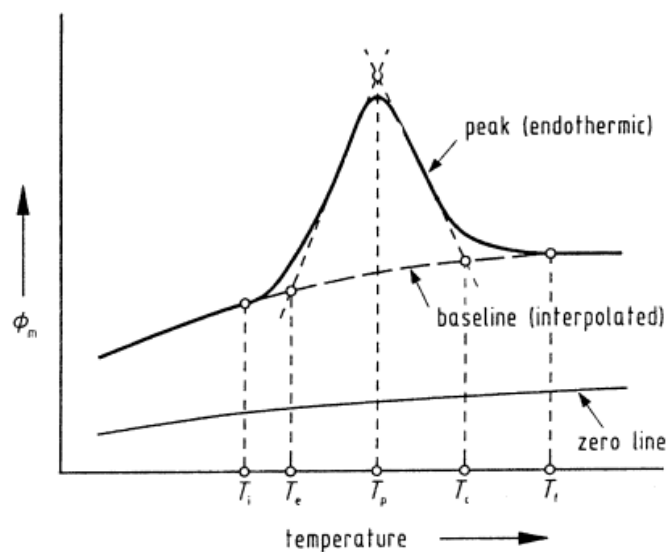


Figure 3.2 – Determination of the characteristic temperatures from the DSC analysis. T_i : initial peak temperature; T_e : extrapolated onset temperature; T_p : peak maximum temperature; T_o : peak offset temperature; T_f : final peak temperature [67].

These characteristic temperatures were obtained from the heating curves, to avoid uncertainties due to supercooling [67].

3.3.2 Viscosity Measurements

Viscosity may be described as the resistance to flow of a fluid in motion. For an ideal behavior of the fluid at a certain temperature and pressure, also known as Newtonian behavior, the viscosity is expressed as follows:

$$\eta = \frac{\tau}{\dot{\gamma}} \quad (3.1)$$

where η is the viscosity and is constant for Newtonian fluids, τ is the shear stress applied to the fluid, and $\dot{\gamma}$ is the shear rate, that is the rate of deformation of the fluid [69]. As described in *Section 2.3.3*, the molten salt's viscosity influences the settling velocity of the metal droplets. If the viscosity of the salt excessively increases, it can hinder the coalescence of the metal. For this thesis work, the 95% wt NaCl – 5% wt KCl salt mixtures' viscosity was investigated to determine how it is affected by the

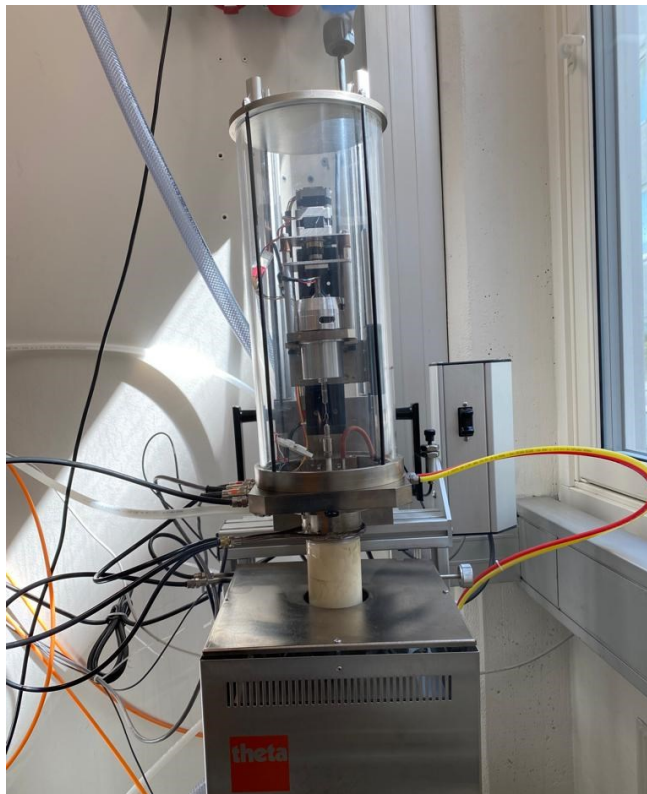


Figure 3.3 – Theta Industries Rheotronic Rotating Viscometer used for the viscosity measurements.

cryolite content. The rheological properties of each sample were examined at the Norwegian University of Science and Technology Laboratories (NTNU, Trondheim, Norway) by means of a Theta Industries Rheotronic II 1700 °C Rotating Viscometer with a Brookfield DV – III Ultra Rheometer measuring head. The apparatus is shown in *Figure 3.3*.

The measurements were carried out by means of a concentric cylinder system: a cylindrical spindle rotates while being immersed in the sample, which is contained in a cylindrical crucible. This is also known as the Searle method, where the spindle is the rotating part of the measuring system [69]. The experiments were performed in Controlled Shear Rate mode (CSR): by setting the rotational speed and thus the shear rate $\dot{\gamma}$, it is possible to obtain the torque, the shear stress τ , and consequently the viscosity η of the sample. A graphite crucible of 69.9 mm height, 36 mm diameter and 3 mm wall thickness was filled with 40 grams of salt mixture. A graphite spindle with the dimensions shown in *Figure 3.4* was utilized.

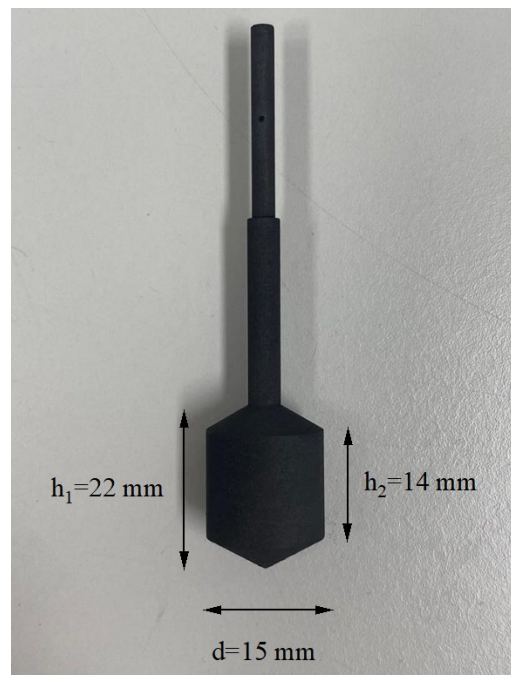


Figure 3.4 – Graphite spindle used for the viscosity measurements.

The crucible is held by alumina rods and is insulated by an alumina tube which can be lowered in the furnace. An S-type thermocouple placed outside the crucible allowed temperature monitoring with a $\pm 5^\circ\text{C}$ accuracy. Calibration of the system was verified by measuring the room temperature viscosity of a Reference Standard mineral

oil (N10, Cannon Instrument Company). The samples were heated up to 820 °C with a 10 °C/min heating rate in Argon atmosphere. The sample was left at 820 °C for 10 minutes before immersing the spindle at a 67 mm depth in the crucible and keeping it at 820 °C for 20 minutes for temperature homogenization. The velocity of the spindle was slowly increased up to 190 RPM, recording the torque and viscosity values shown on the apparatus display. At each spindle velocity, the spindle was kept rotating for 30-45 seconds to allow the torque and viscosity values to stabilize.

3.4 Chemical Characterization

In the next sections, the methodology to characterize the chemical features of the salt mixtures will be discussed in detail. The experimental procedures to determine the alumina dissolution in the molten salts and the salt dissolution in water will be discussed.

3.4.1 Alumina Dissolution

The dissolution of Alumina, Al_2O_3 , in the molten salt mixtures was investigated at the DTG Laboratories of the University of Padua in Vicenza. 30 grams of each salt flux mixture were molten in porcelain crucibles in a muffle furnace. The ability of the salt fluxes in dissolving oxides was evaluated by placing an Al_2O_3 sphere in the molten salt and measuring the sphere's mass loss after the chosen dwelling time. The experimental time of dwelling of the alumina spheres in the molten salts for each cryolite percentage were of 10, 40, 70 and 100 minutes. After each dwelling time, the crucible was taken out of the furnace and the salt was left to cool down; then, the sphere was removed from the solidified salt. The aluminum oxide dissolution in the molten salts was evaluated in terms of mass loss of the alumina sphere by means of the following equation:

$$\text{Alumina Dissolution} [\%] = \frac{w_{i,a} - w_{f,a}}{w_{i,a}} * 100 \quad (3.4)$$

where $w_{i,s}$ and $w_{f,s}$ are the initial and final mass of the Al_2O_3 spheres, respectively. The measurements for each dwelling time and cryolite content in the salt were repeated at least twice.

3.4.2 Salt dissolution in water

The dissolution of the salts in water was evaluated by investigating the mass loss of salt samples after letting them settle in 12 L of distilled water for the chosen experimental times, which were of 25, 50, 100 and 200 minutes. 16 grams of salt flux samples were molten in porcelain crucibles and were left to solidify. Each crucible was weighed before the submersion in water, and after the experimental time the crucibles were heated at 160 °C for 2 hours to remove the water content. The crucibles were then weighed again. The mass loss of the samples was evaluated with the following equation:

$$\text{Salt Dissolution [\%]} = \frac{w_{i,s} - w_{f,s}}{w_{i,s}} * 100 \quad (3.5)$$

where $w_{i,s}$ and $w_{f,s}$ are the weight of the crucible before and after the dissolution of the salt in water, respectively.

4 Results and Discussion

4.1 Thermodynamic calculations

The phase diagrams obtained with the thermodynamic software FactSage show a melting temperature of 757 °C for the 95% wt NaCl – 5% wt KCl without cryolite additions. This is not in agreement with the binary phase diagram in *Figure 2.6*, which does not show a single melting point for the 95% wt NaCl – 5% wt KCl without cryolite, but instead shows a liquidus and a solidus temperature of approximately 775 and 725 °C, respectively. For cryolite concentrations below 1.3%, the liquidus temperature is constant at 757 °C, while the solidus temperature decreases to 661 °C. For cryolite concentrations above 1.3%, the liquidus temperature increases from 757 °C at 1.3% cryolite to 775 °C at 15% cryolite, while the solidus temperature remains constant at 661 °C, as can be seen in *Figure 4.1*.

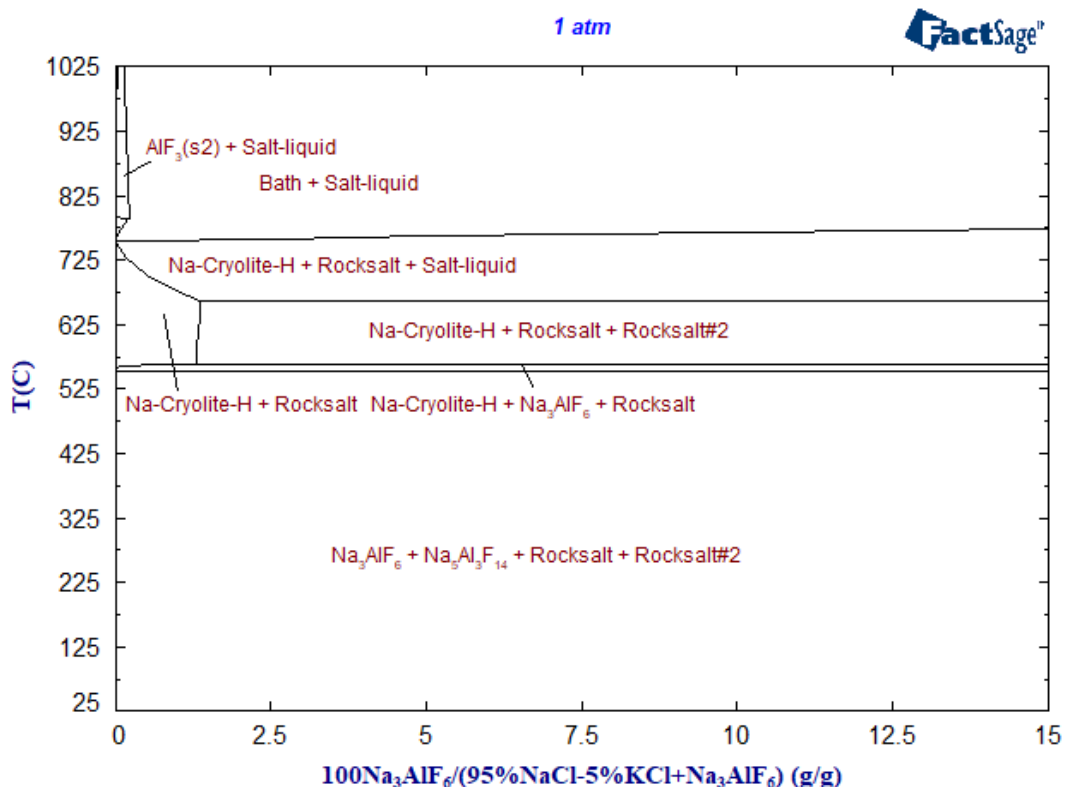


Figure 4.1 – Phase diagram of 95 % wt NaCl – 5 % wt KCl with cryolite additions up to 15% wt.

From the thermodynamical analysis of the 70 % wt NaCl – 30% wt KCl, the mixture without cryolite additions presents a liquid phase at 675 °C, well in agreement with the NaCl-KCl phase diagram [41]. For cryolite concentrations greater than 2% wt. and temperatures above 725 °C, a liquid phase and a sodium-cryolite solid compound are present. Below 725°C, the liquid phase is still noticeable until 620 °C, but a precipitation of rocksalt solid compounds can also be observed. The phase diagram for the 70 % wt NaCl – 30% wt KCl mixture with cryolite concentrations up to 15 % weight is shown in *Figure 4.2*.

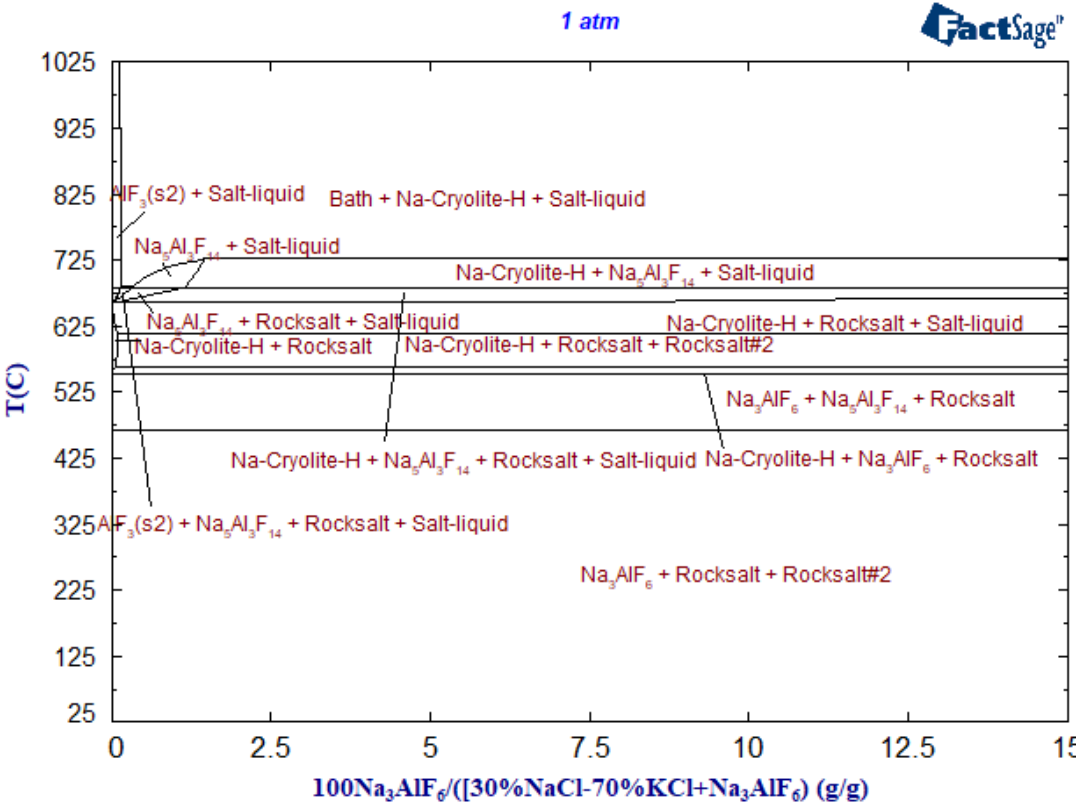


Figure 4.2 – Phase diagram of 70% wt NaCl – 30% wt KCl with cryolite additions up to 15%.

The investigation of the 50 % wt NaCl – 50 % KCl phase diagram at varying cryolite content also reveals the presence of a low-temperature melting phase at 685 °C for cryolite contents below 1%. As the cryolite content increases, the melting temperature increases to 725 °C. Below this temperature, solid phases of rocksalt and fluoride compounds start to precipitate. However, a liquid phase of salt is still present

until 605°C. Below this temperature, only solid phases are present, as can be seen in Figure 4.3.

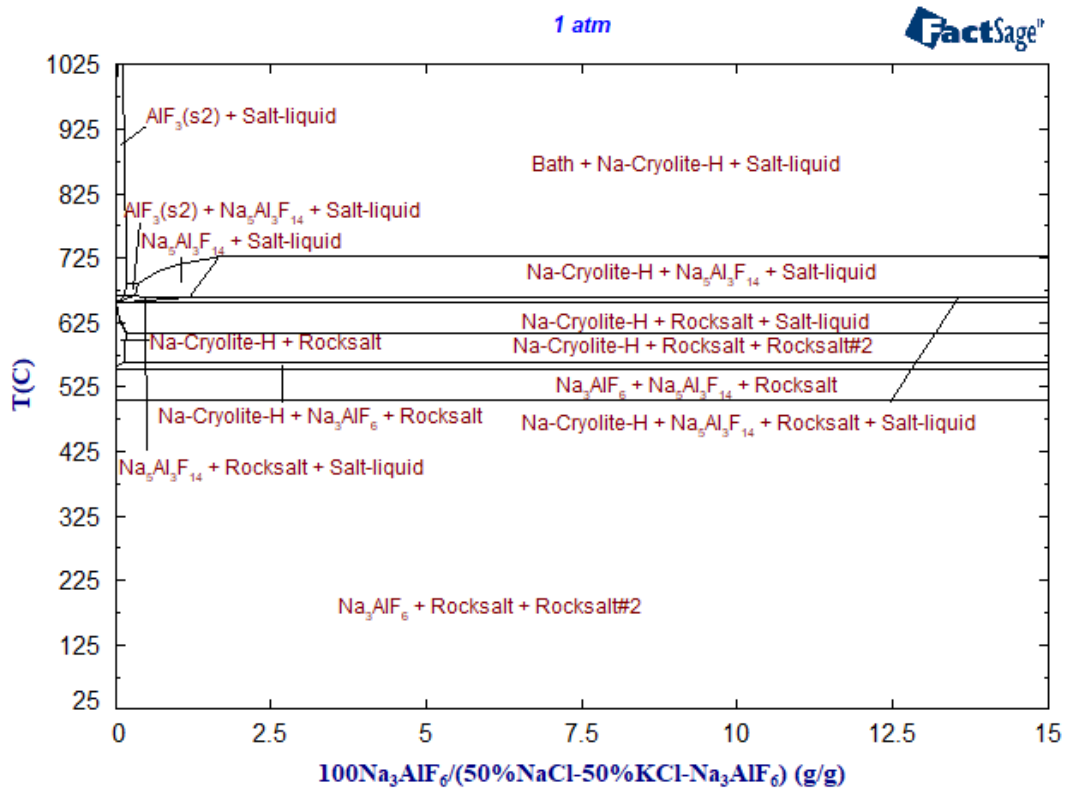


Figure 4.3 – Phase diagram of 50% wt NaCl – 50% wt KCl with cryolite additions up to 15% wt.

According to the binary phase diagrams presented above, the addition of cryolite to the NaCl-KCl mixtures decreases their solidus temperature to a constant value, as shown in the table below:

NaCl/KCl ratio	Cryolite addition [wt%]	Solidus Temperature [°C]	Liquidus Temperature [°C]
95/5	0	757	757
95/5	2	661	760
95/5	3	661	761
95/5	5	661	764
95/5	7	661	767
95/5	10	661	770
95/5	15	661	775
70/30	0	668	668
70/30	2	613	725
50/50	0	657	657
50/50	2	608	725

Table 4-1- Solidus temperature of the salt mixtures with cryolite additions according to the phase diagrams obtained with FactSage.

From an industrial point of view, the liquidus temperature is the most relevant: even a slight increase of the energy required to completely melt the salt flux and the metal could result in a significant rise of the operations cost. Therefore, when aiming to optimize the cost efficiency of the refining process, it is important to minimize the liquidus temperature of the salt flux while still ensuring fair coalescence and metal recovery by adding fluorides, e.g., cryolite.

4.2 Thermal Analysis

In the following sections the results obtained from the thermal analysis will be presented and discussed. In Section 4.2.1, the findings from the preliminary thermal analysis by means of the wetting furnace will be discussed. Section 4.2.2 will concern the results from the Differential Scanning Calorimetry.

4.2.1 Wetting Furnace

By observing the shape of the sample as the temperature increased, it was possible to determine the softening point of the salt, which is the beginning of the melting of the sample. Four main events were identified by observing the shape of the sample as the temperature increased:

- a) The shape of the sample remained unchanged.
- b) The shape of the sample started to be altered by the increasing temperature. This was observed as a shift of position of a fixed point in the image of the sample. The temperature at which this event was observed was determined as the softening temperature of the sample.
- c) The shape of the sample mutated noticeably as it started to collapse and become a droplet.
- d) The sample assumed the shape of a droplet.

The events listed above are shown in Figure 4.4, taken from the experimental procedure of the melting of a 95% NaCl – 5% KCl with 15% cryolite addition. The

red circles in Figure 4.4 (a) and 4.4 (b) highlight the slight movement of the observed point of the sample.

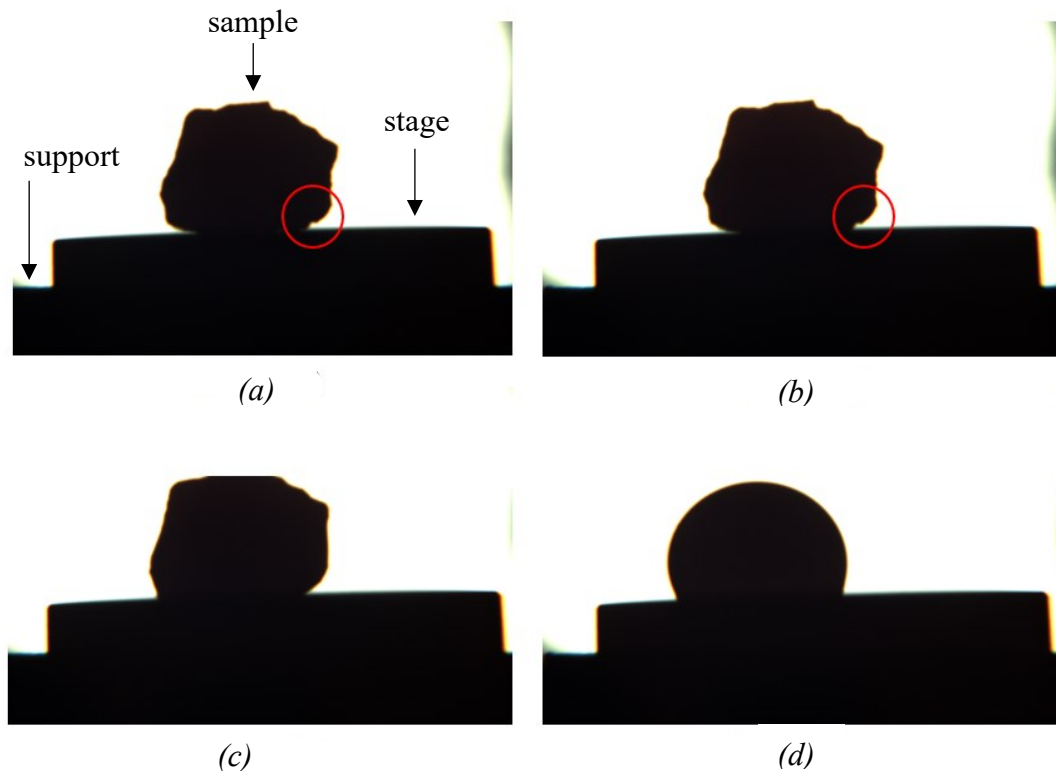


Figure 4.4 – Experimental melting sequence of a 95% wt NaCl – 5% wt KCl with 15 % wt cryolite addition (a) 640 °C; (b) 710 °C; (c) 731 °C; (d) 760 °C.

The softening temperatures of the analyzed samples are reported in *Table 4-2*.

NaCl/KCl ratio	Cryolite content [%wt]	Softening Point [°C]
95/5	0	764
95/5	2	728
95/5	3	722
95/5	5	722
95/5	7	719
95/5	10	708
95/5	15	710
70/30	2	639
50/50	2	628

Table 4-2 – Softening point of the salt mixtures obtained by melting the samples in the wetting furnace

The softening point of the salt mixtures decreases by 54 °C as the cryolite additions range from 0 to 15% wt. The most sensible decrease in the softening temperature, of

approximately 36 °C, is found when comparing the salt without cryolite and the one with just 2% cryolite content. The softening temperature then decreases by 9°C, from 728 °C to 719 °C, with cryolite additions in the range of 2% up to 7%. The salt with 10% cryolite addition shows a sharp decrease in the softening temperature compared to the 7% cryolite-containing salt. However, no further decrease of the softening temperature was noticed when adding cryolite above 10%, as can be seen in *Figure 4.5*.

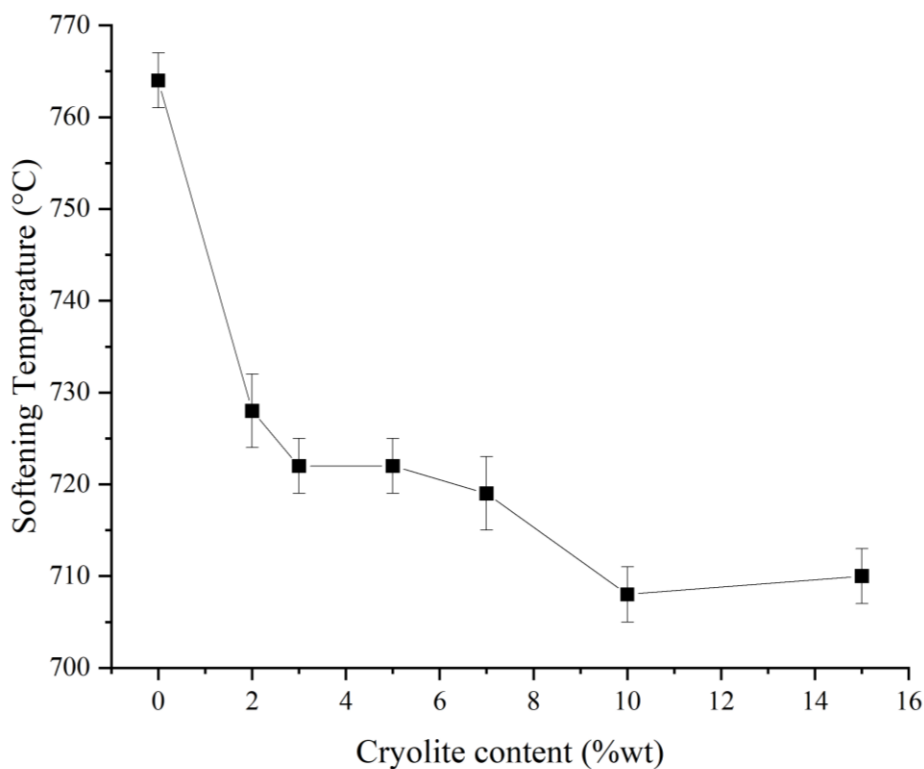


Figure 4.5 – Wetting furnace - Softening temperature of the salt mixtures as the cryolite content increases.

The softening temperature was determined as the temperature at which the sample started to collapse due to the beginning of melting; this implies that the softening temperature may be compared to the solidus temperature in the phase diagrams from factsage. The experimental results obtained with the wetting furnace differ from the results obtained from the thermodynamic analysis: for the 95% wt NaCl – 5% wt KCl mixture with no cryolite addition, the thermodynamic analysis revealed the presence of a liquid phase at 756 °C, whereas the wetting furnace experiments found the softening point at 764 °C. As the cryolite content increases, the softening temperature decreases; however, according to the phase diagrams, the solidus

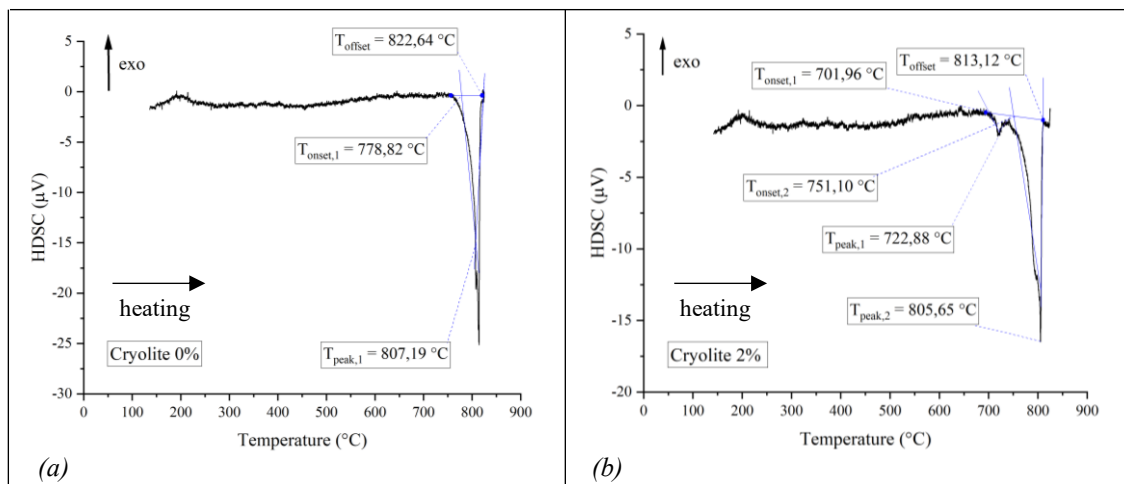
temperature for cryolite contents above 1.3% should be constant. The experimental results were found to deviate from the thermodynamic analysis also for the 70 % *wt* NaCl – 30 % *wt* KCl as well as for the 50 % *wt* NaCl – 50 % *wt* KCl: the experimental results show a softening point of 639 °C and 628 °C, respectively, whereas according to the phase diagram a liquid phase should be present at 612.64 °C and 607.94 °C, respectively.

For industrial applications, a decrease of the solidus temperature may be advantageous in terms of reduced energy requirements to melt the salt; however, the most relevant for industrial considerations is the liquidus temperature.

The inconsistency between the experimental results and the thermodynamic analysis may be related to the deviation from the equilibrium conditions due to the heating rate of the sample in the wetting furnace, which was of 15 °C/min. Moreover, the sensitivity of the apparatus may have affected the accuracy of the results. Lastly, the phase diagrams obtained from the thermodynamic analysis may also be subjected to inaccuracies due to possible imprecisions in carrying out the preliminary thermodynamic calculations as well as to possible lack of information in the software's database for inorganic salts.

4.2.2 DSC Analysis

The measured DSC curves for each mixture containing cryolite showed two events: a peak due to the melting of the eutectic and a peak due to the melting of the remaining phase. The DSC curves for the 95 % *wt* NaCl – 5% *wt* KCl are reported in *Figure 4.6*.



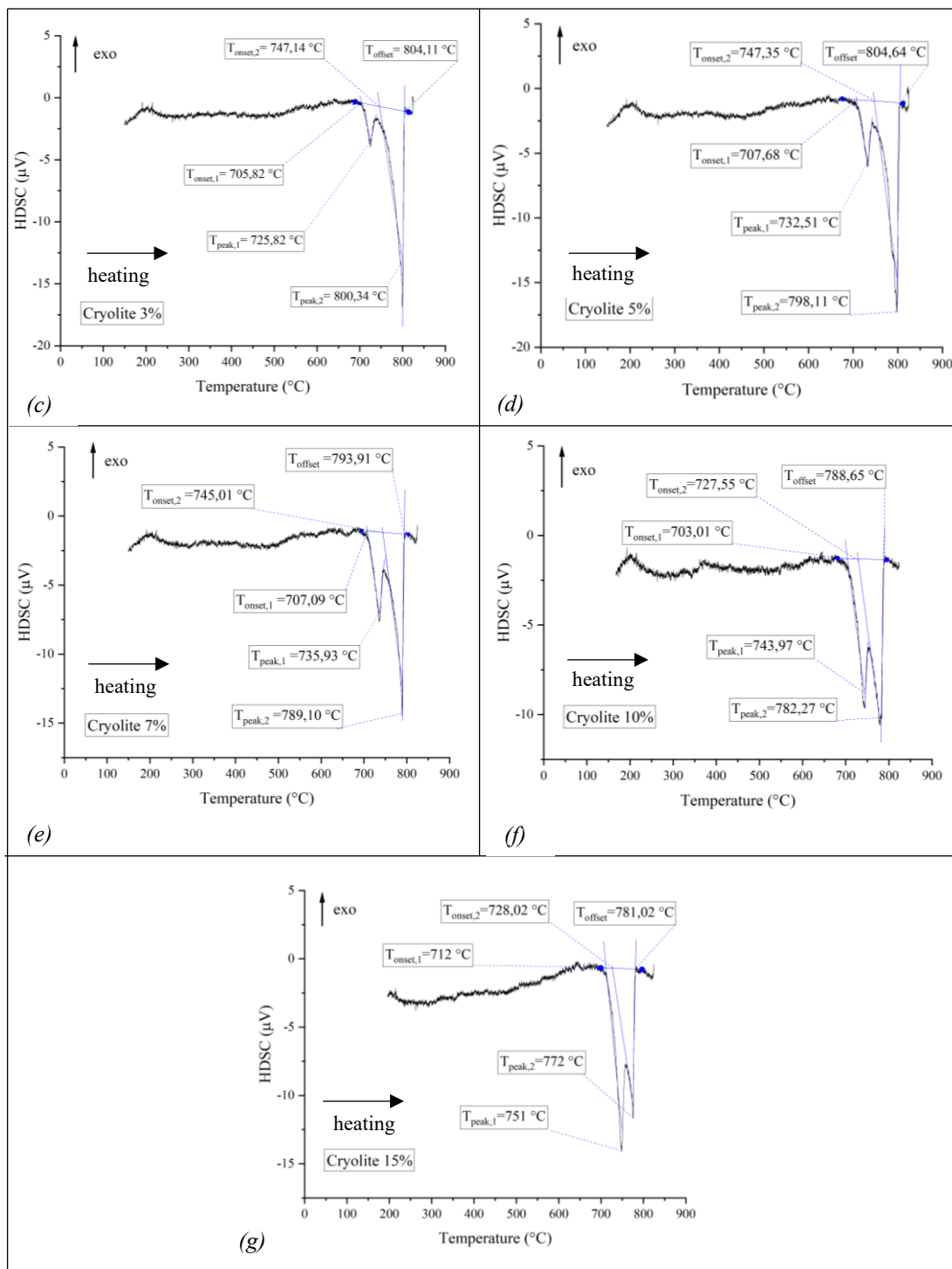


Figure 4.6 – DSC curves of the 95% wt. NaCl – 5% wt. KCl with (a) 0% cryolite; (b) 2% cryolite; (c) 3% cryolite; (d) 5% cryolite; (e) 7% cryolite; (f) 10% cryolite; (g) 15% cryolite.

The extrapolated peak onset temperatures, the peak maximum temperatures and the extrapolated offset temperatures for each mixture are summarized in *Table 4-3*.

Cryolite Content [%]	Tonset,1 [°C]	Tpeak,1 [°C]	Tonset,2 [°C]	Tpeak,2 [°C]	Toffset [°C]
0	-	-	778.8	807.2	822.6
2	702.0	722.9	751.1	805.7	813.1
3	705.8	725.8	747.1	800.3	804.1
5	707.7	732.5	747.4	798.1	804.6
7	707.1	735.9	745.0	789.1	793.3
10	703.0	744.0	727.6	782.3	788.7
15	712.0	751.0	728.0	772.0	781.0

Table 4-3 – Characteristic temperatures obtained from the DSC curves of the 95% wt. NaCl – 5% wt. KCl with different cryolite contents.

The extrapolated onset temperature of the first peak represents the melting of the eutectic, whereas the extrapolated onset temperature of the last peak indicates the beginning of the melting of the remaining phase, which in a phase diagram is represented by the solidus temperature. The extrapolated peak maximum temperature of the last peak can be considered as a good approximation of the liquidus temperature [67]. To provide the reader with a clear overview of the melting behavior of the salt mixtures, the temperatures mentioned above are reported in *Table 4-4* and in *Figure 4.7*.

NaCl/KCl ratio	Cryolite content [%]	T_{eutectic}	T_{solidus}	T_{liquidus}
95/5	0	-	778.8	807.2
95/5	2	702.0	751.1	805.7
95/5	3	705.8	747.1	800.3
95/5	5	707.7	747.4	798.1
95/5	7	707.1	745.0	789.1
95/5	10	703.0	727.6	782.3
95/5	15	712.0	728.0	772.0

Table 4-4 – Eutectic, solidus, and liquidus temperature obtained from the analysis of the extrapolated temperatures from the DSC curves for the 95% wt. NaCl – 5% wt. KCl with increasing cryolite content.

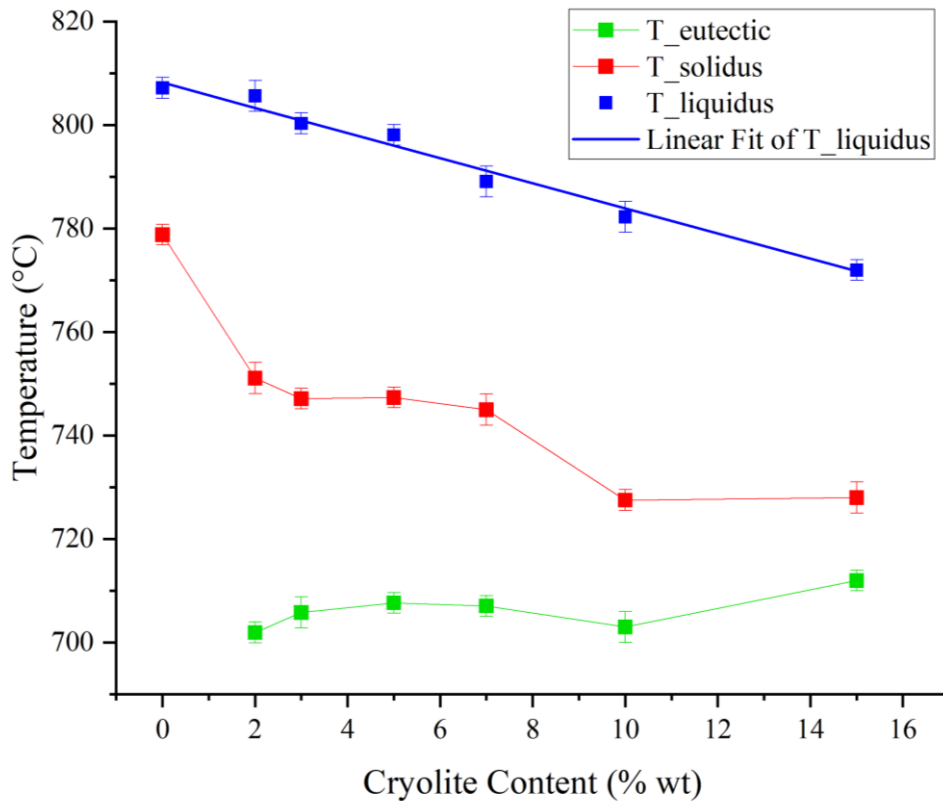


Figure 4.7 – Eutectic, solidus and liquidus temperatures of the 95% wt NaCl – 5% wt KCl salt mixtures as the cryolite content increases from 0 to 15% wt.

The addition of cryolite to the 95%NaCl – 5% KCl salt mixture noticeably affects the liquidus and the solidus temperatures of the salts. The solidus temperature decreases from 778 °C for the salt without cryolite to 728 °C for the 15% cryolite-containing salt. From an industrial point of view, the liquidus temperature is the most relevant: a decrease of the melting point of the salt fluxes implies lower emissions and reduced energy costs. The liquidus temperature was found to decrease linearly as the cryolite content increases.

The eutectic temperature shows a minimum value of 701,96 °C for 2% cryolite, followed by a slight increase to approximately 707 °C for cryolite contents up to 7%. The values of the eutectic temperature then decrease to 703,01 °C for 10% cryolite before reaching the maximum temperature at 712 °C for 15% cryolite.

The decreasing trend of the solidus temperature obtained by the DSC curves was observed to be in agreement with the trend of the softening temperature by melting the samples in the wetting furnace; however, the values of the solidus temperature are

approximately 20 °C higher than the values of the softening temperature, as shown in *Figure 4.8*.

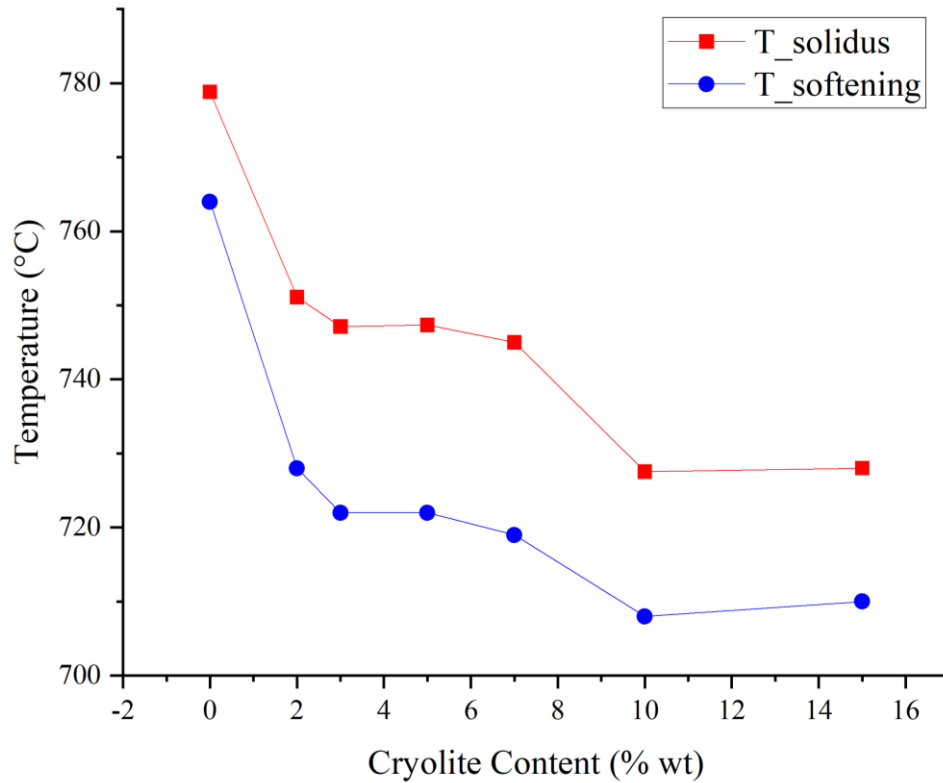


Figure 4.8 – Comparison between the solidus temperature obtained from the DSC analysis and the softening temperature obtained from the wetting furnace experiments.

In the wetting furnace experiments the heating rate was of 15 °C/min, which is far from the equilibrium conditions. Moreover, the sensitivity of temperature recording of the apparatus was characterized by uncertainty. The lower heating rate of the DSC experiments as well as the better accuracy and sensitivity of the apparatus, allow to conclude that the temperatures extrapolated from the DSC curves are more reliable.

The DSC curves for the 70% wt NaCl – 30% wt KCl and 50% wt NaCl – 50% wt KCl with 2% cryolite content are displayed in *Figure 4.9*.

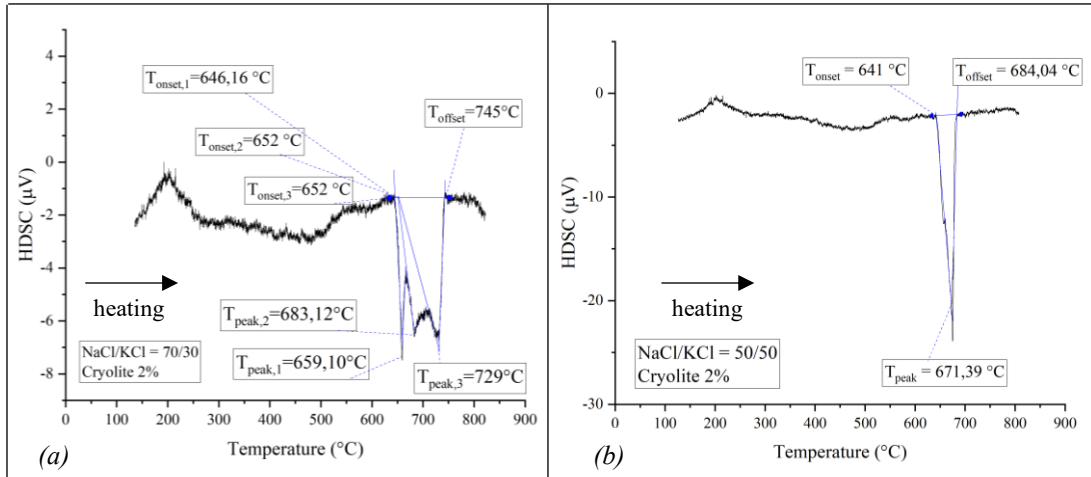


Figure 4.9 - DSC curves of the (a) 70% wt. NaCl – 30% wt. KCl and (b) 50% wt. NaCl – 50% wt. KCl, both with 2% cryolite additions.

The extrapolated peak onset temperatures, the peak maximum temperatures and the extrapolated offset temperatures for each mixture are summarized in the tables below:

NaCl/KCl ratio	Cryolite content [%]	T _{onset,1} [°C]	T _{onset,2} [°C]	T _{onset,3} [°C]	T _{peak,1} [°C]	T _{peak,2} [°C]	T _{peak,3} [°C]	T _{offset} [°C]
70/30	2	646.2	652.0	652.0	659.1	683.1	729.0	745.0
50/50	2	641.0	-	-	671.4	-	-	684.0

Table 4-5 - Characteristic temperatures obtained from the DSC curves of the 70% wt NaCl – 30% wt KCl and the 50% wt NaCl – 50% wt KCl with 2 % cryolite additions.

NaCl/KCl ratio	Cryolite content [%]	T _{eutectic} [°C]	T _{solidus} [°C]	T _{liquidus} [°C]
70/30	2	646.2	652.0	729.0
50/50	2	-	641.0	671.4

Table 4-6 – Eutectic, solidus and liquidus temperatures obtained from the analysis of the characteristic temperatures of DSC curves for the salt mixtures.

The solidus and liquidus temperatures for the 50% NaCl – 50% KCl and 70% NaCl – 30% KCl mixtures with 2% cryolite are lower when compared with the 95% NaCl – 5% KCl mixtures, regardless of the cryolite content. This implies higher energy requirements to melt salt fluxes with higher NaCl content; however, it may be economically viable to decrease the KCl content due to its higher cost compared to NaCl.

The experimental results from the DSC analysis are not in agreement with the preliminary thermodynamic analysis. Again, the empirical results are not easily comparable with thermodynamic calculations, as the experimental conditions are not those of equilibrium. Other possible reasons for this discordance are ascribable to the lack of calibration of the DSC apparatus or else to inaccuracies in the calculations of the phase diagrams, either due to missing information in the FactSage database for inorganic salts or to imprecisions in carrying out thermodynamic calculations.

4.3 Viscosity Measurements

Figure 4.10 shows the variation of viscosity at 170 RPM and 820 °C as the cryolite content in the 95% NaCl – 5% KCl salt flux increases. The experimental results show an increase of viscosity from 3.95 cP to 7.025 cP as the cryolite increases from 0 to 5%. For higher cryolite concentrations, the viscosity shows a decreasing trend.

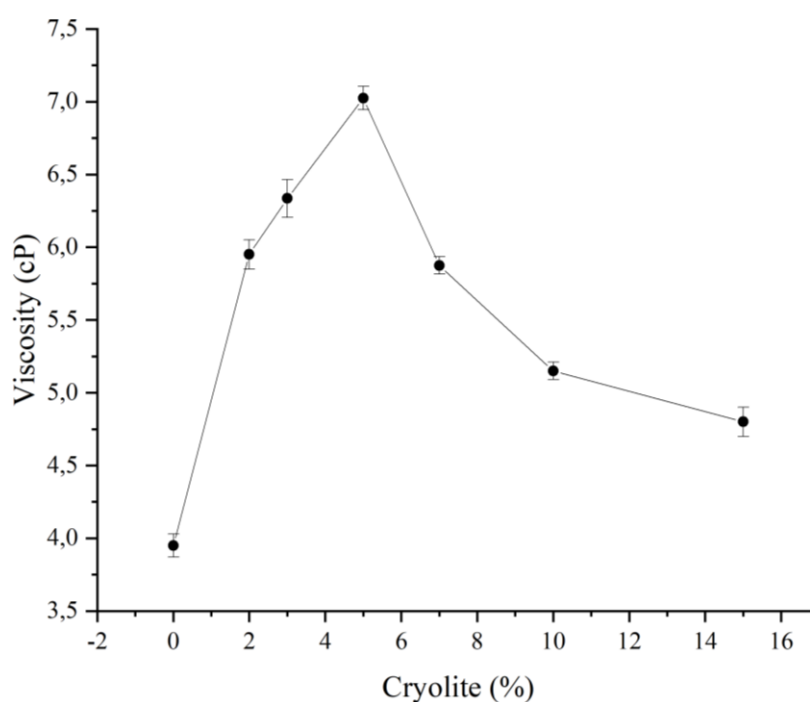


Figure 4.10 – Viscosity of the 95% NaCl - 5% KCl at 820°C and 170 RPM at different cryolite content.

There is no scientific evidence on the viscosity of the 95% NaCl – 5% KCl salt flux with cryolite additions in literature. Tenorio et al. [19] investigated the viscosity

of an equimolar mixture of NaCl and KCl with KF and NaF additions at 810 °C and 760 °C by means of the body falling method. The authors' findings show a decreasing trend of viscosity for fluorides contents up to 20 %. The viscosity ranges from approximately 1.2 cP to 0.4 cP at 810 °C. Roy, Ye and Sahai studied the effect of fluoride additions on the kinematic viscosity of an equimolar NaCl – KCl mixture. For cryolite additions up to 1,5 % mole, the kinematic viscosity showed a decreasing behavior. According to the work of Murgulescu and Zuca [70], who studied the viscosity of molten NaCl-KCl systems at different temperatures with the oscillating sphere method, the viscosity of a 84.77% mol NaCl – 15.23 % mol KCl at 817 °C was of 1.285 cP.

For industrial relevance, an increase in the molten salt's viscosity hinders the metal droplets' coalescence and thus leads to a decrease in the metal recovery [14]. Although the experimental results of this thesis work are not easily comparable with the data in literature due to the different experimental methods, inaccuracies of the data obtained may be related to the measuring system, specifically to the type of spindle utilized, which is more suitable for high-viscosity measurements and may cause turbulence in the molten salt, eventually leading to uncontrolled increasing flow resistance [69].

4.4 Alumina Dissolution in the molten salt mixtures

Figure 4.11 shows the Al_2O_3 dissolution for cryolite content in the 95% NaCl – 5% KCl salt mixtures up to 15%. The addition of cryolite up to 5% shows no relevant effect in the salt’s ability in dissolving the oxide, whereas concentrations equal to 7% or above lead to noticeable improvements already after 10 minutes of holding time of the alumina sphere in the molten salt. The oxide dissolution rate for the 7% and the 10% cryolite contents stabilizes to a constant value after 10 minutes and 40 minutes, respectively, whereas for the 15% cryolite concentration the salt’s ability in dissolving the oxide maintains an increasing trend even at 130 minutes.

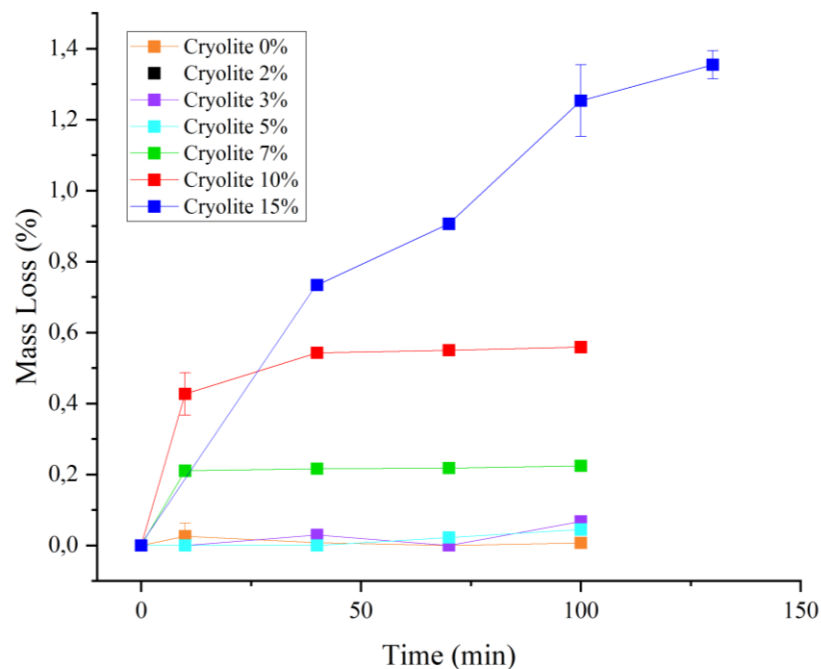


Figure 4.11 – Al_2O_3 dissolution in the molten 95%NaCl-5%KCl salt mixtures at varying cryolite concentrations.

The salt’s ability in dissolving the aluminum oxide is relevant for the oxide’s stripping ability of the salt flux and consequently for its capability in promoting the metal droplets’ coalescence. The experimental results of this study are in agreement with the findings of Tenorio et al. [19], which studied the effect of fluorides (NaF , KF and CaF_2) additions to an equimolar NaCl-KCl salt flux by investigating its ability in dissolving alumina rods. Although the experimental results are not easily comparable due to the different experimental conditions and methodologies, a higher content of

fluorides in the salt flux and a longer holding time lead to an increased aluminum oxide dissolution. From an industrial point of view, the ability of the salt flux in dissolving the aluminum oxide is relevant as it promotes the coalescence of the metal droplets by stripping away the oxide layer that surrounds them, thus leading to an increased metal recovery of the recycling process.

4.5 Salt dissolution in water

Figure 4.12 displays the salt dissolution in water at cryolite contents of 0, 5, 10 and 15% as a function of the holding time. The mass loss of the samples is noticeably different for the 0% and the 15% cryolite-containing salt mixtures, with the salt dissolution decreasing as the cryolite content increases. This is evident for holding times up to 100 minutes, but at 200 minutes there is no significant difference in mass loss for the different samples.

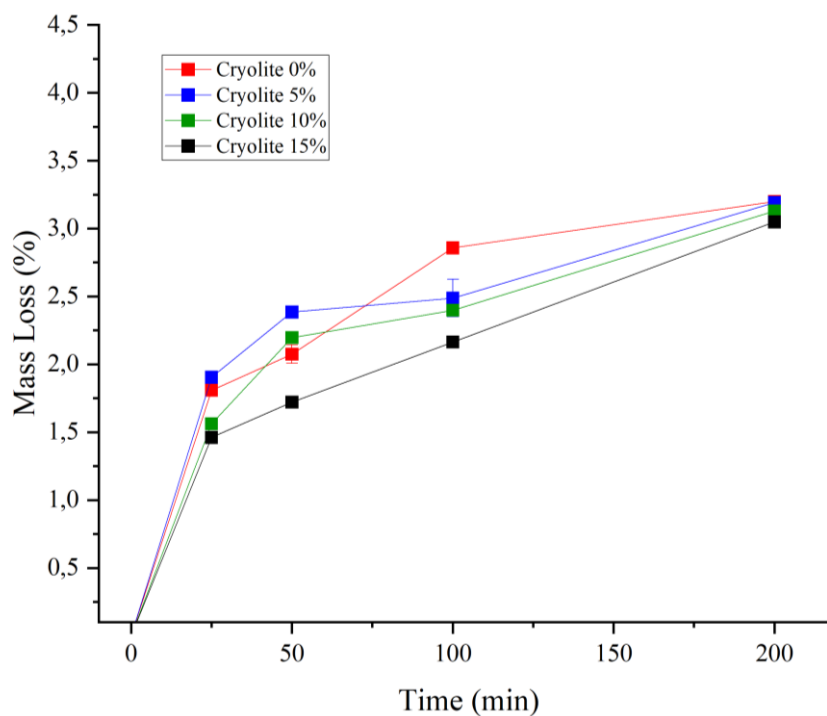


Figure 4.12 – Salt dissolution in water as a function of time for different cryolite contents.

The salt dissolution at varying cryolite concentrations as a function of time is relevant from an industrial point of view for the recovery and leachability of the salt cakes; however, several other parameters influence the recovery of salt cakes in industrial

practice, due to the presence of a large and extremely variable content of compounds, oxides, and impurities, which cannot be neglected. Since high cryolite contents hinder and slow down the dissolution of the salt fluxes, it may be industrially convenient to maintain a low cryolite content in the salts to avoid long cycle times for the recycling process. Moreover, higher cryolite contents in the salt are also a concern from an environmental point of view.

5 Conclusions and future perspectives

In this work, the effect of cryolite additions up to 15% *wt.* to a 95% *wt.* NaCl – 5% *wt.* KCl salt flux was investigated. The melting behavior of the salt mixtures, their rheological properties, their ability in dissolving aluminum oxide, and their dissolution time in water were studied. As a term of comparison for the melting behavior of a 70% NaCl – 30% KCl and a 50% NaCl – 50% KCl with 2% cryolite additions were also considered.

According to a preliminary thermodynamic analysis performed with FactSage, the solidus temperature of the 95% NaCl – 5% KCl salt flux decreases when adding cryolite up to 1.3 %. Further cryolite additions do not lead to a decrease in the solidus temperature. The liquidus temperature slightly increases with cryolite additions. This is not in agreement with the experimental results: both the wetting furnace and the DSC results show a decrease of the solidus and liquidus temperature for the 95% *wt.* NaCl – 5% *wt.* KCl salt flux as the cryolite content increases. The melting characteristics of the salt flux are relevant from an industrial point of view, as a decrease of the melting point implies reduced energy costs and emissions related to energy consumption. Although, experimentally, a higher cryolite content leads to a reduction in the solidus and liquidus temperatures, the melting point of both the 70% NaCl – 30% KCl and the 50% NaCl – 50% KCl with 2% cryolite was lower when compared to the 95% NaCl – 5% KCl salt flux, regardless of the fluoride content. As a matter of fact, the KCl content in the salt flux decreases its melting point; however, the cost of KCl is higher compared to that of NaCl.

The rheology experiments show a maximum viscosity value for a cryolite content of 5%. Overall, the viscosity increases when cryolite is present in the salt flux. The rheological properties of salt fluxes are significant in terms of the metal droplets' coalescence; indeed, an increase in the salt flux's viscosity leads to hindering of the movement of the droplets through the slag layer and therefore to a decreased coalescence and metal recovery.

The experimental results from the alumina spheres' dissolution show a beneficial effect both of longer holding times and of the presence of cryolite in the salt flux for concentrations higher than 7%; below this percentage no relevant effect was noted. For each cryolite content, longer holding times after a certain limit are not beneficial.

The ability of the salt flux in dissolving the aluminum oxide is related to its capability of stripping the oxide layer, which affects the aluminum droplets' coalescence by freeing the molten metal from the surrounding oxide layer, thus increasing the metal recovery of the recycling process.

The findings from the dissolution of the salt mixtures in water show that the presence of cryolite leads to a reduced dissolution of the salt. The salt dissolution rate in water is related to the leachability of salt cakes and therefore to their recovery, which is significant from an industrial point of view in terms of processing times, as well as it affects the environmental impact of the waste products from secondary aluminum production. Since the presence of cryolite hinders the dissolution of the salt in water, the content of fluoride should be kept at the minimum necessary value to avoid excessively long cycle times for the recovery of salt cakes.

In this thesis work, the chemical and physical properties relevant for industrial practice of a NaCl – KCl salt flux were investigated. The next step could include the assessment of the specific heat capacity of the salt mixtures by means of a calibrated DSC, as specific heat capacity is significant in terms of energy requirements for the melting of the salt flux. The rheological properties should be revised and carried out by means of a spindle for low-viscosity measurements. Lastly, more repetitions of the alumina dissolution in the molten salt mixtures and of the salt's dissolution time in water should be carried out.

6 References

- [1] National Oceanic and Atmospheric Administration (NOAA), «Climate.gov - Climate Change: Global Temperature,» 12 August 2021. [Online]. Available: <https://www.climate.gov/news-features/understanding-climate/climate-change-global-temperature>. [Consultato il giorno 15 April 2022].
- [2] ClimateWatch, «World Greenhouse Gas Emissions in 2018 by Sector, End Use and Gases (static),» 2018. [Online]. Available: <https://www.climatewatchdata.org/key-visualizations?visualization=4>.
- [3] Intergovernmental Panel on Climate Change, «SPECIAL REPORT "Global Warming of 1.5 °C", Summary for Policymakers,» 2018. [Online]. Available: https://www.ipcc.ch/site/assets/uploads/sites/2/2019/05/SR15_SPM_version_report_LR.pdf.
- [4] D. Raabe, D. Ponge, P. J. Uggowitzer, M. Roscher, M. Paolantonio, C. Liu, H. Antrekowitsch, E. Kozeschnik, D. Seidmann, B. Gault, F. De Geuser, A. Deschamps, C. Hutchinson, C. Liu, Z. Li, P. Prangnell, J. Robson, P. Shanthraj, S. Vakili, C. Sinclair, L. Bourgeois e S. Pogatscher, «Making sustainable aluminum by recycling scrap: The science of “dirty” alloys,» *Progress in Materials Science*, vol. 128, 2022.
- [5] A. T. Tabereaux e R. D. Peterson, «Chapter 2.5 - Aluminum Production,» in *Treatise on Process Metallurgy - Volume 3: Industrial Processes*, Elsevier Ltd., 2014, pp. 839-917.
- [6] M. Gautam, B. Pandey e M. Agrawal, «Chapter 8 - Carbon Footprint of Aluminum Production: Emissions and Mitigation,» in *Environmental Carbon Footprints: Industrial Case Studies*, Butterworth-Heinemann, 2018, pp. 197-228.
- [7] International Aluminium Institute - IAI, «BEYOND 2 DEGREES - The outlook for the aluminium sector,» 2018. [Online]. Available: <https://international-aluminium.org/resource/beyond-2-degrees-the-outlook-for-the-aluminium-sector-factsheet/>.
- [8] J. A. Greene, *Aluminum Recycling and Processing for Energy Conservation and Sustainability*, ASM International, 2007.

- [9] C. Schmitz, Handbook of Aluminum Recycling, Vulkan, 2006.
- [10] M. E. Schlesinger, Aluminum Recycling, Rolla, MO, U.S.A.: Taylor & Francis Group, 2007.
- [11] S. Capuzzi e G. Timelli, «Preparation and melting of scrap in aluminum recycling: a review,» *Metals*, vol. 8, n. 4, p. 249, 2018.
- [12] R. D. Peterson, «Effect of Salt Flux Additives on Aluminum Droplets Coalescence,» in *Second International Symposium - Recycling of Metals and Engineered Materials - TMS*, 1990.
- [13] R. R. Roy e Y. Sahai, «Coalescence behavior of aluminum alloy drops in molten salts,» *Materials Transactions, JIM*, vol. 38, n. 11, pp. 995-1003, 1997.
- [14] S. Besson, A. Pichat, E. Xolin, P. Chartrand e B. Friedrich, «Improving coalescence in Al-Recycling by salt optimization,» *Proceedings of EMC*, 2011.
- [15] Y. Xiao, M. A. Reuter e U. Boin, «Aluminium recycling and environmental issues of salt slag treatment,» *Journal of Environmental Science and Health*, vol. 40, pp. 1861-1875, 2005.
- [16] J. A. S. Tenorio e D. C. R. Espinosa, «Effect of salt/oxide interaction on the process of aluminum recycling,» *Journal of Light Metals*, vol. 2, pp. 89-93, 2002.
- [17] R. R. Roy e Y. Sahai, «Interfacial tension between aluminum alloy and molten salt flux,» *Materials Transactions, JIM*, vol. 38, n. 6, pp. 546-552, 1997.
- [18] R. R. Roy, J. Ye e Y. Sahai, «Viscosity and density of molten salts based on equimolar NaCl-KCl,» *Materials Transactions, JIM*, vol. 38, n. 6, pp. 566-570, 1997.
- [19] J. A. S. Tenorio, M. C. Carboni e D. C. R. Espinosa, «Recycling of aluminum - effect of fluoride additions on the salt viscosity and on the alumina dissolution,» *Journal of Light Metals*, vol. 1, pp. 195-198, 2001.
- [20] T. A. Utigard, K. Friesen, R. R. Roy, J. Lim, A. Silny e C. Dupuis, «The Properties and Uses of Fluxes in Molten Aluminum Processing,» *JOM*, vol. 50, n. 11, pp. 38-43, 1998.

- [21] A. Gil e S. A. Korili, «Management and valorization of aluminum saline slags: current status and future trends,» *Chemical Engineering Journal*, vol. 289, pp. 74-84, 2015.
- [22] NASA's Goddard Institute for Space Studies (GISS), «Global Climate Change,» 22 March 2022. [Online]. Available: <https://climate.nasa.gov/vital-signs/global-temperature/>.
- [23] United States Environmental Protection Agency, «EPA.gov,» 2021. [Online]. Available: <https://www.epa.gov/ghgemissions/overview-greenhouse-gases>.
- [24] EPA - United States Environment Programme, «Greenhouse Gases Emissions - Understanding Global Warming Potentials,» 18 October 2021. [Online]. Available: <https://www.epa.gov/ghgemissions/understanding-global-warming-potentials>.
- [25] United Nations, «UN News - Global perspective Human stories,» 2020. [Online]. Available: <https://news.un.org/en/story/2020/03/1059061>.
- [26] R. Rupasinghe, B. B. Chomel e B. Martinez-Lopez, «Climate change and zoonoses: A review of the current status, knowledge gaps, and future trends,» *Acta Tropica*, vol. 226, 2022.
- [27] Internal Displacement Monitoring Center, «Global Report on Internal Displacement 2021,» 2021. [Online]. Available: <https://www.internal-displacement.org/global-report/grid2021/>.
- [28] UNEP United Nations Environment Programme, «Emissions Gap Report,» 2021.
- [29] M. Bui, C. S. Adjiman, A. Bardow, E. J. Anthony, A. Boston, S. Brown, P. S. Fennell, S. Fuss, A. Galindo, L. A. Hackett, J. P. Hallett, H. J. Herzog, G. Jackson, J. Kemper, S. Krevor, G. C. Maitland, M. Matuszewski, I. S. Metcalfe, C. Petit, G. Puxty, J. Reimer, D. M. Reiner, E. S. Rubin, S. A. Scott, N. Shah, B. Smit, J. P. Martin Trusler, P. Webley, J. Wilcox and N. Mac Dowell, "Carbon Capture and Storage (CCS): the way forward," *Energy & Environmental Science*, pp. 1062-1176, 5 January 2018.
- [30] Ellen McArthur Foundation, «Completing the Picture: How the Circular Economy Tackles Climate Change,» 2019. [Online]. Available: <https://ellenmacarthurfoundation.org/completing-the-picture>.

- [31] European Aluminium Association , «Aluminium in cars - Unlocking the light-weighting potential,» 29th July 2013. [Online]. Available: <https://www.european-aluminium.eu/media/3371/aluminium-in-cars-unlocking-the-lightweighting-potential.pdf>.
- [32] European Aluminium Association, «The aluminum effect - A unique metal with unique properties,» 2013. [Online]. Available: <https://www.european-aluminium.eu/about-aluminium/the-aluminium-effect/>. [Consultato il giorno 2022].
- [33] International Aluminium, «International Aluminium Statistics,» 2019. [Online]. Available: <https://international-aluminium.org/statistics/primary-aluminium-smelting-energy-intensity/>.
- [34] G. Gaustad, E. Olivetti e R. Kirchain, «Improving aluminum recycling: A survey of sorting and impurity removal technologies,» *Resources, Conservation and Recycling*, vol. 58, pp. 79-87, 2012.
- [35] T. Arink e M. I. Hassan, «Metal scrap preheating using flue gas waste,» *Energy Procedia*, vol. 105, pp. 4788-4795, 2017.
- [36] D. Kopeliovich, «SubsTech - Substances and Technologies: Degassing treatment of molten aluminum alloys,» 28 07 2012. [Online]. Available: https://www.substech.com/dokuwiki/doku.php?id=degassing_treatment_of_molten_aluminum_alloys. [Consultato il giorno 05 08 2022].
- [37] S. Padamata, A.-. Yasinskyi e P. Polyakov, «A review of secondary aluminum production and its byproducts,» *JOM*, vol. 73, n. 9, pp. 2603-2613, 2021.
- [38] E. Velasco e J. Nino, «Recycling of aluminum scrap for secondary Al-Si alloys,» *Waste Management & Research: The Journal For A Sustainable Circular Economy*, vol. 29, n. 7, pp. 686-693, 2011.
- [39] A. Morris, «Industrial Heating - Minimizing melt loss in aluminum recycling,» 4 February 2014. [Online]. Available: <https://www.industrialheating.com/articles/91516-minimizing-melt-loss-in-aluminum-recycling>.
- [40] T. A. Utigard, R. R. Roy e K. Friesen, «The Roles of Molten Salts in the Treatment of,» *Canadian Metallurgical Quarterly*, vol. 40, n. 3, pp. 327-334, 2013.

- [41] R. Beheshti, *Sustainable Aluminium and Iron Production - Doctoral Thesis*, 2017.
- [42] S. Capuzzi, G. Timelli, L. Capra e L. Romano, «Study of fluxing in Al refining process by rotary and crucible furnaces,» *International Journal of Sustainable Engineering*, vol. 12, n. 1, pp. 38-46, 2019.
- [43] A. Pirker, H. Antrekowitsch, W. Fragner, H. Suppan e M. Kettner, «Optimization of the Al-recycling Process for Low Grade Scraps,» *BHM - Berg- und Hüttenmännische Monatshefte*, vol. 160, n. 7, pp. 320-327, 2015.
- [44] R. Bolivar e B. Friedrich, «The influence of increased NaCl:KCl ratios on metal yield in salt bath smelting processes for aluminium recycling,» *World of Metallurgy - ERZMETALL*, vol. 62, n. 6, pp. 366-371, 2009.
- [45] M. Thoraval e B. Friedrich, «Metal entrapment in slag during the aluminium recycling process in tilting rotary furnace,» *Proceedings of European Metallurgical Conference (EMC)*, 2015.
- [46] Y. Kim, E. Yoon, K. Kim, W. Jung e D. Jo, «Effects of salt flux and alloying elements on the coalescence behaviour of aluminum droplets,» *Journal of Korea Foundry Society*, vol. 20, pp. 39-45, 2000.
- [47] J. H. L. Van Linden e D. L. Stewart, Jr., «Molten salt flux composition effects in aluminum scrap remelting,» *Light Metals*, pp. 391-398, 1989.
- [48] K. J. Friesen e T. A. Utigard, «Coalescence behaviour of aluminum droplets under a molten salt flux cover,» *Light Metals*, pp. 857-867, 1997.
- [49] A. Sydykov, B. Friedrich e A. Arnold, «Impact of parameter changes on the aluminum recovery in a rotary kiln,» *Light Metals*, pp. 1045-1052, 2002.
- [50] B. Wan, W. Li, F. Liu, T. Lu, S. Jin, K. Wang, A. Yi, J. Tian e W. Chen, «Determination of fluoride component in the multifunctional refining flux used for recycling aluminum scrap,» *Journal of Materials Research and Technology*, vol. 9, n. 3, pp. 3447-3459, 2020.
- [51] M. F. Jordan e D. R. Milner, «The removal of oxide from aluminum by brazing fluxes,» *Journal of Institute of Metals*, vol. 85, pp. 33-40, 1956.
- [52] E. I. Storchai e N. S. Baranov, «Optimizing the production operation of brazing aluminum structures in flux baths,» *Khim. Neft. Mashinostr*, vol. 3, pp. 28-30, 1976.

- [53] S. Capuzzi, A. Kvithyld, G. Timelli, A. Nordmark, E. Gumbmann e T. A. Engh, «Coalescence of clean, coated and decoated aluminum for various salts, and salt-scrap ratios,» *Light Metals*, pp. 1115-1121, 2017.
- [54] A. Sully, H. K. Hardy e T. J. Heal, «An investigation of thickening and metal entrapment in a light alloy melting flux,» *Journal of Institute of Metals*, vol. 82, p. 49, 1954.
- [55] B. F. M. Thoraval, «Metal entrapment in slag during the aluminium recycling process in tilting rotary furnace,» *Proceedings of EMC*, 2015.
- [56] A. Vallejo-Olivares, H. Philipson, M. Gokelma, H. J. Roven, T. Furu, A. Kvithyld e G. Tranell, «Compaction of aluminium foil and its effect on oxidation and recycling yield,» *Light Metals*, pp. 735-741, 2021.
- [57] P. Palimaka, «Thermal cleaning and melting of fine aluminium alloy chips,» *Polska Akademia Nauk - Archives of Foundry Engineering*, vol. 2020, n. 4, pp. 91-96, 2020.
- [58] S. Eggen, K. Sandaunet, L. Kolbeinsen e A. Kvithyld, «Recycling of aluminum from mixed household waste,» *Light Metals*, pp. 1091-1100, 2020.
- [59] O. Majidi, S. G. Shabestari e M. R. Aboutalebi, «Study of fluxing temperature in molten aluminum refining process,» *Journal of Materials Processing Technology*, vol. 182, pp. 450-455, 2007.
- [60] Y. Xiao e M. A. Reuter, «Recycling of distributed aluminium turning scrap,» *Minerals Engineering*, vol. 15, pp. 963-970, 2002.
- [61] M. Thoraval, *Understanding metal losses in salt slags during aluminium recycling in tilting rotary furnaces - Doctoral Thesis Dissertation*, 2021.
- [62] I. Padilla, M. Romero, S. L. Andres e A. L. Delgado, «Sustainable management of salt slag,» *Sustainability*, vol. 14, n. 9, pp. 4887-5000, 2022.
- [63] P. E. Tsakiridis, «Aluminium salt slag characterization and utilization - A review,» *Journal of Hazardous Materials*, Vol. %1 di %2217-218, pp. 1-10, 2012.
- [64] E. C. -. C. -. E. r. results, «Efficient aluminium salt cake recycling technology,» 2017. [Online]. Available: <https://cordis.europa.eu/article/id/223757-inhouse-salt-slag-processing-solution-which-turns-waste-into-a-product>.

- [65] S. Bao, *Filtration of Aluminium - Experiments, Wetting and Modelling. Doctoral Thesis.*, Norwegian University of Science and Technology (NTNU), Trondheim, Norway, 2011.
- [66] P. J. Haines, M. Reading e F. W. Wilburn, «Chapter 5 - Differential Thermal Analysis and Differential Scanning Calorimetry,» in *Handbook of Thermal Analysis and Calorimetry. Vol. 1: Principles and Practice.*, Elsevier, 1998, pp. 279-361.
- [67] G. W. H. Höhne, W. F. Hemminger e H. J. Flammersheim, *Differential Scanning Calorimetry - Second Edition*, Springer, 2003.
- [68] J. Harvey, N. Saadatkah, G. D. Vandewinkel, S. L. Ackermann e G. S. Patience, «Experimental methods in chemical engineering: Differential Scanning Calorimetry -DSC,» *The Canadian Journal of Chemical Engineering*, vol. 96, pp. 2518-2525, December 2018.
- [69] T. G. Mezger, *The Rheology Handbook: for users of rotational and oscillational rheometers. 2nd Revised Edition*, Hannover, Germany: Vincentz Networks, 2006.
- [70] G. J. Janz, R. P. T. Tomkins, C. B. Allen, J. R. Downey, G. L. Garner, U. Krebs e S. K. Singer, «Molten salts: Volume 4, part 2, chlorides and mixtures - electrical conductance, density, viscosity, and surface tension data,» in *Journal of physical and chemical reference data*, 1975, pp. 871-1178.
- [71] Linseis, «STA PT 1600 (TG-DSC),» [Online]. Available: <https://www.linseis.com/en/products/simultaneous-thermal-analyzer-tga-dsc/sta-pt-1600/>.

Appendix A

Tables

A.1 – Chemical Compositions

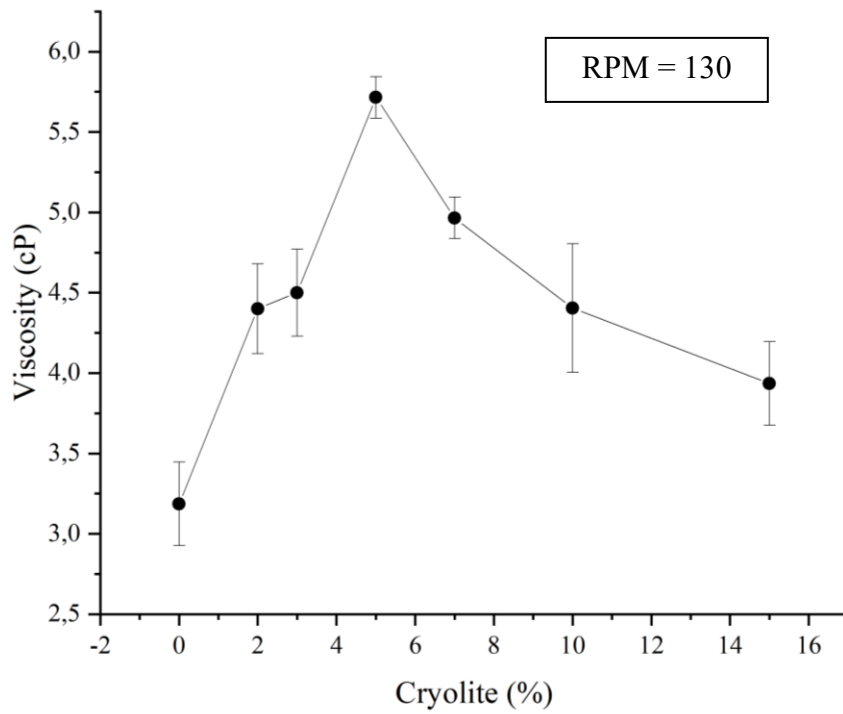
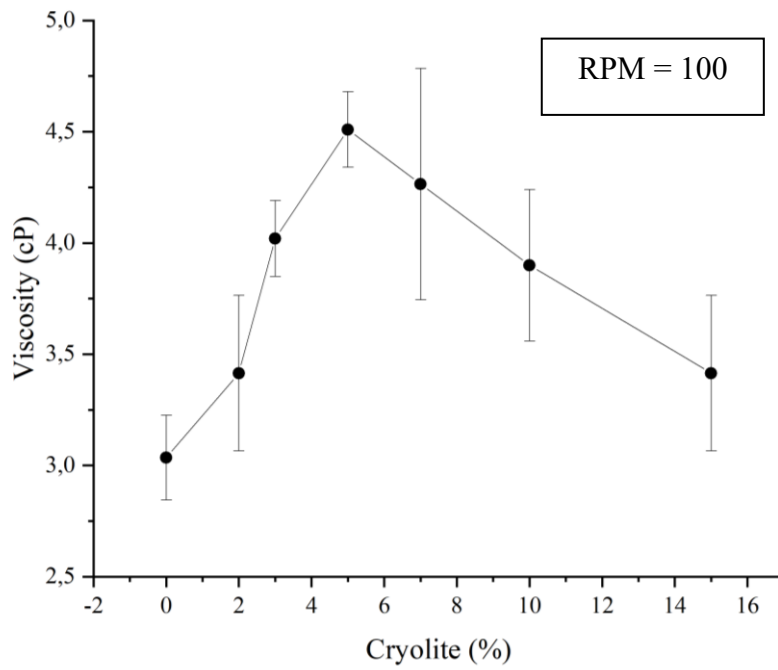
NaCl/KCl ratio	Total mass of mixture [g]	Cryolite % wt.	Cryolite mass [g]	NaCl+KCl mass [g]	NaCl mass [g]	KCl mass [g]
95/5	100	0	0	100	95	5
95/5	100	2	2	98	93,1	4,9
95/5	100	3	3	97	92,15	4,85
95/5	100	5	5	95	90,25	4,75
95/5	100	7	7	93	88,35	4,65
95/5	100	10	10	90	85,5	4,5
95/5	100	15	15	85	80,75	4,25
70/30	100	2	2	98	68,6	29,4
50/50	100	2	2	98	49	49

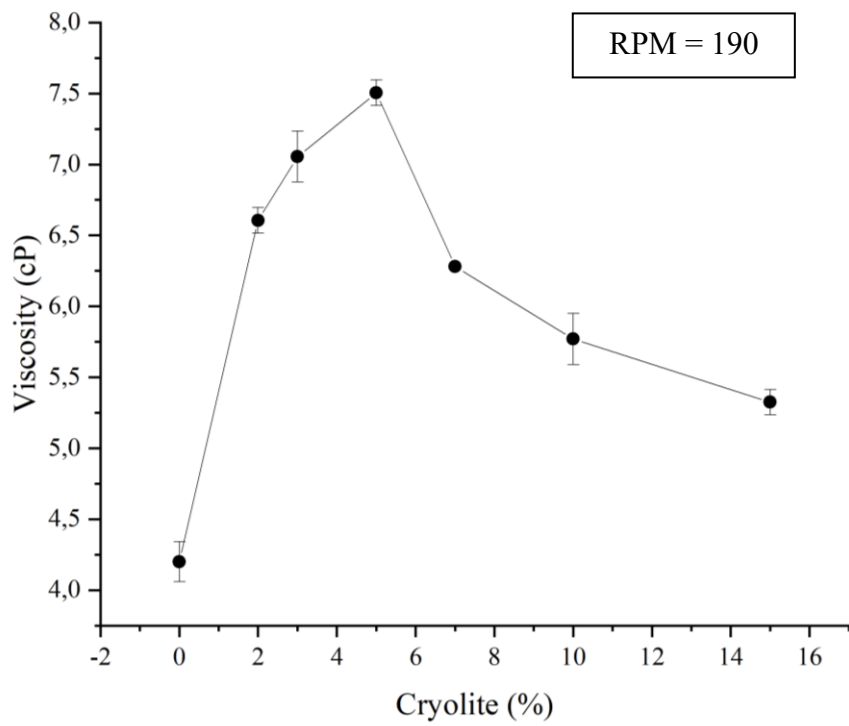
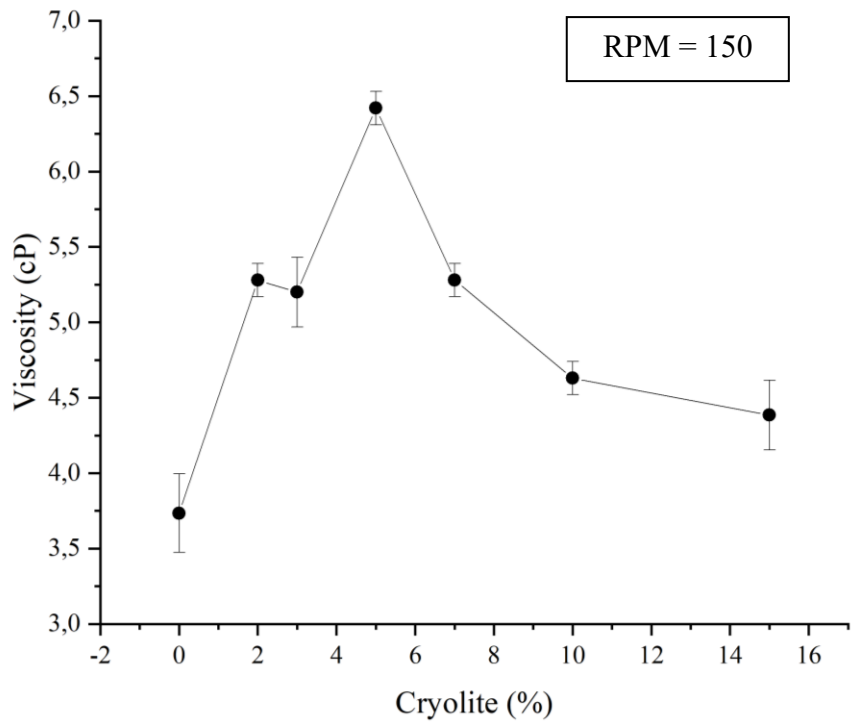
A.2 – Viscosity Measurements on the 95% NaCl – 5% KCl salt flux

Spindle velocity [RPM]	Cryolite %	Viscosity_1 [cP]	Viscosity_2 [cP]	Mean_viscosity [cP]	ST.DEV
100	0	2,9	3,17	3,035	0,19
100	2	3,17	3,66	3,415	0,35
100	3	3,9	4,14	4,02	0,17
100	5	4,39	4,63	4,51	0,17
100	7	3,9	4,63	4,265	0,52
100	10	3,66	4,14	3,9	0,34
100	15	3,17	3,66	3,415	0,35
130	0	3	3,37	3,185	0,26
130	2	4,2	4,6	4,4	0,28
130	3	4,31	4,69	4,5	0,27
130	5	5,62	5,81	5,715	0,13
130	7	4,87	5,06	4,965	0,13
130	10	4,12	4,69	4,405	0,40
130	15	3,75	4,12	3,935	0,26
150	0	3,57	3,9	3,735	0,23
150	2	5,2	5,36	5,28	0,11
150	3	5,04	5,36	5,2	0,23
150	5	6,34	6,5	6,42	0,11
150	7	5,2	5,36	5,28	0,11
150	10	4,55	4,71	4,63	0,11
150	15	4,22	4,55	4,385	0,23
170	0	3,89	4,01	3,95	0,08
170	2	5,88	6,02	5,95	0,10
170	3	6,26	6,45	6,355	0,13
170	5	6,97	7,08	7,025	0,08
170	7	5,88	5,88	5,88	0,00
170	10	5,16	5,16	5,16	0,00
170	15	4,73	4,87	4,8	0,10
190	0	4,1	4,3	4,2	0,14
190	2	6,54	6,67	6,605	0,09
190	3	6,93	7,18	7,055	0,18
190	5	7,44	7,57	7,505	0,09
190	7	6,28	6,28	6,28	0,00
190	10	5,64	5,9	5,77	0,18
190	15	5,26	5,39	5,325	0,09

Appendix B

B.1 – Viscosity Measurements





B.2 – Salt dissolution in water

